1989

ANALYSIS OF ORGANIC SAMPLES BY PLASMA SPECTROMETRY

EVANS, EVAN HYWEL

A thesis entitled

ANALYSIS OF ORGANIC SAMPLES BY PLASMA SPECTROMETRY

presented by

EVAN HYWEL EVANS, B.Sc., GRSC

in part fulfilment of the
requirements for the degree of

DOCTOR OF PHILOSOPHY
of the
COUNCIL FOR NATIONAL ACADEMIC AWARDS

Department of Environmental Sciences
Polytechnic South West
Drake Circus, Plymouth PL4 8AA.

Collaborating establishment:
ICI Wilton Materials Research Centre
Materials Analysis and Testing Group
PO Box 90, Wilton
Middlesbrough, Cleveland, TS6 8JE

October 1989

ANALYSIS OF ORGANIC SAMPLES BY PLASMA SPECTROMETRY

Evan Hywel Evans, B.Sc., GRSC

ABSTRACT

The application of inductively coupled plasma (ICP) spectrometry to the analysis of organic compounds is reviewed. Problems associated with such analyses are identified and methods to overcome them are described.

Simplex optimisation has been used to optimise ICP operating conditions for ICP-atomic emission spectrometry (ICP-AES) and the introduction of organic solvents. The temperature of the spray chamber was also included in the optimisation. Maximum signal-to-background ratios were achieved at lower power for hard lines compared to soft lines, and lower carrier gas flow, spray chamber temperature and power were found to be optimal for organic solvents compared to water. Lower detection limits were achieved using organic solvents compared to water, and the introduction of an organic solvent did not necessarily cause a reduction in excitation temperature in comparison to water when using optimum conditions.

Results are presented for the elemental analysis of organic samples by ICP-AES using either direct introduction of solvents, slurry atomisation or dissolution in sodium hydroxide solution.

A study of matrix effects caused by an organic solvent in ICP-mass spectrometry (ICP-MS) was undertaken. These effects were eliminated by employing the simultaneous nebulisation of aqueous and organic phases together with the use of an internal standard.

Operating conditions for standard and low-flow torches were optimised for ICP-MS using simplex optimisation. The low-flow torch was found to yield a greater proportion of doubly charged ions, but exhibited greater plasma stability on the introduction of volatile solvents compared to the standard torch. The low-flow torch was used for semi-quantitative elemental determinations in organic samples.

Finally, the effect of an organic solvent and molecular gases on polyatomic ion interferences in ICP-MS was investigated. Substantial reductions in, or elimination of, these interferences was achieved, allowing the interference free determination of arsenic and selenium.

ACKNOWLEDGEMENTS

First and foremost I would like to thank Professor Les Ebdon for his expert guidance and beneficial influence throughout the course of this project.

I would also like to thank the Science and Engineering Research Council for providing funding through a SERC-CASE award, and the Wilton Materials Research Centre who collaborated on the project. Thanks must go to Dr. Neil Barnett, my second supervisor for much of the project, for his steadying influence at work and his unsteadying influence in the bar, and also to Dr. John Marshall for his support during visits to Wilton and throughout the course of the work.

I owe a debt of gratitude to many other people including all my friends and colleagues at Plymouth, my wife Sian and Beverley for typing the thesis.

Last but not least I wish to dedicate this thesis to my parents.

CONTENTS

LIST OF TABLES

LIST OF FIGURES

CHAPTER 1

INTRODUCTION

1.1 Elemental Analysis in the Petrochemicals and Polymers Industry

The determination of major, minor, trace and ultra-trace elements plays a vital role in the operation of a modern petrochemicals and polymers business, where the efficient running of the plant and maintenance of a quality product are at a premium. Broadly speaking elemental analysis is required in four main categories.

(i) Petrochemical feedstocks are checked for catalyst poisons and trace elements which may affect the composition of the final product.

(ii) Petrochemical and polymeric products must be monitored for catalyst residues, additives and impurities which may affect their chemical or physical properties or be detrimental to health.

(iii) Catalysts must be periodically assayed to check their composition, and monitored for catalyst poisons.

(iv) Environmental monitoring of wastes from chimneys and outfalls is becoming increasingly important.

It is evident that a great proportion of the analyses

carried out in the industry involves the analysis of organic compounds. From the point of view of elemental determinations this instantly poses a problem, since most of the instrumentation currently in use has been designed for the analysis of aqueous samples. The analyst is therefore faced with two choices: either to transform the organic samples so that they can be solubilised in aqueous media; or to modify the instrumentation to allow the direct introduction of organic samples. Whichever method is chosen, economic constraints will still apply, as the analyst is also under pressure to complete the analysis in the minimum amount of time without resorting to possibly hazardous procedures. Obviously, therefore there is much scope for the development of new instrumentation, sample preparation procedures and analytical methodology to meet the challenge presented by the bewildering variety of sample types encountered in the petrochemicals and polymers industry. This task is not made easier by the continuing development of polymeric materials which are resistant to chemical attack and are thermally stable to relatively high temperatures, therefore constantly presenting the analyst with new sample preparation problems.

The analytical methods and techniques commonly used in the petrochemical and polymers industry for elemental analysis have been reviewed elsewhere (1), however, the most common are flame atomic absorption spectrometry (FAAS), flame atomic emission spectrometry (FAES), X-ray fluorescence

spectrometry (XRFS), neutron activation analysis (NAA), electrothermal atomisation - atomic absorption spectrometry (ETA-AAS), laser/spark/arc ablation atomic - emission spectrometry (laser/spark/arc-AES), inductively coupled plasma - atomic emission spectrometry (ICP-AES), inductively coupled plasma - mass spectrometry (ICP-MS) and classical techniques of analysis. This work will deal exclusively with ICP-AES and ICP-MS, which have found widespread application in the petrochemicals and polymers industry because of their sensitivity and rapid multielement capability.

1.2 Inductively Coupled Plasma - Atomic Emission Spectrometry

Since the inductively coupled plasma (ICP) was first recognised as an almost ideal atom cell for atomic emission spectrometry (AES) by Greenfield et al.,(2) in the UK and Fassel et al. (3), in the USA it has become one of the principal tools for trace element determination in the analytical laboratory (4). The ICP is generated by coupling the energy from a radio-frequency generator into a suitable gas via a magnetic field surrounding a three turn, water-cooled, copper coil. The radio frequency generator normally operates at 27.12 MHz delivering forward power of between 1000 - 3000 W. The gas, usually argon, flows through the outer tubes of a concentric three-tube quartz torch which is positioned axially in the copper coil (Fig. 1.1). When the gas is seeded with electrons, usually by means of a spark, the electrons

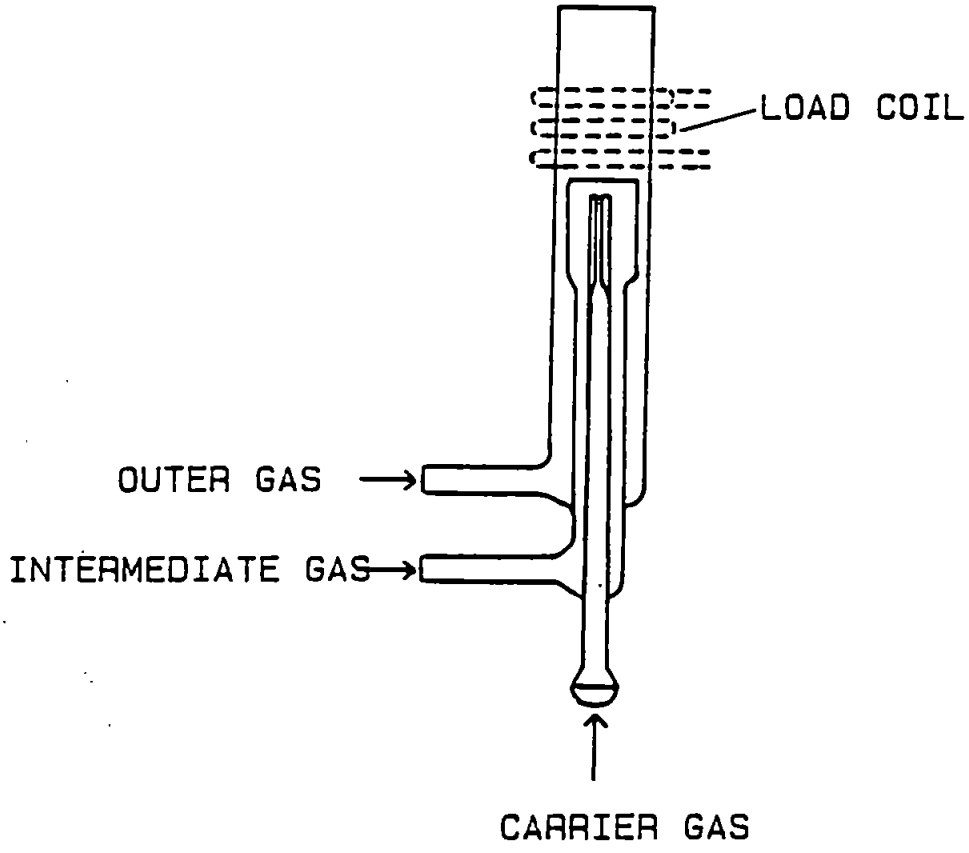

Figure 1.1 Schematic diagram of an ICP torch

accelerate in the magnetic field and reach energies sufficient to ionise gaseous atoms in the field. Subsequent collisions with other gaseous atoms causes further ionisation and so on, so that the plasma becomes self-sustaining. This occurs almost instantaneously. The magnetic field causes the ions and electrons to flow in the horizontal plane of the coil, thereby heating the neutral argon by collisional energy exchange, and a hot fireball is produced. The hottest part of the ICP has a temperature measured at between 8000 - 10000 K, though the analytically useful region in the tail flame has a temperature between 5000 - 6000 K. Since the plasma is not in local thermal equilibrium, however, the gas temperature, ionisation temperature and excitation temperature have different values. The sample is introduced via the injector gas which punches a hole through a weak spot at the base of the plasma producing a torus.

The advantages of the ICP over flames are the much higher excitation temperatures obtainable, with a consequent improvement in detection limits, long linear calibration ranges because its optical thinness reduces self absorption, relative freedom from chemical interferences due to the high temperature, and reproducible generation. The main disadvantages are the initial capital outlay and running costs.

The incorporation of the ICP into an atomic emission

spectrometer is shown schematically in Fig. 1.2. The system basically comprises a sample introduction system, the ICP source, a monochromator and detector, and commonly an integrated microcomputer for collection and manipulation of data and instrument control. During operation the sample, usually a liquid, is introduced by pneumatic nebulisation to form an aerosol containing the analyte. Larger droplets settle out in the spray chamber, allowing the smaller droplets to pass into the plasma via the injector tube. Here, the droplets are desolvated and the molecules decomposed, atomised and ionised. The atoms and ions are excited, then fall back to the ground state emitting characteristic radiation, which is separated with respect to wavelength by the monochromator and detected usually by a photomultiplier tube (PMT). The PMT allows conversion of the signal to an electrical current which can then be processed by various electronics and output to a digital display or microcomputer. This is a description of operation in its simplest form. In practice complications can arise, and new developments are constantly being made at each of the stages of operation.

1.2.1 Applications to Organics Analysis

Inductively coupled plasma - atomic emission spectrometry has been used to determine trace metals in a wide variety of organic solvents and compounds, including wear metals in lubricating oils and other petroleum products (5-10), metal impurities in a wide range of organic solvents (11, 12), and biological samples (13). The so called 'organic'

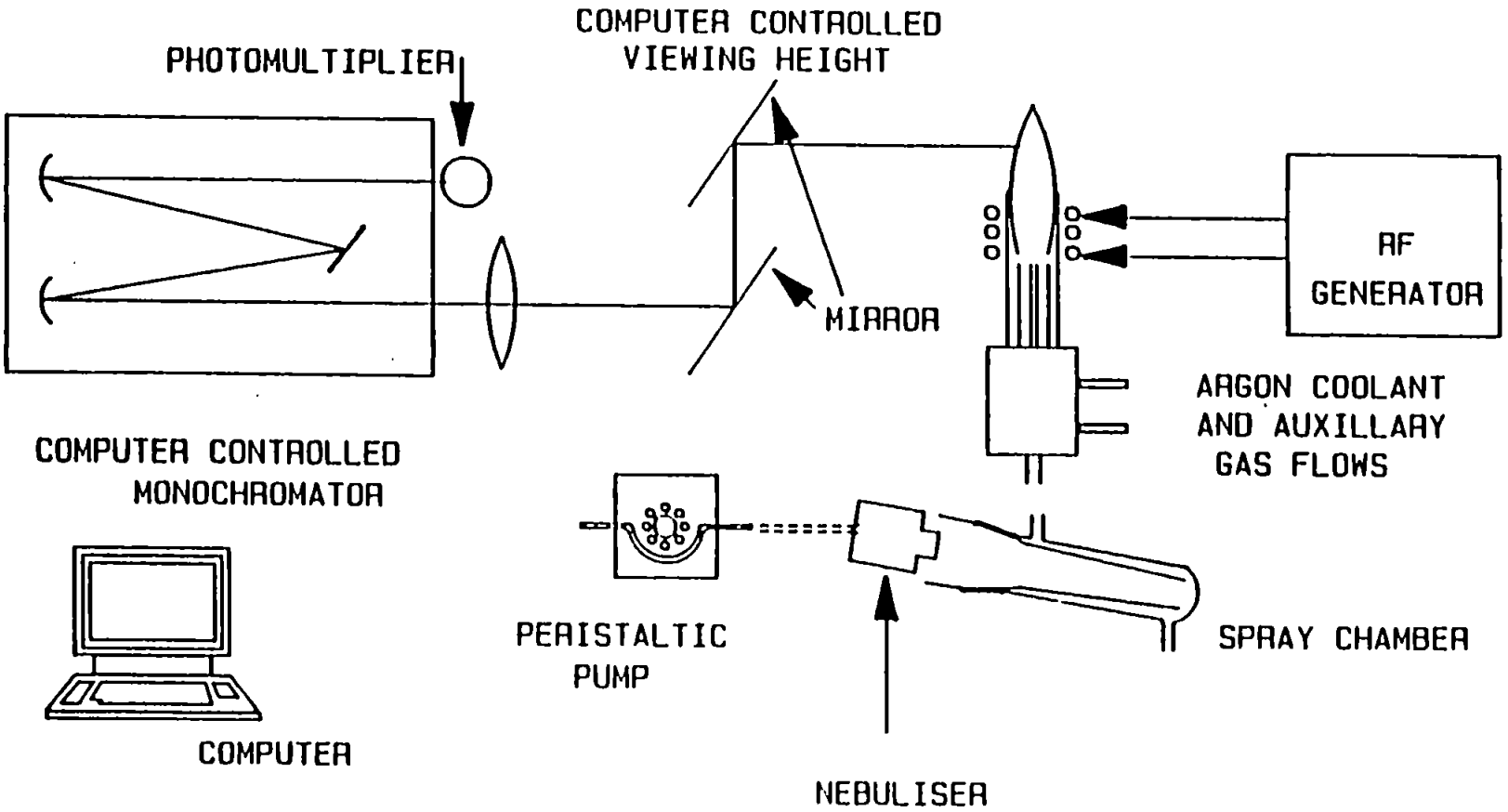

Figure 1.2 Schematic diagram of an inductively coupled plasma - atomic emission spectrometer (from reference 88)

ICP is also necessary for determinations after solvent extraction (14-19) and coupled to liquid and gas chromatography (20-22). Much work has also been carried out into the effect of various organic solvents on plasma stability, excitation conditions, interference from molecular spectra and the optimisation of operating parameters with regard to these effects (23-35). This area of more fundamental work is discussed in greater detail in Chapter 2.

1.3 Inductively Coupled Plasma - Mass Spectrometry

Inductively coupled plasma - mass spectrometry (ICP-MS) is an outstanding example of the marriage of two well developed analytical techniques. The ICP has long been recognised as an extremely efficient ion source, and MS as offering excellent sensitivity. However, coupling of the two has presented a problem due to the difficulty in transferring ions from an ICP operated at atmospheric pressure into the MS operated in a vacuum. This was ingeniously overcome by the groups of Gray and Fassel (36). Gray and Date (37) developed the system and interface shown in Fig. 1.3. The ICP is positioned horizontally (in most cases), end-on to an aperture of between 0.5 and 1.5 mm in the water-cooled sampling cone. Ions are sampled from the central channel of the ICP, pass through the aperture and into the expansion chamber. There the sampled gas expands rapidly forming a 'barrel-shock' region fronted by the 'mach disc'. The skimmer cone protrudes through the mach disc into the so-called

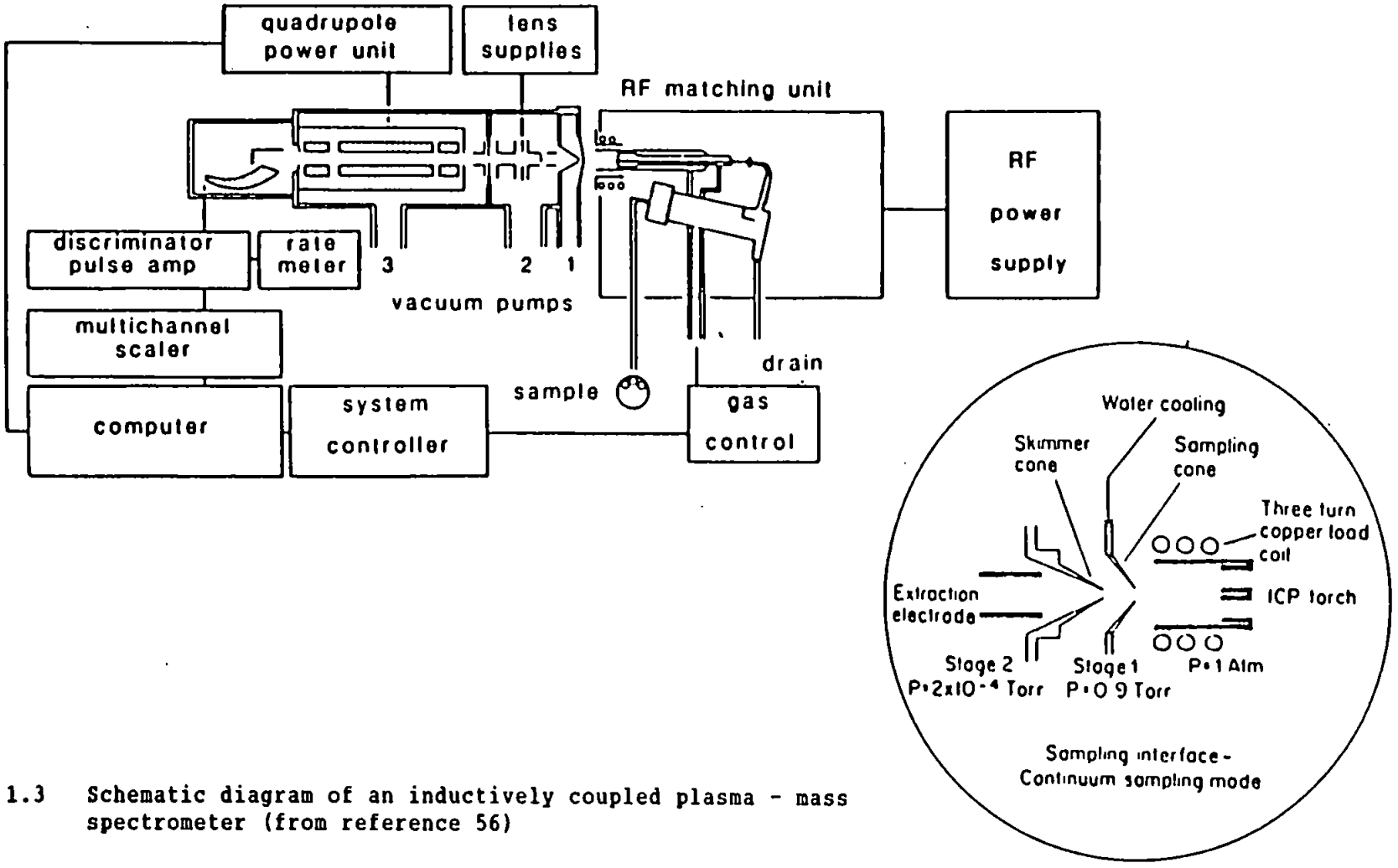

Figure 1.3 Schematic diagram of an inductively coupled plasma - mass spectrometer (from reference 56)

'zone of silence'. A small percentage of the ions that passed through the sampling cone now pass through the aperture in the skimmer cone (ca. 1 mm in diameter) forming a relatively collimated ion beam. This ion beam passes into a second vacuum stage where it is focused by means of ion-focusing lenses, and thence into a third vacuum stage containing the quadropole MS where the ions are separated with respect to the mass-to-charge ratio (m/z) and detected by means of an electron multiplier. The electron multiplier is positioned off-axis to minimise noise caused by photons from the intensely bright ICP source. The resultant mass spectrum is far simpler than that obtained in optical spectroscopy because it is comprised to a large extent only of isotopes of the elements, although interferences due to polyatomic species formed from argon, atmospheric gases, the sample matrix and acids used for dissolution cause problems below 80 m/z units (38).

These interferences can be overcome to a certain extent by modification to sample preparation procedures or utilisation of an alternative isotope. Interferences caused by doubly charged ions and refractory oxides can largely be overcome by careful choice of operating conditions (39, 40). The main advantages of ICP-MS are the possibilities of quantitative isotope determination (41-44), isotope dilution analysis (42, 45-50), rapid spectral scanning due to the peak hopping capability of the mass spectrometer and semi-quantitative determinations

to within a factor of 2 or 3. Additionally, detection limits are commonly an order of magnitude better than in ICP-AES, and it is better suited for determination of the rare earth elements (51-53) and halogens (54).

1.3.1 Applications to Organics Analysis

Since ICP-MS is a relatively new technique there is comparatively little published material, and much of the literature on the subject currently deals with fundamental aspects of research. Most of the material to date has been reviewed elsewhere (55, 56). The number of publications dealing purely with the analysis of organic matrices is very small (57-59), however, mixtures of organic and aqueous solutions have been introduced as mobile phases in coupled high performance liquid chromatography ICP-MS (60-64).

1.4 Problems Associated with Organics Analysis

The development of sample introduction systems, torches and plasma generation for both ICP-AES and ICP-MS has centred mainly around the utility of the techniques for determinations in aqueous media. Consequently their application to determinations in other media, specifically organic solvents and compounds, has been relatively unexploited, perhaps because of the particular difficulties associated with such analyses. The major difficulties associated with organics analysis concern either dissolution of inert polymeric materials such as victrex or polypropylene or introduction of volatile

organic solvents into the ICP whilst still maintaining stable plasma operation, and calibration of the instrument for a variety of solvent types. These problems apply equally to both ICP-MS and ICP-AES, and methods developed to overcome them can be used in the operation of either instrument, since they are essentially concerned with the 'ICP part'. Where the two techniques diverge is at the interface between ICP and spectrometer, and subsequent to this. In ICP-AES there is no physical interface between plasma and spectrometer, therefore giving rise to no problematical effects other than the interferences caused by molecular emission spectra. However, in ICP-MS there is an intimate relationship between the ICP and sampling interface which critically affects the sampled ion beam with respect to singly charged, doubly charged and polyatomic ions. Also, in the ion beam itself discrimination between ions may vary depending on operating conditions, the interface configuration and the sample matrix. These parameters influence the final spectrum, especially with regard to polyatomic ion interferences and doubly charged ion response.

1.4.1 Sample Introduction

Viscous samples such as high molecular weight petroleum fractions can be difficult to nebulise efficiently using conventional pneumatic nebulisers. Algeo et al., (8) overcame this problem by using a heated Babington type nebuliser in conjunction with ICP-AES, and found that aerosols could be produced from undiluted oils containing

a high proportion of particulate matter, as well as a reduction in resultant emission intensity variations due to viscosity differences between oils. An ultrasonic nebuliser has been used to increase transport efficiency of organic solvents into an 'air' ICP (65), while the grid type nebuliser has been evaluated for use with coupled HPLC techniques (66). The glass frit nebuliser has also been tested (67) and found to produce finer aerosols and improved plasma stability compared to a conventional pneumatic nebuliser. Whatever nebuliser is used however, it is desirable to control the solvent uptake rate by peristaltic or syringe pump. For extremely volatile solvents it is necessary to reduce the amount of solvent vapour entering the plasma by means of a condenser (32-35) or other desolvation interface combined with flow injection (68).

An alternative approach of electrothermal vaporisation (ETV) sample introduction has been studied by Ohls and Hutsch (10) and Ng and Caruso (69). The latter group of workers eliminated the background contribution from organic solvents by vaporisation of the solvent in the 'dry' stage. However, they found that Zn gave variable responses in different solvents, and that inorganic and organic Zn species gave different responses. The differing volatilities of various organometallic compounds of the same element is one of the major disadvantages in this approach since 'real samples' of organic nature often contain several species.

1.4.2 Stable Plasma Generation

Ng et al., (70) have used a low-power, low-flow torch in ICP-AES to improve plasma stability when introducing organic solvents, at the same time achieving improvements in signal to background ratio. However, the maintenance of a stable plasma is mainly dependent on the amount of solvent vapour entering it per unit time, therefore any measures taken to reduce the solvent vapour loading will also improve plasma stability.

1.4.3 Carbon Deposition

Inevitably, the destruction of organic solvents and compounds in the plasma leads to significant carbon generation, which may build up on the torch surfaces, thereby altering torch geometry and hence gas flow. The obvious way to counteract this in ICP-AES has been to adjust the intermediate gas flow, thereby 'lifting' the plasma away from the torch. However, this procedure is less than satisfactory, particularly when organics with high H/C ratios are introduced. In ICP-MS operation the problem is even more acute since the carbon builds up on the sampling cone, thereby effectively blocking the orifice. The most effective way to combat this problem is to introduce a small amount (ca. 2%) of O_2 into the carrier gas stream to promote carbon combustion in the plasma (58). This has been investigated by Lancione and Evans (71) for ICP-AES, and Hutton (58) and Hausler (59) for ICP-MS.

A more ambitious approach has been adopted by Meyer (65), who has investigated a 40.68 MHz air-ICP for atomic emission spectrometry, which has the advantage of better sample decomposition and cheapness of operation. He found that it yielded detection limits for nine elements comparable with those obtainable in organic solutions with an argon-ICP. This approach would only be possible in ICP-MS if the sampling cone was fabricated from a non-oxidizable material.

1.4.4 Background Spectra

During ICP-AES operation organic solvents contribute to the background spectra due to atomic carbon and hydrogen emission, molecular emission and certain elements which may be found in organic reagents in some quantity (20, 26, 28). However, the spectral region from 190-300 nm is relatively free from background spectra with the exception of the CS and NO band systems and broadened atomic carbon lines. Above 300 nm CN and C_2 band systems can cause spectral interferences during determination of the lanthanides. These interferences are well documented for ICP-AES (4) and can usually be overcome if sufficient care is exercised.

The problems associated with ICP-MS are less well defined (58, 59). Polyatomic ion interferences arise due to the large quantities of carbon from organic solvents, oxygen used to prevent carbon deposition on the cones, and sulphur which is found in large quantities in many organic

samples. More serious than this, considering the very low detection limits obtainable with ICP-MS, may prove to be the relative dirtiness of organic solvents with respect to blank levels of trace elements (58), necessitating solvent clean-up before sample preparation.

1.5 Aims and Objectives

The work described in this thesis was directed towards an investigation of the application of both ICP-AES and ICP-MS to the determination of trace elements in a variety of organic matrices. Optimisation of instrumentation for organic solvent introduction was investigated using a modified, variable step-size simplex algorithm. Novel methods of sample introduction were attempted, in particular for the introduction of volatile organic solvents and the direct introduction of organic compounds as slurries with particular reference to samples which present dissolution problems. The problem of calibration for a wide variety of organic solvents was addressed from the point of view of internal standardisation for ICP-MS. Additionally, since ICP-MS is a relatively new technique some work was undertaken to investigate more fundamental aspects, particularly polyatomic ion-interferences and how they are affected by the introduction of organic solvents and molecular gases.

CHAPTER 2

SIMPLEX OPTIMISATION OF ICP-AES FOR ORGANIC SOLVENT INTRODUCTION

2.1 Introduction

2.1.1 Sample Transport Effects

The nebulisation of organic samples, whilst sometimes problematical, is relatively straightforward to achieve. However, the transport of the resultant aerosol from nebuliser to the plasma, via a spray chamber, has posed a major problem due to the different physical characteristics of various solvents.

Boorn et al., (27) used a theoretical approach to predict the aerosol droplet size distributions of a range of organic solvents. They suggested that the major factors affecting the distributions, and hence nebulisation and transport efficiency, were surface tension, viscosity, evaporation rate, solvent density and vapour pressure. They proposed that viscosity and surface tension affected the primary droplet size distribution (i.e. the size distribution immediately after nebulisation), while evaporation rate, solvent density and vapour pressure affected the droplet size distribution as the aerosol passed through the spray chamber. Their reasons may be summarised as follows.

(i) Viscosity affects solvent uptake rate. The more viscous the solvent, the lower will be the

aspiration rate, and hence the droplet size distribution shifts to smaller droplets.

(ii) Surface tension determines the droplet size distribution at the moment of nebulisation. Hence, lower surface tension leads to smaller droplets.

(iii) Solvent density determines the amount of gravitational settling of the larger droplets on the way through the spray chamber.

(iv) Evaporation rate and vapour pressure determine the extent to which a particular solvent evaporates from the aerosol droplets as they pass through the spray chamber, hence affecting the droplet size distribution.

They concluded that the differences in nebulisation efficiencies between water and organics were caused mainly by (i) and (ii), and the differences between various organics were caused mainly by (iv). These points are important to remember when considering the overall effect of organic solvent introduction into the ICP.

One of the main consequences of the variability in droplet size distributions is the necessity to carefully matrix match standards and samples with respect to the physical parameters mentioned, or use an internal standard, which is itself fraught with difficulty. Botto (31) has studied

the matrix effects of various organic solvents and petroleum products compared to standards dissolved in xylene and/or tetralin. He found a suppression effect that was greater for 'hard' than 'soft' lines, and was dependent upon the amount of plasma cooling caused by the solvent vapour loading. Likewise, Nisamaneepong et al., (67) found an increasing suppression effect on Cd emission at the 228.802 nm line, for increasing concentration of methanol in water. Surprisingly, Fassel et al., (5) determined 15 wear metals in lube oil and reported no matrix effects. However, the oils were diluted 1:10 (m/v) in methyl isobutyl ketone (MIBK), which may not be practical in most instances.

Undoubtedly the main causes of matrix interferences are changes in the droplet size distribution, and plasma cooling caused by increased solvent load as vapour evaporates from more volatile solvents.

2.1.2 Effect of Solvent Vapour Load on Plasma Stability and Emission Signal

Boorn and Browner (28) have investigated the tolerance of a low power argon ICP to 30 organic solvents. They defined the 'limiting aspiration rate' of a solvent as the rate at which the solvent could be introduced with stable plasma operation and no carbon build up on the inner torch tube for 1 hour. In general they found that those solvents with high evaporation factors (Eqn. 2.1) had lower limiting aspiration rates.

$$E = 48 \quad D_V \delta P_S M^2 (\partial RT)^{-2} \qquad (2.1)$$

where: E = evaporation factor

D_V = the diffusion coefficient for a solvent vapour

M = the molecular mass of the solvent

R = the gas constant

T = the absolute temperature

P_S = the saturated vapour pressure

δ = the surface tension

∂ = the density

Also observed were signal enhancements for an atom line in many solvents, while suppression was observed for ion lines. These results are broadly in agreement with Miyazaki et al., (15), who found that solvents with low vapour pressure were more easily introduced, and Botto (31) who observed not only similar matrix effects on signal, but also suggested that solvents with higher H/C ratios require more plasma power.

These effects demonstrate the "trade-off" between lower droplet size distributions and higher solvent vapour loading for more volatile solvents. However, condensation of solvent vapour using some form of condenser or cooled spray chamber has been shown to cause signal enhancements (21, 31), due to a reduction in the solvent vapour loading, while still allowing the formation of smaller droplets, and hence greater transport efficiencies compared to water. Aerosol vapour condensation has been

extensively investigated by Maessen and co-workers (32 - 35) with respect to "optimisation" of the ICP for organic solvent introduction, and is discussed in more detail in section 2.1.4.2.

2.1.3 Effect of Organic Solvents on Excitation Temperature

It has been shown by two groups of workers (29, 35) that the introduction of an organic solvent reduces the excitation temperature in the central channel of the plasma for fixed viewing height, power and nebuliser gas flow rate in comparison to an aqueous plasma. Additionally, an axial peak in excitation temperature and a corresponding peak in analyte emission at 'hard' lines was observed only after full dissociation of C_2 molecular species had occurred when an organic solvent was introduced. This is thought to be due to energy transfer from the plasma gas to the dissociation of molecular species, primarily C_2, thereby making less energy available for excitation until the dissociation is complete. These axial peaks occurred at a lower height in the aqueous plasma.

Observations of electron density (29) supported these results, the introduction of an organic solvent causing a corresponding decrease in electron density compared to aqueous plasma operation.

2.1.4 Optimisation for Organic Solvent Introduction

2.1.4.1 Classification of Spectral Lines

Any discussion of optimisation studies for ICP-AES must include reference to the behaviour of various spectral lines in relation to their spectroscopic properties. This is primarily dictated by the ionisation potential of the species and the excitation potential of the line. Boumans and Lux-Steiner (30) have classified lines into two broad categories, namely 'hard' and 'soft' lines. They classified atomic lines of elements with low to medium first ionisation potentials as 'soft', and atomic and ionic lines of elements with a high first or second ionisation potential as 'hard'. The behaviour of 'hard' and 'soft' lines differ with respect to changes in operating conditions such as power, gas flow and viewing height, which relate directly to the excitation conditions in the plasma. In simple terms, for a particular figure of merit such as net emission intensity, a different set of optimum conditions apply to 'hard' lines than to 'soft' lines. There is no abrupt transition between the two groups, though for comparison it is generally accepted that representative lines from each group suffice.

2.1.4.2 Optimisation Studies

Boumans and Lux-Steiner (30) have investigated "optimisation" of a 50 MHz ICP for the introduction of methyl isobutyl ketone (MIBK). Trends of net line and background signals, and signal-to-background ratios with ICP parameters were studied, and the authors reported

similar trends in the 'organic' compared to an 'aqueous' ICP. Significantly they found that signal-to-background ratios (SBR's) have maxima that shift to higher power with increasing line hardness, though this study was confined to the solvent MIBK. While the above study was not a true multi-variate optimisation, other studies (13, 70) have led to similar conclusions.

Probably the most comprehensive work performed in this field is that of Maessen and co-workers (32 - 35). Initial studies (32) employing a condenser to control the amount of solvent vapour entering the plasma, led to the conclusions that lower condenser temperatures resulted in higher SBR's for both hard and soft lines, and that SBR's increased for both hard and soft lines at lower powers only if condenser temperatures were "reoptimised" for the lower power. In two further studies (33, 34) these workers employed the continuous weighing method to determine the 'solvent plasma load' (i.e. measuring the quantity of solvent entering the plasma in unit time by using a balance to weigh the uptake and drain) controlled by aerosol thermostatting, and its effect on the analytical performance of the ICP for a number of organic solvents and analytical lines of differing 'hardness'. Their conclusions exemplify the difficulty in choosing optimum operating conditions, and of predicting the effects of various organic solvents on analytical performance. This stems mainly from the fact that the effects of evaporation rate on aerosol droplet size, and

hence analyte delivery rate, and saturation vapour pressure on solvent load, and hence plasma excitation conditions are so interdependent that conventional univariate optimisation regimes are inadequate.

2.1.4.3 Simplex Optimisation

The simplex optimisation algorithm is based on a simple set of rules originally described by Spendley et al., (72), further modified by Nelder and Mead (73) and Yarbro and Deming (74), and now referred to as the "modified" or "variable step-size" simplex algorithm. This optimisation algorithm is attractive in that the mathematically based rules are applied in a rigorous and iterative manner to the particular system being optimised, making it ideal for the optimisation of novel systems with several interdependent variables, and a response surface about which little or nothing is known.

The algorithm has found wide application in analytical chemistry (75) for the optimisation of novel and conventional analytical methods and instrumentation. It has been found to be particularly suited to the optimisation of ICP-AES (76 - 83) where a large number of parameters may affect the analytical performance of the plasma, hence a multivariate optimisation technique is essential to find the true optimum. Commonly, the parameters to be optimised are carrier, intermediate and outer gas flows, forward power and viewing height. However, other parameters such as spray chamber

temperature, sample introduction rate and spectrometer settings can be optimised with equal facility. Such an approach is extremely useful when comparing different instrumental configurations such as low power argon cooled plasmas with high power nitrogen cooled plasmas (76), or different torch and sample introduction configurations (78), since a true comparison can only be made between systems operating at optimum conditions. The intrinsic figure of merit is often taken to be signal-to-background ratio (SBR) which has been shown to be independent of the spectrometer (84), thereby making comparisons between plasmas and operating conditions valid.

The technique has also been used in ICP-AES for removal of spectral interferences (85), matrix interferences caused by easily ionisable elements (86), and significantly with respect to this work, for the removal of effects caused by varying concentrations of acetic acid in water, compared to pure aqueous solutions (87).

In this study the application of simplex optimisation to ICP-AES for spectral lines of different 'hardness', covering a wide range of organic solvents will be investigated. In practice an initial set of simplex vertices are generated using a matrix designed by Yarbro and Deming (74) to allow the investigation of the maximum of factor space. The set of operating conditions defined by each vertex are tried, and the response factors noted, thus generating the initial simplex. The optimisation

then proceeds in an iterative manner, until further iterations produce vertices with no further significant improvement in response over the other vertices within the simplex. The centroid of the final simplex is taken as the optimum operating conditions. The conditions can be confirmed by univariate searches of each parameter in turn, while the others are held constant at their optimum values. The univariate searches are also useful in that they provide extra information about the effect of each parameter on the optimum.

In this study simplex optimisation was used merely as a tool, a more detailed discussion from a theoretical, as well as practical viewpoint, is contained elsewhere (88).

2.2 Experimental

2.2.1 Instrumentation

All experiments were performed using an integrated, computer controlled, inductively coupled plasma - atomic emission spectrometer (S35 Plasmakon, Kontron Spectroanalytik, Eching, West Germany), of the rapid sequential type. Details are given in Table 2.1. The injector tube used was of 1.8 mm internal diameter.

2.2.2 Temperature Controlled Spray Chamber

The temperature controlled spray chamber was of a Scott-type, double pass design, jacketed to allow circulation of the cooling fluid. Temperature control was achieved by means of an open propanol reservoir into which was

Table 2.1 Details of the inductively coupled plasma - atomic emission spectrometer used in this work

Nebuliser	PTFE, v-groove high solids nebuliser (Ebdon Nebuliser, P.S. Analytical, Sevenoaks, Kent, U.K.)
Spray chamber	Scott type, double pass, jacketed spray chamber
Torch assembly	Fused quartz, Greenfield type torch with a choice of injector tubes
Power supply	27.12 MHz crystal controlled, radio-frequency power supply, with an output of between 0 - 3.5 kW under normal conditions, and automatic tuning
Spectrometer	Czerny-Turner type sequential monochromator with a 2,400 grooves mm^{-1} grating capable of wavelength selection to within 0.0015 nm, under computer control.
Gas flows	All argon gas flows
	Carrier gas 0.2 - 3.0 1 min^{-1} Intermediate gas 0 - 10 1 min^{-1} Outer gas 0 - 35 1 min^{-1}
Plasma viewing height	Variable viewing height commonly between 0 - 60 mm above the load coil, under computer control

immersed a recirculation pump with a heating element (Tecam Tempunit, Techne Ltd., Cambridge, U.K.), to pump the coolant/heating fluid around the system. The reservoir and tubing was lagged to minimise temperature fluctuations. Cooling was achieved by the addition of a suitable amount of liquid nitrogen to the reservoir, and heating by means of the heating element. The temperature at the outside surface of the spray chamber was monitored by means of a contact Ni-Cr/Ni-Al thermocouple and electronic thermometer (model 2001, Comark Electronics Ltd., Rustington, West Sussex, U.K.).

A schematic diagram of the system described above is shown in Fig. 2.1. This arrangement was preferred because it allowed rapid cooling or heating of the recirculating fluid.

2.2.3 Parameters Optimised

The parameters which were optimised are listed in Table 2.2, with the possible ranges over which optimisation experiments could be conducted. In practice the ranges were carefully selected for each organic solvent in turn, taking into account the practical problems of maintaining a stable plasma, freezing point of the solvent and coupling of power.

2.2.4 Representative Spectral Lines

One representative line from each of the 'hard' and 'soft' line categories was chosen. They are listed in Table 2.3,

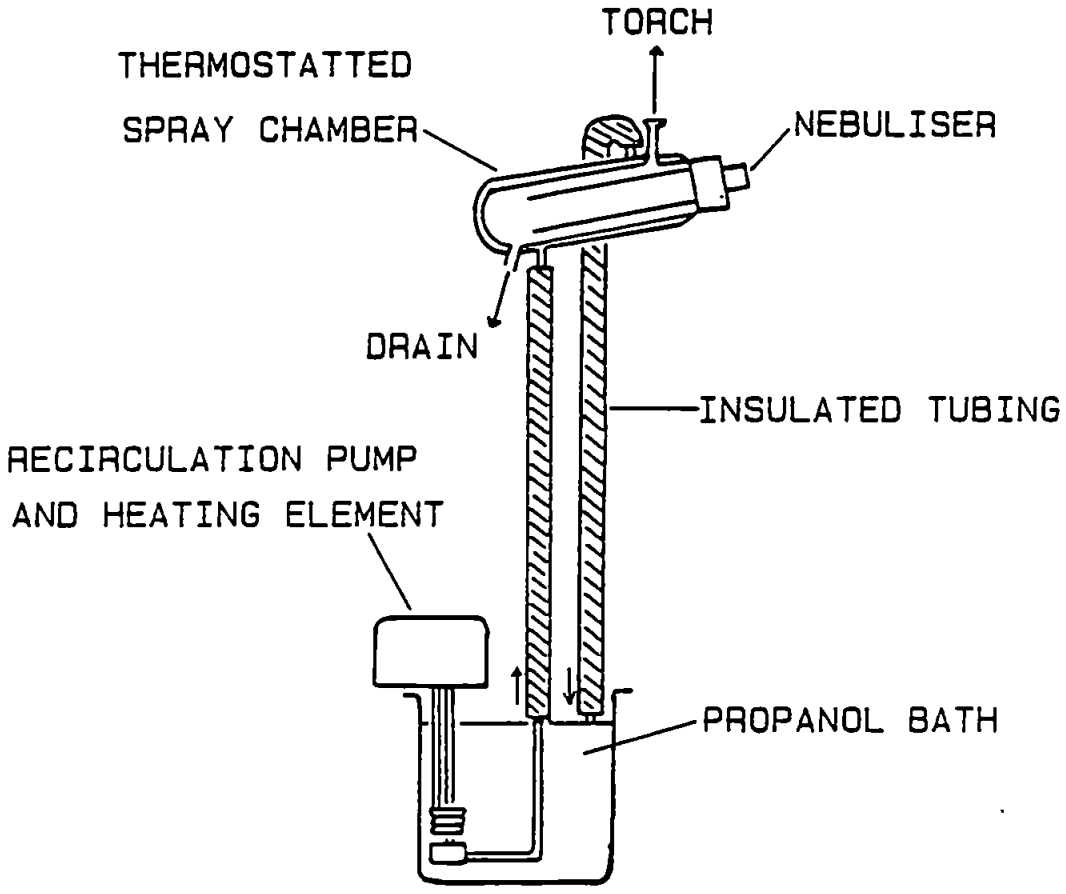

Figure 2.1 Schematic diagram of the spray chamber thermostatting system

Table 2.2 Boundary limits of parameters studied during the simplex optimisation

Parameter	Range
Carrier gas	0.4 - 3.0 l min^{-1}
Intermediate gas	0 - 3.0 l min^{-1}
Outer gas	15 - 35 l min^{-1}
Forward power	1.0 - 2.5 kW
Viewing height	0 - 60 mm
Spray chamber temperature	-25 - +55 ^{o}C

Table 2.3 Wavelength, excitation and ionisation energies of the spectral lines studied

Species	Wavelength/nm	Excitation energy/eV	Ionisation energy/eV		Sum/eV
			1	2	
Mn II	257.610	4.81	-	15.64	20.45
Cu I	324.754	3.82	7.72	-	11.54

together with the ionisation potentials of the species and excitation potentials as appropriate.

2.2.5 Reagents and Standards

The organic solvents used were of AnalaR, General Purpose or Laboratory Reagent grade (BDH Chemicals Ltd., Poole, Dorset, U.K.) since high purity was not a critical factor. Stock solutions of organometallic standards, 250 - 1000 μg ml^{-1} were made up from Spectrosol cyclohexylbutyrate salts of the metals (BDH Chemicals Ltd.) dissolved in xylene, for dilution in those solvents which were immiscible with water. Aqueous stock solutions of inorganic salts, 1000 μg ml^{-1} (Spectrosol, BDH Chemicals Ltd.) were used for dilution in solvents which were miscible with water. For optimisation studies, 10 μg ml^{-1} solutions from the appropriate Mn and Cu stock solutions, in the organic solvents were used.

For the excitation temperature measurements the thermometric species was Ti. A stock solution of Ti, 1000 μg ml^{-1} (BDH Chemicals Ltd.) in aqueous medium was used for dilution in those solvents miscible with water. A stock solution of Ti, 1500 μg ml^{-1} in chloroform was used for dilution in those solvents immiscible with water. This solution was made up using a solution of tetra-n-butyl titanate, (14.2% Ti) in xylene (Spectrosol, BDH Chemicals Ltd.).

2.2.6 Simplex Optimisation

Simplex optimisation experiments were performed using a software package developed previously (88) and run on a microcomputer (Apple IIe, Apple Computer Inc., Cupertino, California, USA). Net signal-to-background ratio (SBR) was taken as the criterion of merit, since it has been shown to be independent of the type of spectrometer used (84).

After each optimisation univariate searches were performed for each parameter in turn while holding the others at the optimum established by the simplex procedure.

2.2.7 Temperature Measurements

When the optimisation experiments were completed, measurements of rotational and excitation temperature were performed while operating the ICP using the various sets of optimum conditions, and introducing the corresponding organic solvents.

Rotational and excitation temperatures were calculated using the 'Boltzmann plot' method described by Mermet (4). Rotational temperature (T_{rot}) was calculated by measuring the emission intensity of the Q_1 branch of the OH (0-0) band and using equation 2.2.

$$\log (I\lambda/A) = -0.625/T_{rot} \cdot E \qquad (2.2)$$

where I = net emission intensity

λ = wavelength/nm

A = transition probability

E = energy/cm^{-1}

T = temperature/K

Log ($I\lambda/A$) was plotted against E and the slope of the line used to calculate T_{rot}.

Line assignments, wavelengths, transition probabilities and energies taken from reference 4 and used in this work are given in Table 2.4.

Excitation temperature (T_{exc}) was calculated by measuring the emission intensity of ionized Ti lines and using equation 2.3

$$\log (I\lambda^3/gf) = -0.625/T_{exc} \cdot E \qquad (2.3)$$

where g = the statistical weight of the excited energy level

f = oscillator strength.

Log ($I\lambda^3/gf$) was plotted against E and the slope of the line used to calculate T_{exc}.

Wavelengths, statistical weights, energies and log gf values taken from reference 4 and used in this work are given in Table 2.5.

Table 2.4 Assignment (k), wavelengths (λ), energies (E) and transition probabilities (A) for the Q_1 branch of the OH (0 - 0) band

k	λ(nm)	E(cm^{-1})	A(10^8 s^{-1})
1	307.844	32,475	0.0
2	307.995	32,543	17.0
4	308.328	32,779	33.7
5	308.520	32,948	42.2
6	308.734	33,150	50.6
8	309.239	33,652	67.5
9	309.534	33,952	75.8

Table 2.5 Wavelengths (λ), statistical weights (g), energies (E) and log gf values for Ti

λ(nm)	gi	gk	E(cm^{-1})	log gf*
321.827	10	8	43,741	-0.06
322.284	6	8	31,114	-0.49
322.424	12	10	43,781	0.04
322.860	4	2	39,675	-0.20
323.228	8	6	39,927	-0.25
323.452	10	10	31,301	0.31
323.657	8	8	31,114	0.16
323.904	6	6	30,959	-0.02
323.966	6	4	39,603	-0.24

* Originally taken from reference 89

2.3 Results and Discussion

Table 2.6 shows the optimum conditions established in this study. Univariate searches at the established optimum conditions for signal-to-background ratio net signal and background signal are shown in Figures 2.2 - 2.15 for the organic solvents and spectral lines studied. The vertical arrows indicate the optima determined by the simplex procedure. The Mn II 257.610 nm and Cu I 324.754 nm lines are referred to as the hard and soft lines respectively in the following discussion.

2.3.1 Effects of Different Parameters

2.3.1.1 Carrier Gas

It is evident from Fig. 2.2 that carrier gas flow was a critical parameter with regard to maximum SBR. More so for the complex organic solvents than for water, or a simple organic molecule like methanol. Cyclohexane produced a particularly sharp optimum at the hard line, demonstrating that care is necessary when determining compromise operating conditions for different solvents and lines of different hardness. In every case the carrier gas flow was lower for the hard compared to the soft line, demonstrating the effect of the solvent on plasma excitation conditions. Increasing carrier gas flow may have three effects, namely decreased residence time, increased plasma cooling and an influence on analyte delivery to the plasma, which is determined by the optimum nebuliser gas flow for a particular solvent. In the case of the hard line plasma cooling appears to be more

Table 2.6 Optimum conditions established for the solvents studied, and the hard and soft lines

	Optimum Conditions											
	Water		Cyclohexane		Methanol		Hexane		Chloroform		Acetone	
	CuI	MnII	CuI	MnII	CuI	MnII	CuI	MnII	CuI	MnII	CuI	MnII
Carrier gas/l min^{-1}	1.84	1.24	1.10	0.85	1.57	1.23	1.66	1.01	-	0.95	1.32	0.94
Intermediate gas/ l min^{-1}*	0.5	0.5	1.8	1.8	0.7	0.8	1.6	1.6	-	1.6	1.6	1.6
Outer gas/l min^{-1}*	23	23	23	23	25	29	22	22	-	22	22	22
Forward power/kW	2.11	1.58	1.31	1.17	1.34	1.32	1.71	1.79	-	1.55	1.60	1.51
Viewing height/mm	41	18	32	12	18	12	51	20	-	16	32	18
Spray chamber temperature/°C	+24	+27	-5	-7	-6	-12	-23	-11	-	-10	-20	-4
Sample introduction rate/ml min^{-1}	0.65	0.65	0.10	0.10	0.70	0.70	0.15	0.15	-	0.25	0.25	0.25

* for hexane, chloroform and acetone the intermediate gas was maintained at a constant 1.6 l min^{-1} and the outer gas at 22 l min^{-1} as these had marginal influence on the optimum

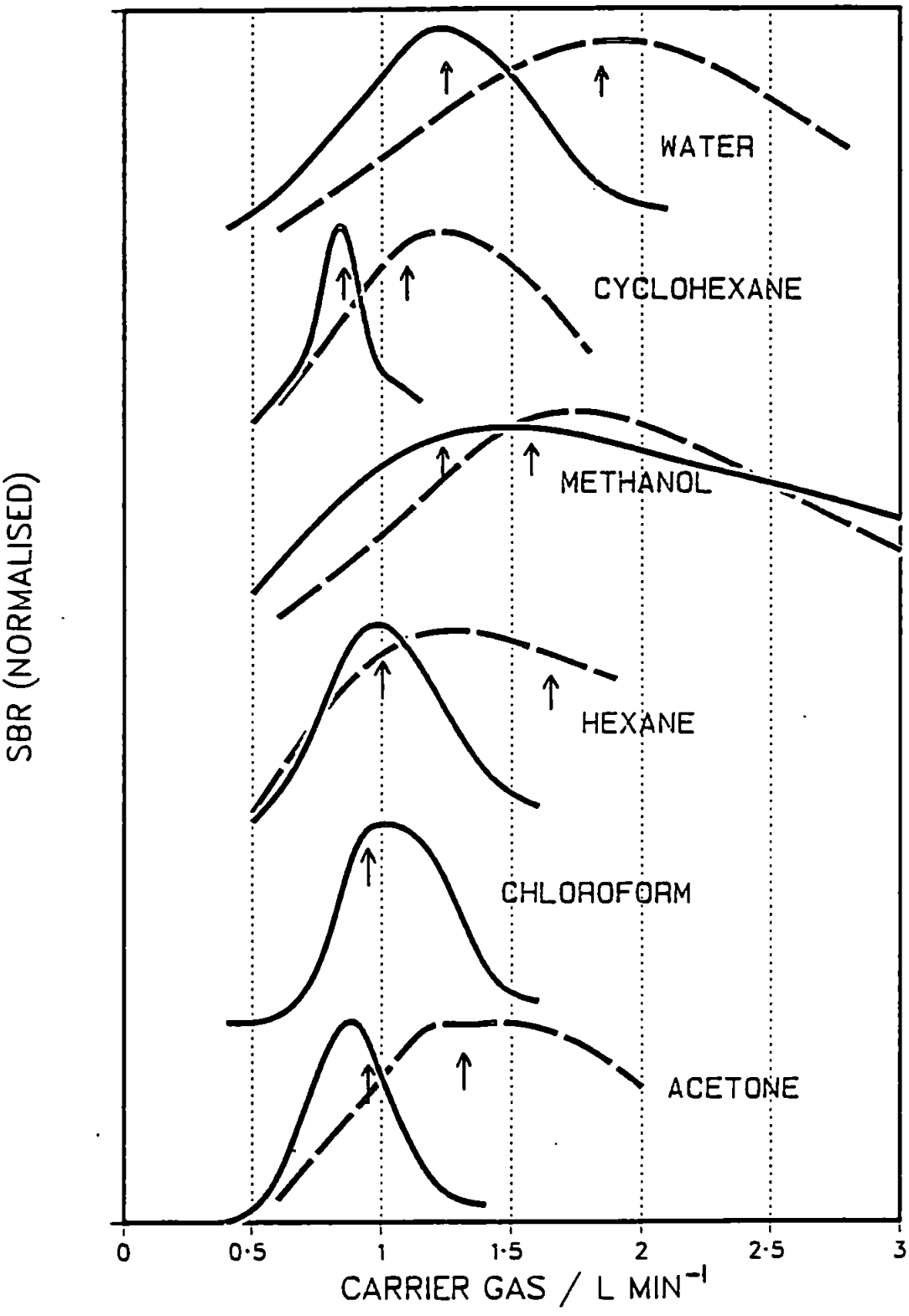

Figure 2.2 Carrier gas flow vs signal to background ratio for the various solvents and the spectral lines:
_____ Mn II 257.610 nm; ------ Cu I 324.754 nm

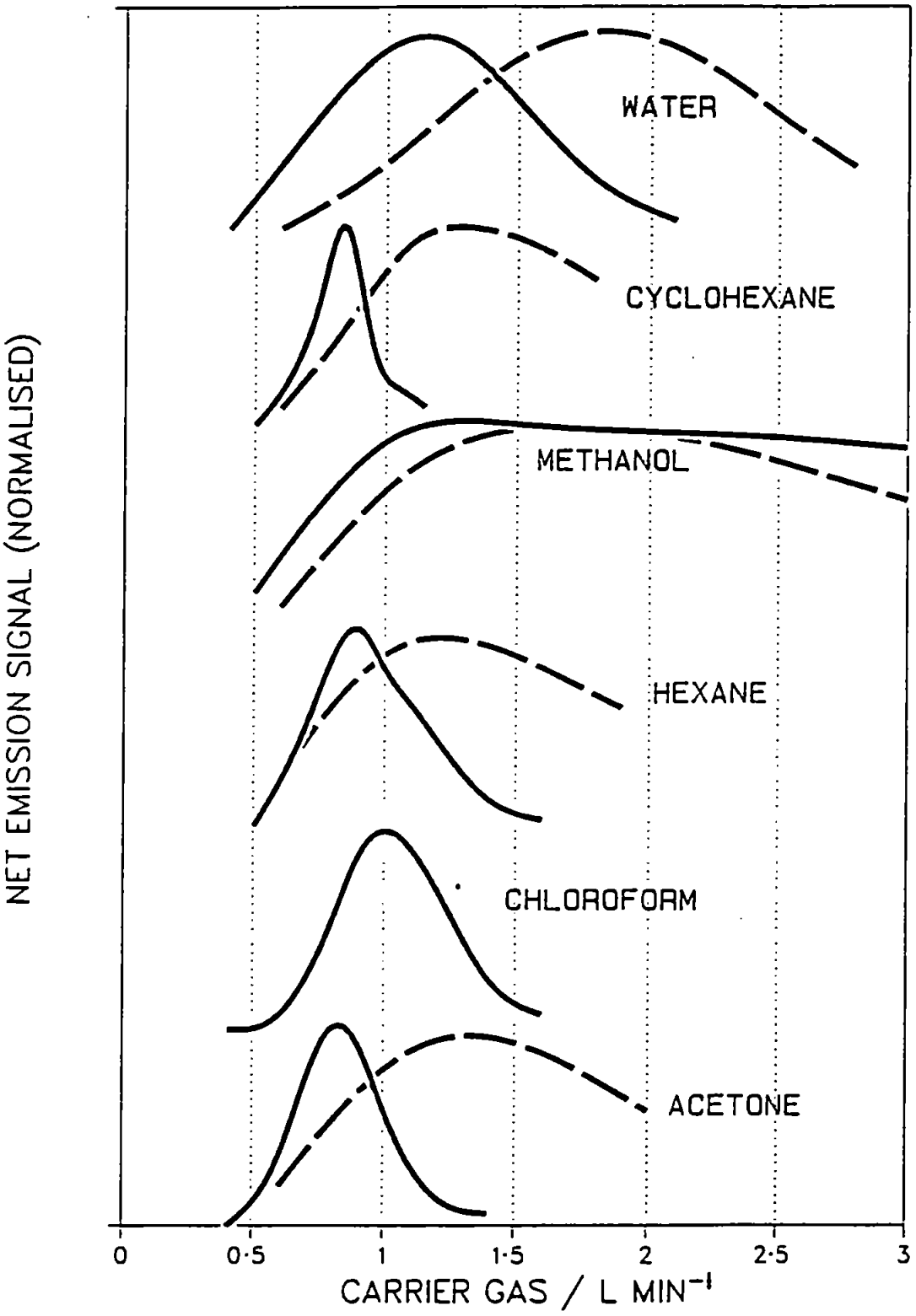

Figure 2.3 Carrier gas flow vs net signal for the various solvents and the spectral lines:
_____ Mn II 257.610 nm; ------ Cu I 324.754 nm

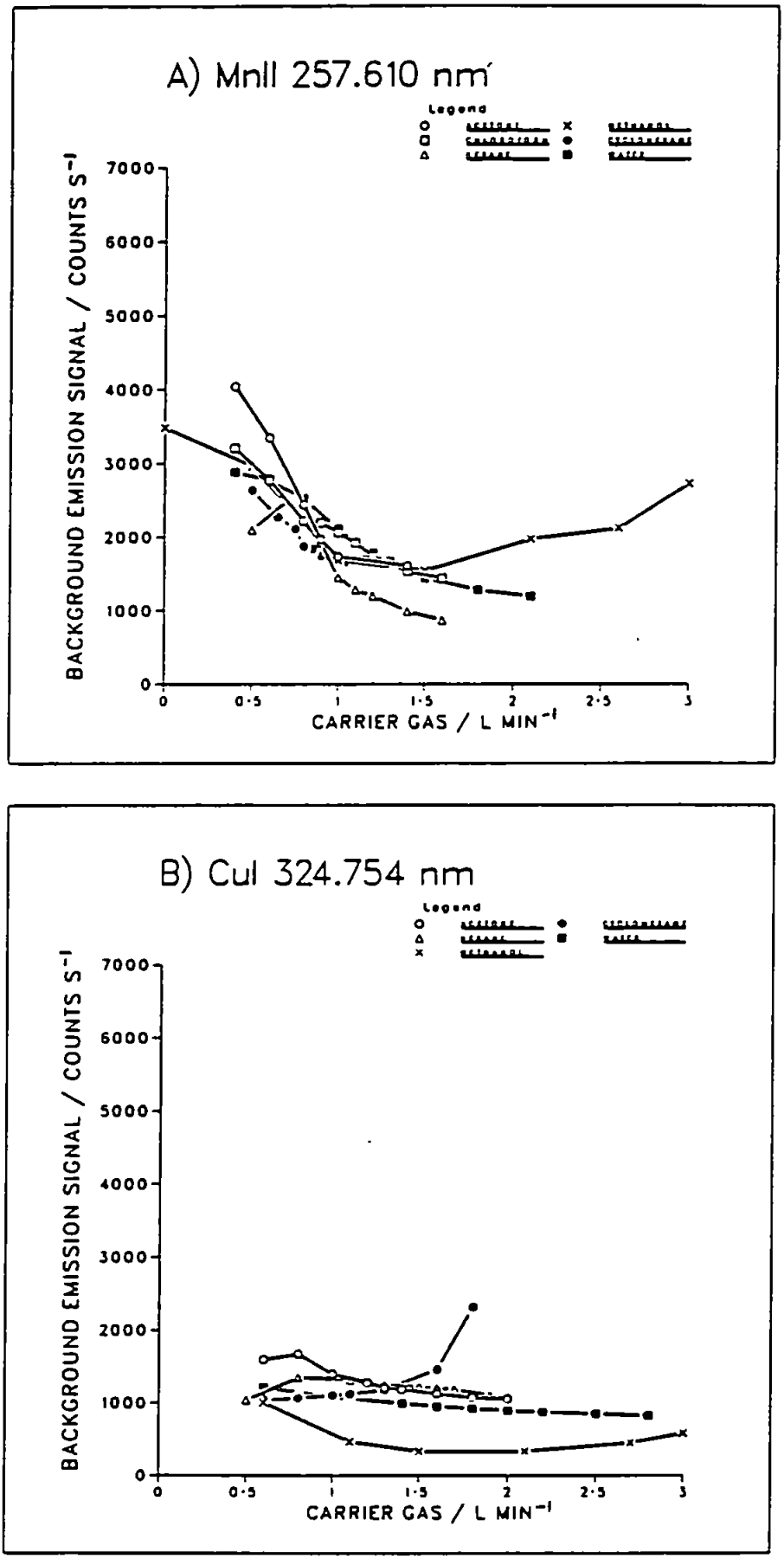

Figure 2.4 Carrier gas flow vs background signal at the spectral lines studied using the solvents: acetone (O); chloroform (□); hexane (Δ); methanol (X); cyclohexane (●); and water (■)

critical, since a higher temperature is necessary to ionise and excite the species in comparison to the soft line. Similarly, the more volatile organic solvents generally led to lower optimal carrier gas flows than for water, though the extent to which nebulisation efficiency influences these optima is unclear.

Variations in net signal with carrier gas flow (Fig. 2.3) mirror almost exactly the trends in SBR (Fig. 2.2) for the lines and solvents studied, suggesting that the optimisation was influenced primarily by net signal rather than variations in continuum background. This is borne out by reference to the corresponding plots of background signal against carrier gas flow (Fig. 2.4). For both hard (Fig. 2.4A) and soft (Fig. 2.4B) lines background signal shows a gradual degradation, more pronounced for the former, which is probably due to a reduction in continuum intensity caused by plasma cooling. The exception is that of cyclohexane at the hard line, the background signal showing a marked increase at higher carrier gas flows (Fig. 2.4B). This may be due to destabilisation of the plasma, or molecular emission not seen under normal operating conditions.

2.3.1.2 Forward Power

The optimum conditions determined for power (Table 2.6) initially appear to contradict the findings of other workers, namely that the organic ICP requires more power than the aqueous ICP, and that hard lines require more

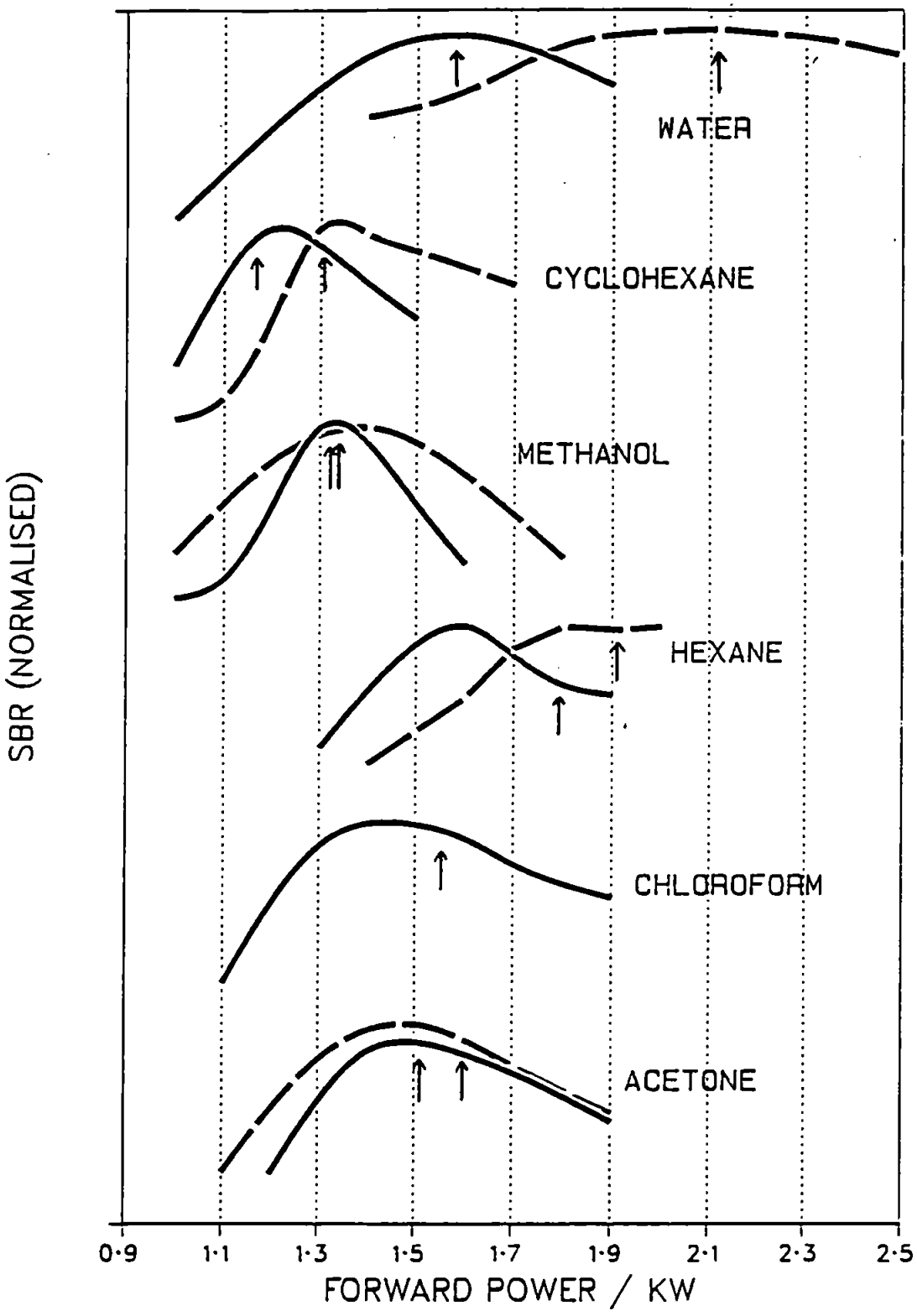

Figure 2.5 Forward power vs signal to background ratio for the various solvents and the spectral lines:
_____ Mn II 257.610 nm; ------ Cu I 324.754 nm

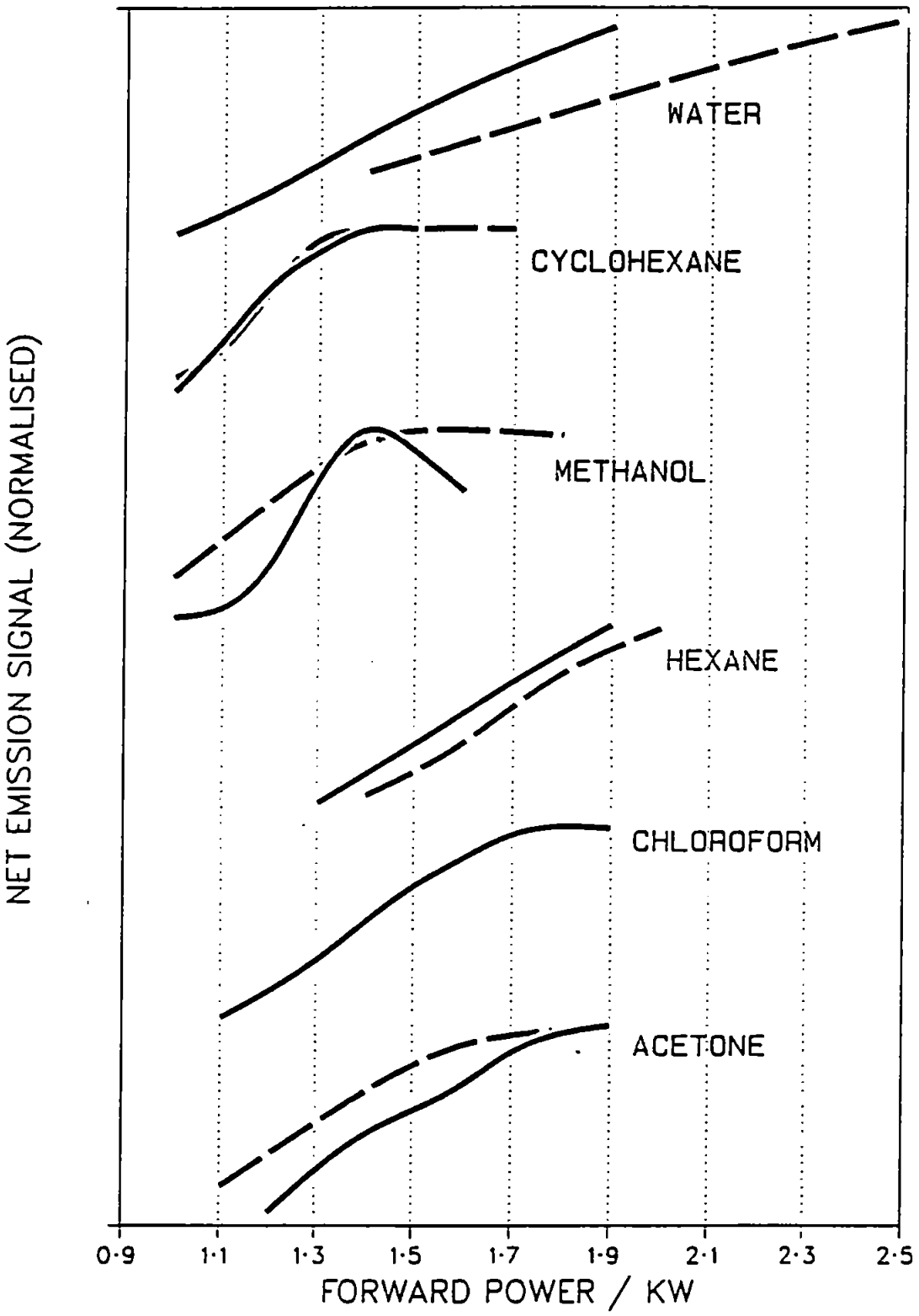

Figure 2.6 Forward power vs net signal for the various solvents and the spectral lines:
_____ Mn II 257.610 nm; ------ Cu I 324.754 nm

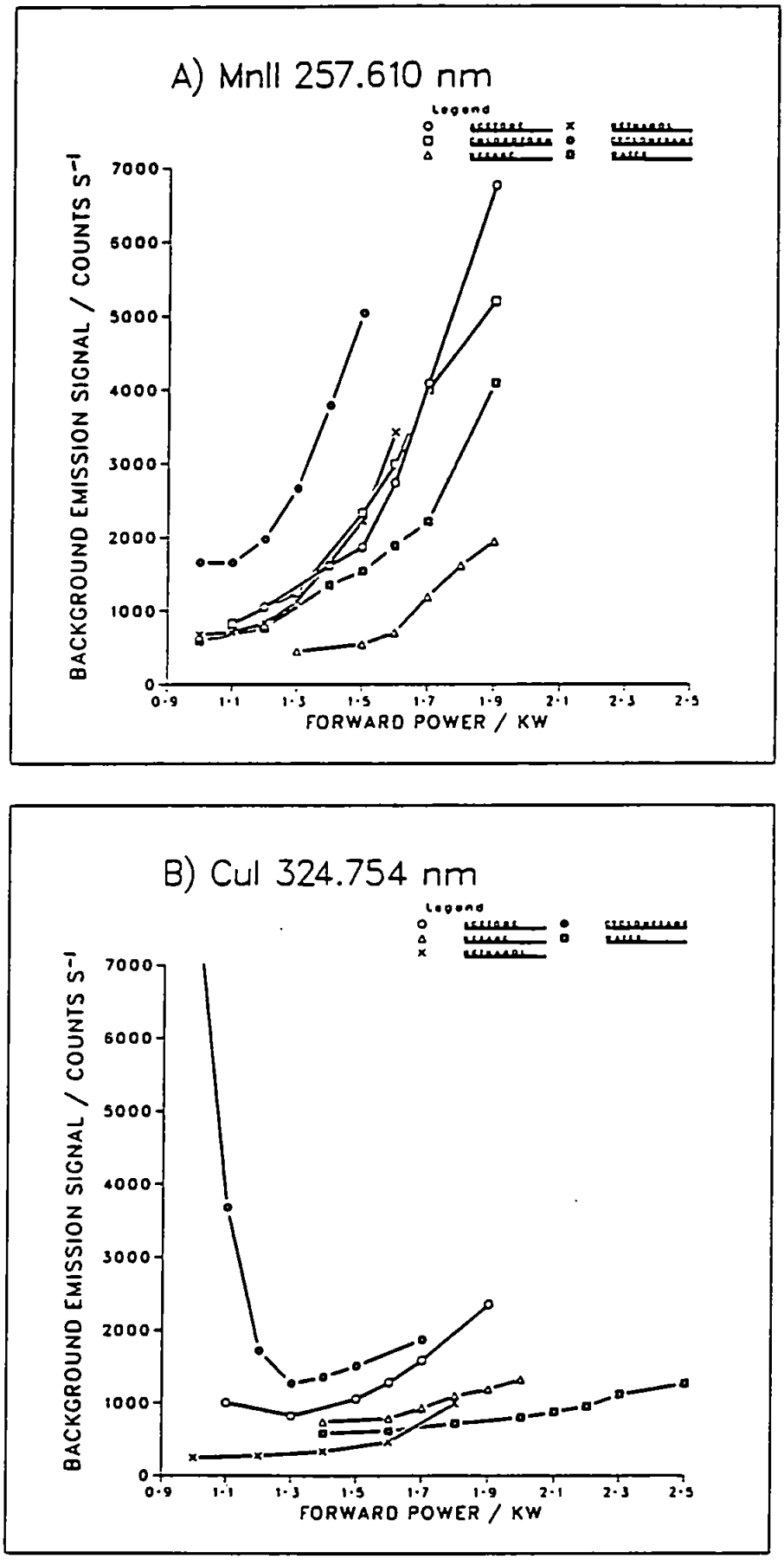

Figure 2.7 Forward power vs background signal at the spectral lines studied using the solvents: acetone (O); chloroform (□); hexane (Δ); methanol (X); cyclohexane (O); and water (□)

power than soft lines. Fig. 2.5 indicates that this is not necessarily the case when other parameters are included in the optimisation.

The organic solvents actually yielded optima at lower power for maximum SBR compared to water. This may be due to the combined effects of lower carrier gas flow and spray chamber cooling, resulting in a much reduced solvent load in the plasma, though the plasma exhibited a surprisingly high tolerance to the solvent chloroform which has a relatively high vapour pressure.

Significantly in this work, without exception, lower power was optimal for the hard line compared to the soft line. However, it must be remembered that the other operating parameters, in particular carrier gas flow and spray chamber temperature, were at different optimal values.. This demonstrates the facility of simplex optimisation to find the true optimum, especially in the case of organic solvents.

The variation of net signal with power (Fig. 2.6) indicates that in all but one case, i.e. methanol at the hard line, maximum signal was obtained at the maximum power studied. This means that maximum SBR was limited by the background signal. This is demonstrated clearly in Fig. 2.7. For the hard line the lowest background signal was obtained at low power for all solvents (Fig. 2.7A). Optimum powers for these solvents at the hard line

(Fig. 2.5) correspond to just above the mid-points in the curves in Fig. 2.7A for all solvents. The same is true for the soft line. Background signal is lowest at low power for water, hexane and methanol, and shows a minimum for cyclohexane and acetone (Fig. 2.7B). As in the previous case optimum powers were determined by the influence of background signal.

2.3.1.3 Spray Chamber Temperature

The spray chamber temperature proved to be more critical for some solvents than others. This is illustrated in Fig. 2.8. For water, both hard and soft lines were relatively insensitive to spray chamber temperature in the range investigated. The steady increase in SBR could well be due to a shift to a smaller droplet size distribution caused by evaporation in the spray chamber, and hence improved analyte transport. Surprisingly, considering the relatively high vapour pressure of chloroform, spray chamber temperature had little effect on SBR, though this solvent has been shown to be anomalous by other workers (28).

The greatest dependence on spray chamber temperature was seen in the case of cyclohexane. In practice the optimum temperature could not be reached because it was well below the freezing point of the solvent, resulting in a build up of frozen solvent in the spray chamber with consequent effects on analyte transport.

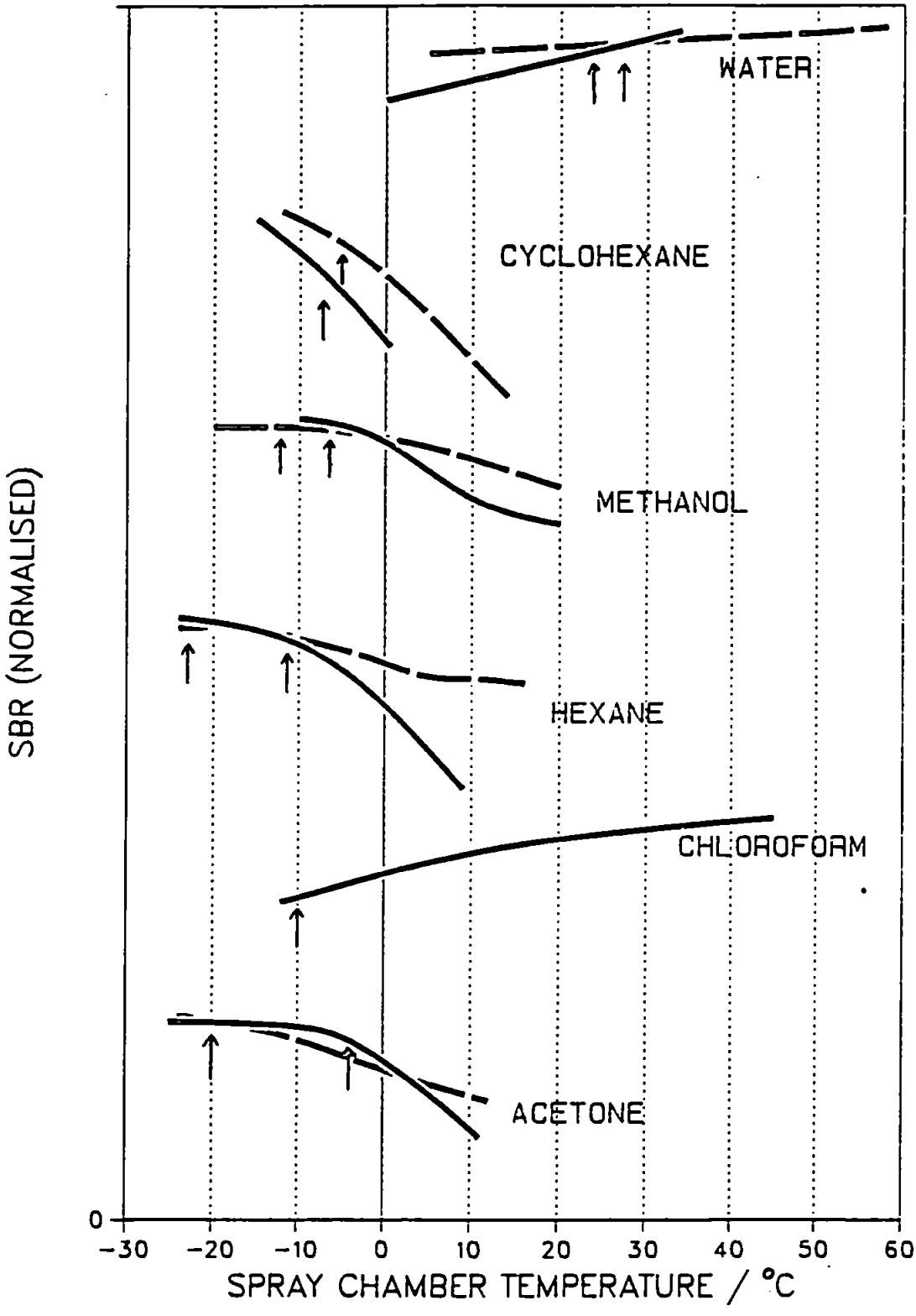

Figure 2.8 Spray chamber temperature vs signal to background ratio for the various solvents and the spectral lines: _____ Mn II 257.610 nm; ------ Cu I 324.754 nm

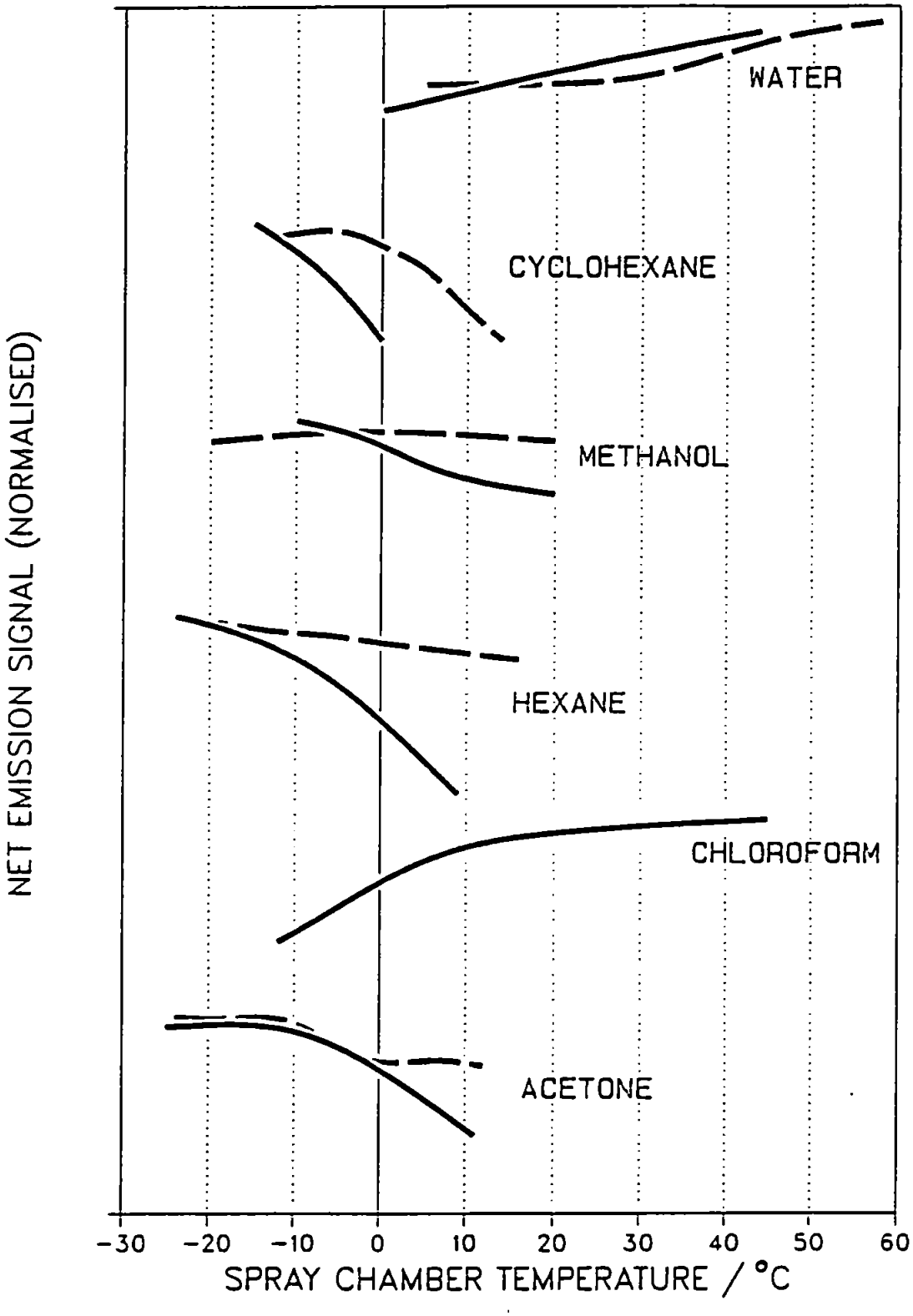

Figure 2.9 Spray chamber temperature vs net signal for the various solvents and the spectral lines:
_____ Mn II 257.610 nm; ------ Cu I 324.754 nm

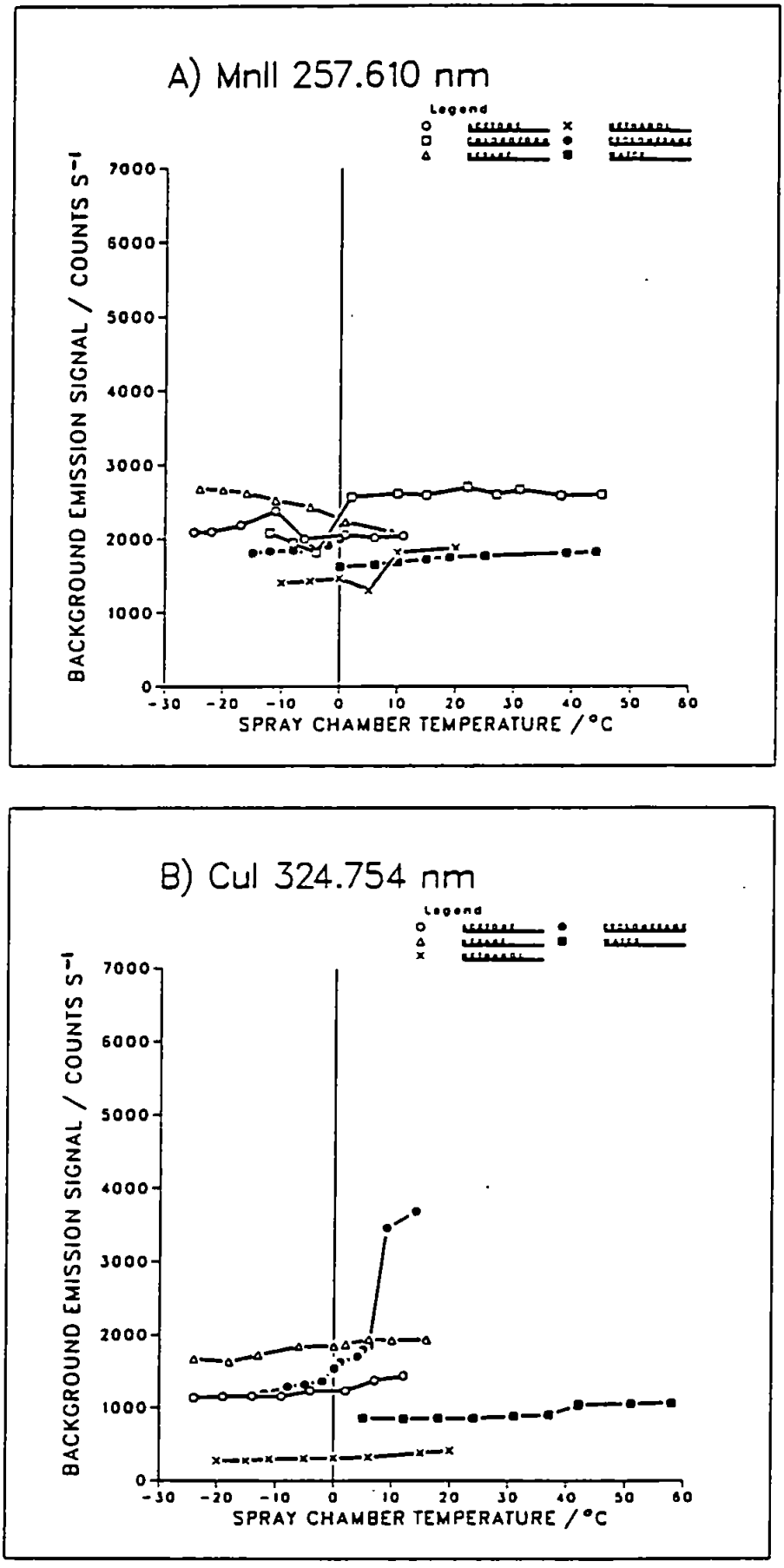

Figure 2.10 Spray chamber temperature vs background signal at the spectral lines studied using the solvents: acetone (O); chloroform (□); hexane (Δ); methanol (X); cyclohexane (●); and water (■)

The organic solvents required a temperature of about -10°C in general at both hard and soft lines. The vapour pressures of the solvents at 20°C and at optimum spray chamber temperatures are shown in Table 2.7. It is evident that for most solvents the requirement is to reduce the vapour pressure to the order of 10 - 30 torr or so.

Figures 2.9 and 2.10 indicate that the optimum spray chamber temperature was influenced primarily by the net signal, since the trends of net signal against spray chamber temperature (Fig. 2.9) closely resemble those in Fig. 2.8. Spray chamber temperature had no great influence on background signal for all solvents at the hard line (Fig. 2.10A) and only for cyclohexane at the soft line (Fig. 2.10B). As in the case for carrier gas flow this may be due to plasma instability at high cyclohexane loadings.

2.3.1.4 Viewing Height

As would be expected, for all solvents the optimum viewing height for the hard line was lower than that for the soft line (Fig. 2.11). Differences between solvents were probably due to a combination of carrier gas flow, intermediate gas flow, background signal and power which are difficult to separate. For instance, the relatively high power and carrier gas flow associated with the soft line for water is probably the cause of the high viewing height shown as optimal in Fig. 2.11. Such unexpected

Table 2.7 Vapour pressures (VP) of the solvents studied at 20°C (VP_{20}) and at optimised spray chamber temperature (VP_{opt})

Solvent	VP_{20}/torr	VP_{opt}/torr	
		Mn II	Cu I
Water	17.5	27	22
Cyclohexane	77.5	19	20
Methanol	95.6	13	20
Hexane	121	24	11
Chloroform	159	35	58
Acetone	182	64	22

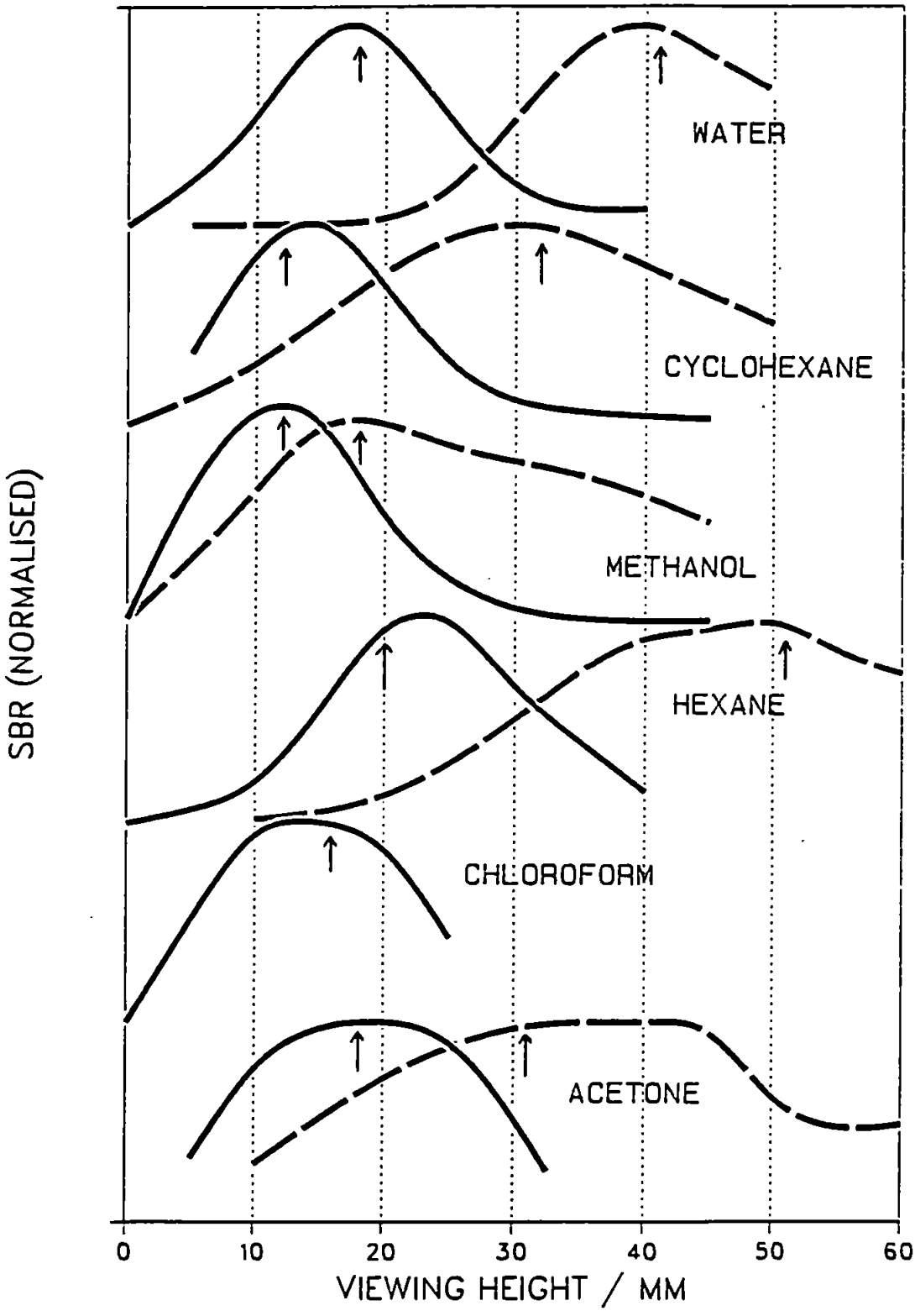

Figure 2.11 Viewing height vs signal to background ratio for the various solvents and the spectral lines:
_____ Mn II 257.610 nm; ------ Cu I 324.754 nm

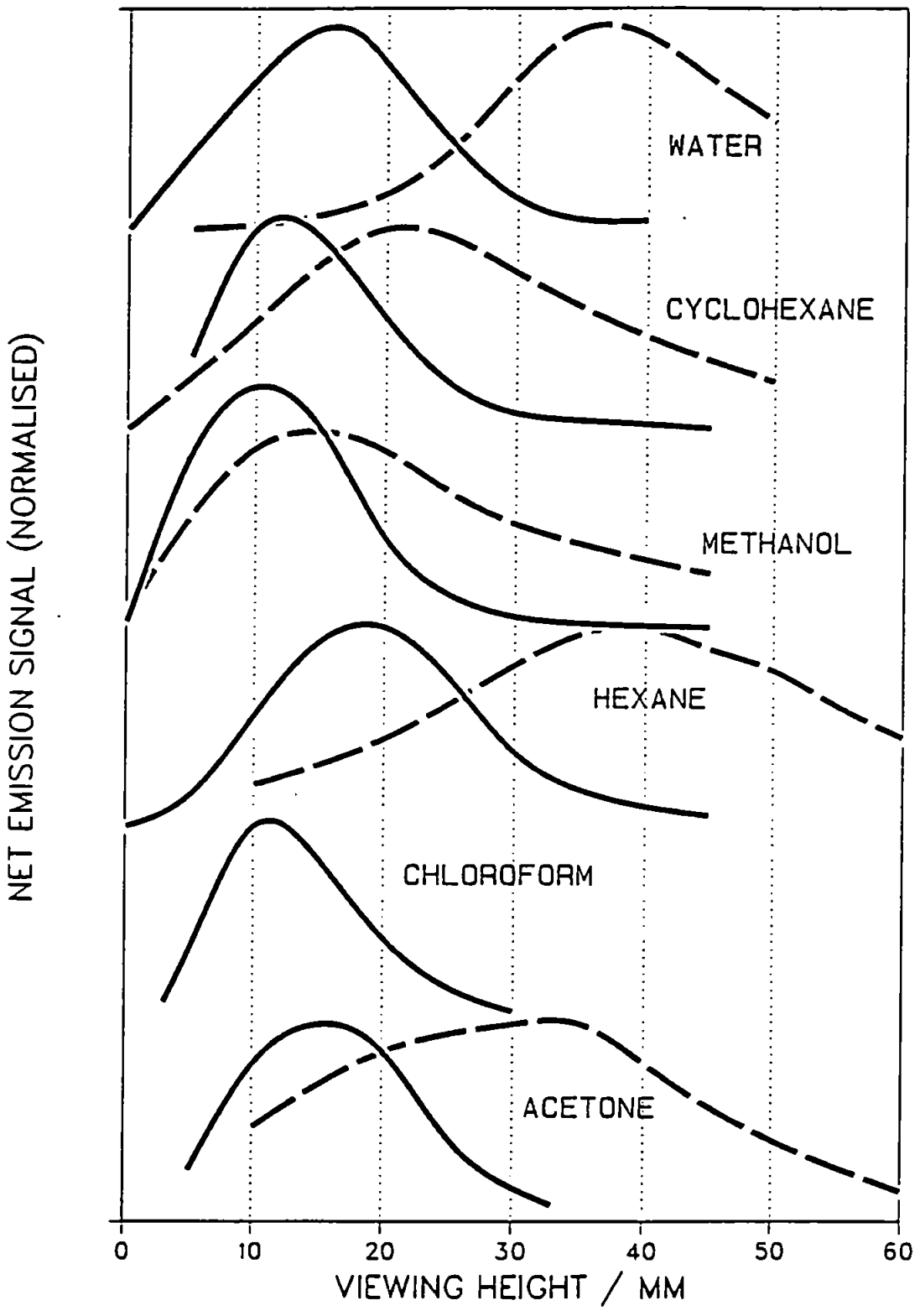

Figure 2.12 Viewing height vs net signal for the various solvents and the spectral lines:
_____ Mn II 257.610 nm; ------ Cu I 324.754 nm

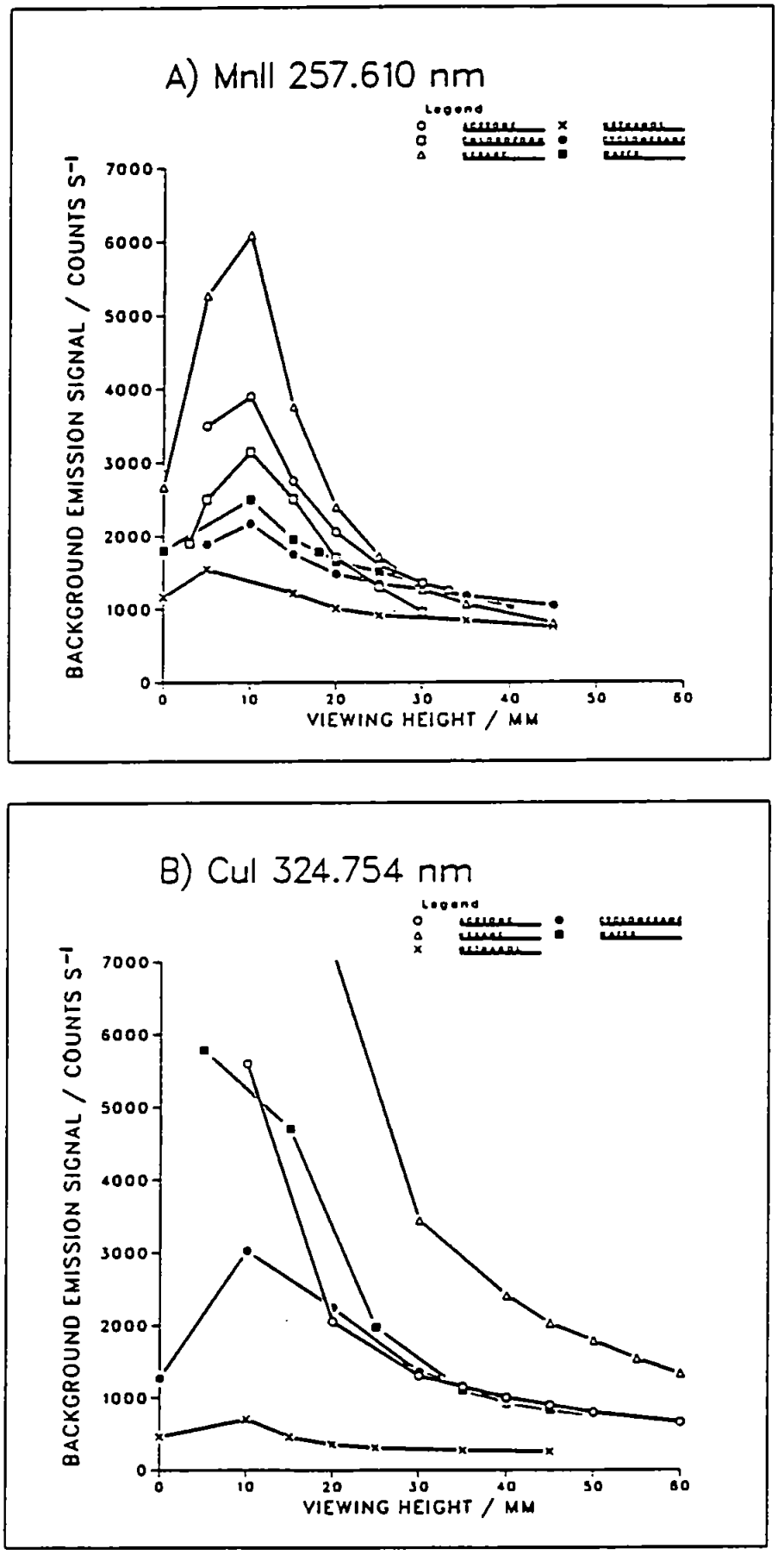

Figure 2.13 Viewing height vs background signal at the spectral lines studied using the solvents: acetone (O); chloroform (□); hexane (Δ); methanol (X); cyclohexane (●); and water (■)

conclusions illustrate the utility of simplex optimisation studies when parameters are strongly interrelated.

The trends of net signal against viewing height (Fig. 2.12) are similar to those of SBR (Fig. 2.11), though they show maxima at slightly lower viewing heights for all solvents and both lines. This can be explained by the behaviour of the background signal, which decreased as viewing height increased above 10 mm for all solvents and at both hard (Fig. 2.13A) and soft (Fig. 2.13B) lines. The result of this was a shift in maximum SBR to a slightly higher viewing height, in all cases, in comparison to maximum net signal.

2.3.1.5 Intermediate and Outer Gas

Intermediate and outer gas flows had less critical effect on SBR (Figs. 2.14 and 2.15). The main effect of the intermediate gas is to alter the position of the plasma in the torch, and hence the viewing height. However, it is desirable to use a relatively high intermediate gas flow when introducing organic solvents to prevent carbon deposition on the injector and intermediate torch tube. Likewise, a high outer gas flow helps to prevent carbon deposition and maintains a more stable plasma. Consequently, these two parameters were included in the optimisation only for the solvents water, methanol and cyclohexane. For the remaining solvents compromise conditions of 1.6 l min^{-1} and 22 l min^{-1} for intermediate and outer gas flows respectively were chosen for the

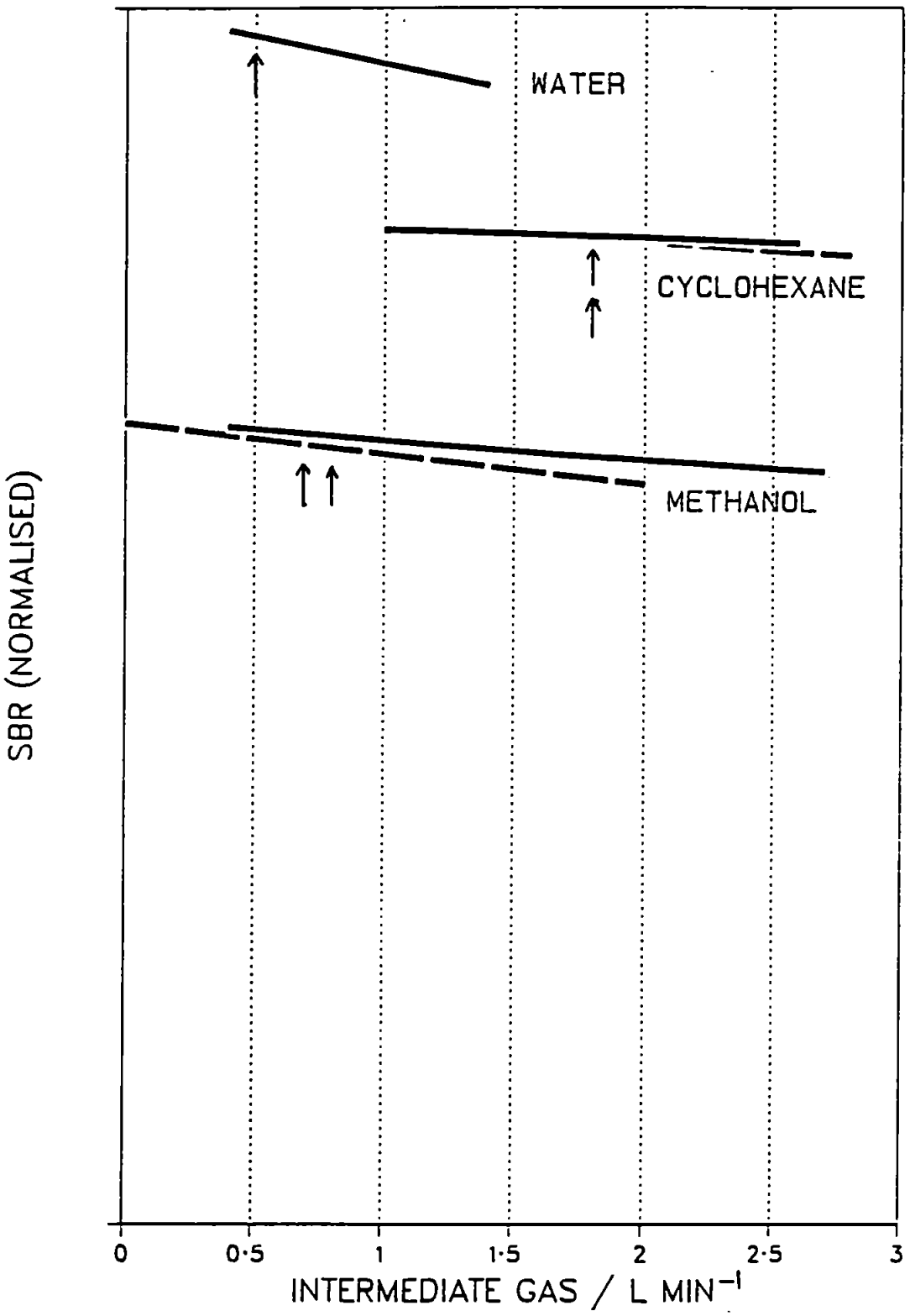

Figure 2.14 Intermediate gas vs signal to background ratio for the various solvents and the spectral lines:
_____ Mn II 257.610 nm; ------ Cu I 324.754 nm

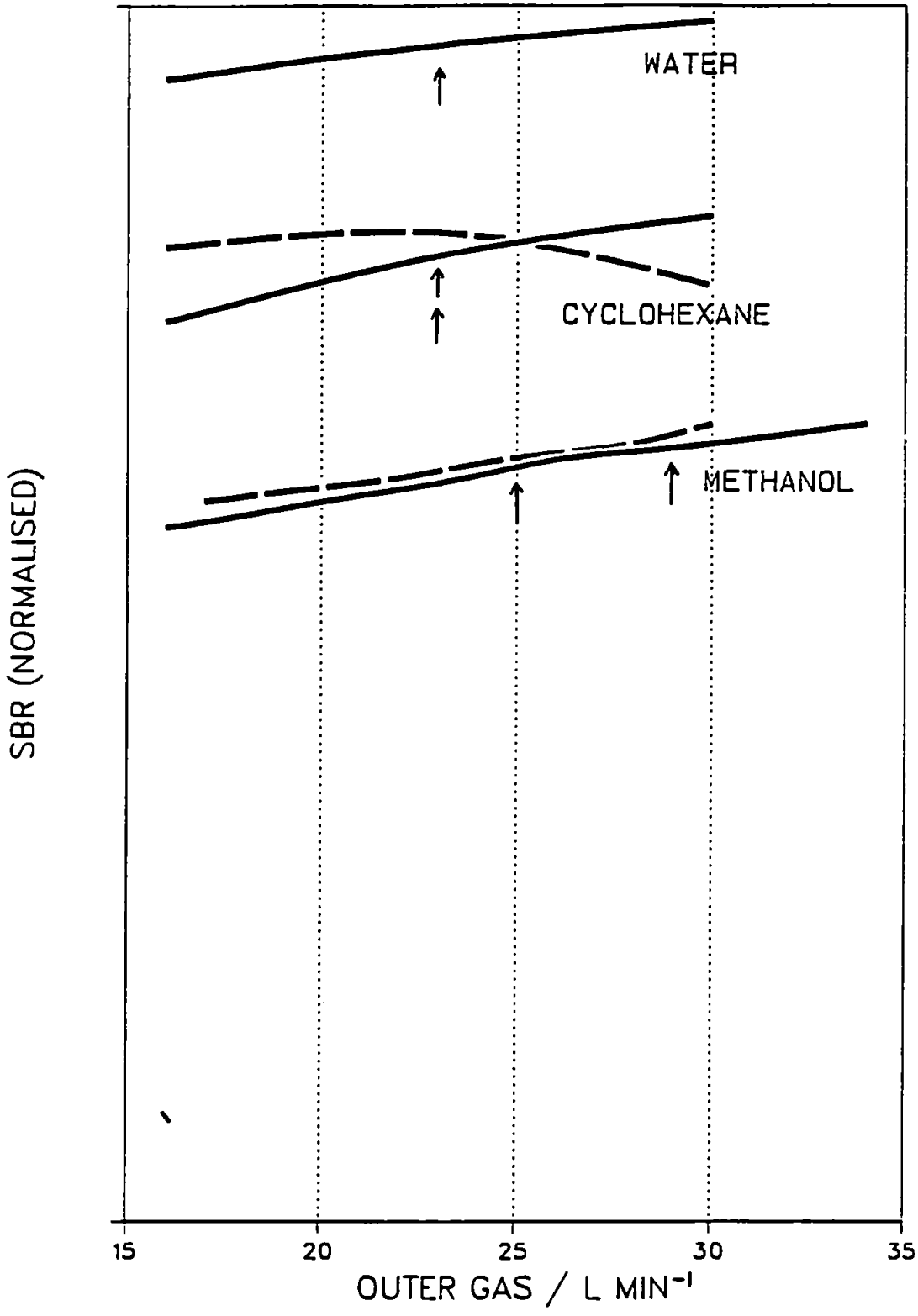

Figure 2.15 Outer gas vs signal to background ratio for the various solvents and the spectral lines:
_____ Mn II 257.610 nm; ------ Cu I 324.754 nm

reasons stated above.

2.3.2 Detection Limits

Detection limits were calculated (Table 2.8) at the spectral lines studied and for the various solvents using equation 2.4.

$$C_L = Z(RSD)_B \frac{(Co)}{(SBR)} \qquad (2.4)$$

where C_L = detection limit/$\mu g\ ml^{-1}$

Z = 3, i.e the number of standard deviations

$(RSD)_B$ = the relative standard deviation of the background expressed as a fraction

Co = analyte concentration/$\mu g\ ml^{-1}$

SBR = signal to background ratio associated with concentration Co.

This was not meant to be a rigorous determination of detection limits, but rather a simple comparison, hence the detection limits should be regarded only in relation to one another and not in isolation.

It is evident that in every case the organic solvent yielded a lower detection limit than water. This was thought to be due to enhanced analyte transport into the plasma caused by the formation of smaller droplets in the case of the organic solvents. However, effects on the excitation conditions in the plasma cannot be excluded.

Table 2.8 Detection limits in the various solvents at the spectral lines studied

Solvent	Detection limit/μg ml^{-1}	
	Mn II	Cu I
Water	0.021	0.046
Cyclohexane	0.012	0.012
Methanol	0.003	0.017
Hexane	0.003	0.006
Chloroform	0.014	not determined
Acetone	0.002	0.005

2.3.3 Temperature Measurements

2.3.3.1 Rotational Temperature

Rotational temperatures (T_{rot}) calculated using the method described in Section 2.2.7, using optimum operating conditions for the spectral lines and solvents studied are shown in Table 2.9. An Abel inversion was not performed so the values represent T_{rot} for a large cross section of the plasma.

There appear to be no significant differences between T_{rot} values for different solvents, except the low value associated with cyclohexane at the hard line. This is probably because these measurements were integrated across the whole plasma rather than indicatve of T_{rot} in the central channel. However, for the hard line, a plot of T_{rot} against forward power corresponding to the various solvents reveals a trend (Fig. 2.16A). As forward power increases so does T_{rot}. This is probably not as surprising as it first seems, since T_{rot} is closely related to the gas temperature in the plasma, which one would expect to increase with forward power, especially at the low viewing heights found to be optimum at the hard line, i.e. in close proximity to the plasma fireball.

At the soft line there appears to be no relationship between T_{rot} and forward power (Fig. 2.16B), the temperature remaining relatively the same at all powers associated with the various solvents. This can be explained by the fact that the optimum viewing heights

Table 2.9 Rotational temperature (T_{rot}) calculated while using optimum operating conditions for the solvents and spectral lines studied

Solvent	T_{rot}/k	
	Mn II	Cu I
Water	2770	2800
Cyclohexane	1130	2850
Methanol	2100	2620
Hexane	2863	2750
Chloroform	2440	not determined
Acetone	2400	3170

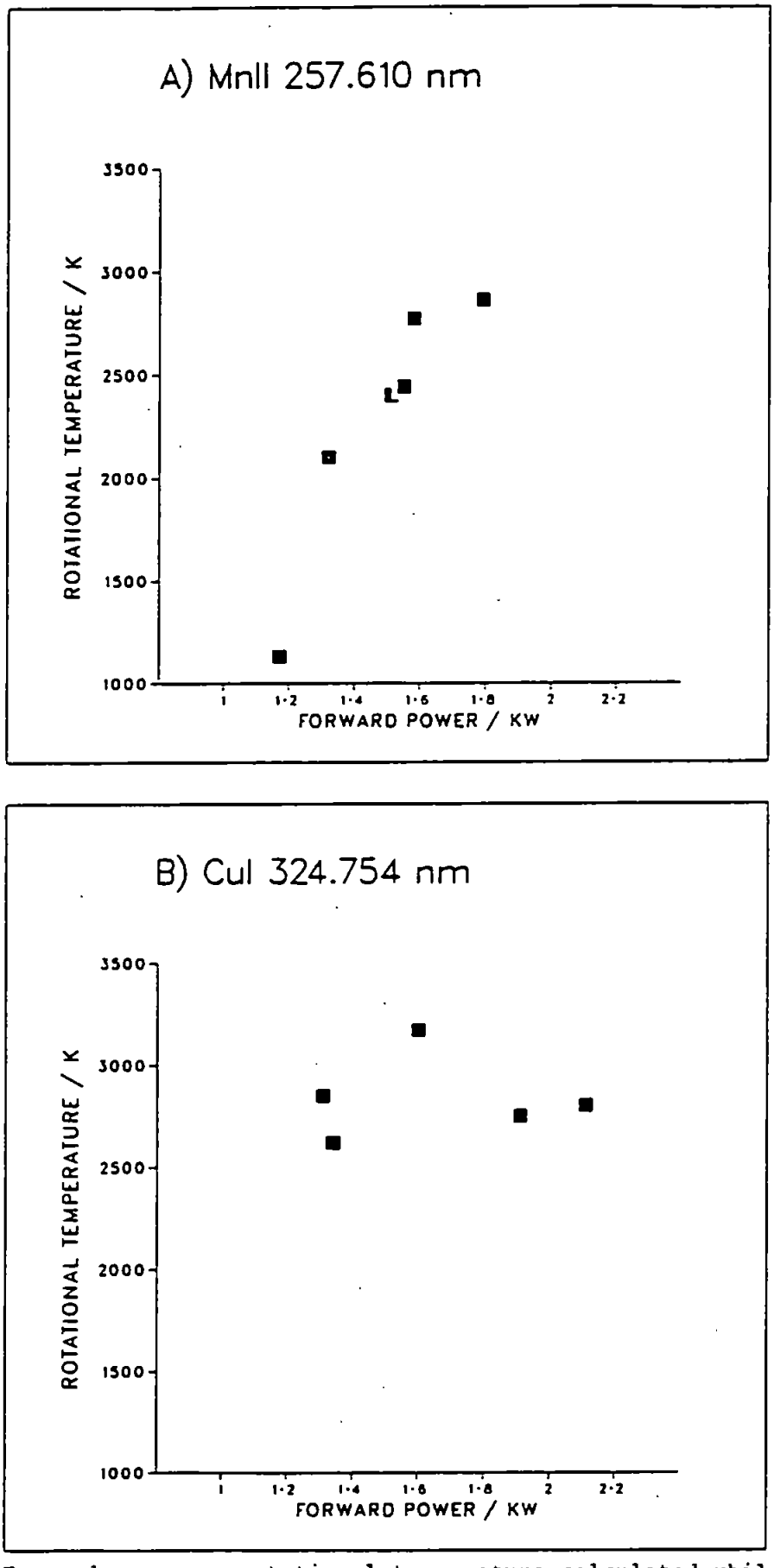

Figure 2.16 Forward power vs rotational temperature calculated while introducing the various solvents at optimum operating conditions for the spectral lines:
A) Mn II 257.610 nm; B) Cu I 324.754 nm

associated with the soft line were rather higher in the plasma, where it is more diffuse, and where changes in forward power would have less effect.

In summary, the organic solvents do not appear to influence T_{rot} to any great extent, given that the plasma has been optimised for each. At the low viewing heights and carrier gas flows associated with the hard line T_{rot} appears to be a function of the forward power, but this relationship disappears at the higher viewing heights and carrier gas flows associated with the soft line. The identification of any other trends is made difficult by the fact that operating conditions varied considerably between solvents, and no Abel inversion was carried out.

2.3.3.2 Excitation Temperature

Excitation temperatures (T_{exc}) calculated using the method described in Section 2.2.7, while using optimum operating conditions for the spectral lines and solvents studied, are shown in Table 2.10. T_{exc} was calculated only for four of the solvents because the organometallic titanium salt used as the thermometric species had a tendency to precipitate rapidly in the two remaining solvents, i.e. hexane and cyclohexane.

It is evident from Table 2.10 that T_{exc} showed a significant increase in the presence of chloroform and acetone compared to water, using optimum operating conditions for both spectral lines. Other workers (29,

Table 2.10 Excitation temperature (T_{exc}) calculated while using optimum operating conditions for the solvents and spectral lines studied

Solvent	T_{exc}/k	
	Mn II	Cu I
Water	6250	5690
Methanol	5680	5220
Chloroform	7350	not determined
Acetone	7130	6140

35) observed a decrease in T_{exc} on the introduction of organic solvents compared to water, however, these workers used identical operating conditions for all solvents. It has been shown (29) that T_{exc} is a function of power, provided other operating conditions are constant. From the point of view of this work it is probable that carrier gas flow and spray chamber temperature, with their consequent effects on solvent vapour load in the plasma, also exerted a great influence on T_{exc}. This can be demonstrated by a comparison between Tables 2.6 and 2.10. More or less the same forward power was found to be optimum for the solvents water, acetone and chloroform at the hard line (Table 2.6). However, the lower carrier gas flows and spray chamber temperatures associated with acetone and chloroform correlate with higher excitation temperatures compared to water (Table 2.10). The same carrier gas flow was found to be optimum for the solvents water and methanol at the hard line, though in the latter case the optimum power and spray chamber temperature was lower than that for water (Table 2.6). In the case of methanol these two factors resulted in a T_{exc} that was lower in comparison to water (Table 2.10).

A general conclusion that can be drawn from Table 2.10 is that for each solvent T_{exc} was lower for operating conditions associated with the soft line in comparison to the hard line. This was probably due to the higher carrier gas flows and viewing heights associated with the soft line, and illustrates the greater dependence of the

hard line on T_{exc}. However, since no Abel inversion was carried out these conclusions must be regarded tentatively.

2.3.4 Conclusions

It is clear that there is no simple relationship between the solvents studied and optimum operating conditions. However, several important points can be identified.

(i) For solvents of higher volatility a lower carrier gas flow and spray chamber temperature were preferable.

(ii) Maximum signal-to-background ratios were achieved at lower power for hard lines compared to soft lines, and lower power was found to be optimal for organic solvents compared to water.

(iii) Lower detection limits were achieved using the organic solvents compared to water.

(iv) Rotational temperature was found to be a function of power at low viewing heights and carrier gas flows.

(v) Excitation temperature was found to be extremely dependent on carrier gas flow and to some extent power, and the introduction of an organic solvent did not necessarily cause a reduction in excitation temperature in comparison to water when using optimum operating conditions.

(vi) The value of a multivariate optimisation technique, namely the variable step-size simplex procedure,

has once again been established for plasma spectrometry.

CHAPTER 3

THE DETERMINATION OF TRACE ELEMENTS IN ACETIC ACID AND TEREPHTHALIC ACID BY ICP-AES

Acetic acid is a feedstock used for the manufacture of terephthalic acid, which is itself an important bulk product used in the manufacture of terylene. To maintain a quality product and ensure the smooth operation of the plant it is necessary to monitor both the feedstock and the product for trace elements, for the reasons discussed in Chapter 1. In this chapter some of the problems associated with such analyses and novel methods to overcome them will be described.

3.1 Analysis of Acetic Acid

3.1.1 Experimental

3.1.1.1 Instrumentation

All analyses were performed using an inductively coupled plasma - atomic emission spectrometer (S35 Plasmakon, Kontron Spectroanalytik) described in Section 2.2.1. A jet injector of 2 mm internal diameter was used throughout. Operating conditions are shown in Table 3.1. The spectral lines studied and used for analysis are shown in Table 3.2

The same samples were also analysed by flame atomic absorption spectrometry (FAAS) both at Plymouth and by an independent analyst at the laboratory of ICI Materials Research Centre, Wilton, Cleveland, U.K. for comparison.

Table 3.1 Inductively coupled plasma operating conditions used for acetic acid analysis

Carrier gas/l min^{-1}	2.0
Intermediate gas/l min^{-1}	0.6
Outer gas/l min^{-1}	15
Forward power/kW.	1.4

Table 3.2 Wavelengths (λ), viewing heights above the load coil (H), excitation energies (E), ionisation energies (I) and their sums (E+I) for the spectral lines studied[#] and used for analysis*

				I/eV		
Species	λ/nm	H/mm	E/eV	1	2	E+I/eV
*Cu I	324.754	36	3.8	7.72	-	11.52
*Fe II	259.940	15	4.77	-	16.18	20.95
*Mn II	257.610	6	4.81	-	15.64	20.45
*Co I	345.350	45	4.0	7.86	-	11.86
*Na I	330.237	35	3.7	5.14	-	8.34
[#]Mn I	403.076	29	3.1	7.43	-	10.53
[#]Fe II	259.940	18	4.77	-	16.18	20.95

3.1.1.2 Procedure

Four different samples of acetic acid mother liquor were diluted 1 + 1 (v/v) in deionised, double-distilled water and trace elements determined in each. Calibration was performed using multielement standards, made up from 1000 $\mu g\ ml^{-1}$ stock solutions (Spectrosol, BDH Chemicals Ltd.), matrix matched in acetic acid (AnalaR, BDH Chemicals Ltd.).

3.1.2 Results and Discussion

Figure 3.1 shows the effect of increasing acetic acid concentration on the net emission signal for 10 $\mu g\ ml^{-1}$ of analyte. The acetic acid used was checked for contamination by Fe and Mn, and none was found. Therefore, the trends of increasing net signal with acetic acid concentration could only have been due to nebulisation, transport, atomisation, ionisation or excitation effects. The effect of acetic acid on ionisation and excitation is probably shown in Fig. 3.1, where the increase in net signal is proportionally greater at the Fe II ion line compared to the Mn I atom line. This is slightly puzzling because the expected result would be the converse due to the supposed cooling effect of acetic acid vapour in the central channel of the plasma. However, acetic acid is a relatively involatile organic solvent and is similar to water in many respects. It may be that the vapour loading in the plasma due to the solvent had the effect of conducting more energy from the anular region into the central channel, but was not so

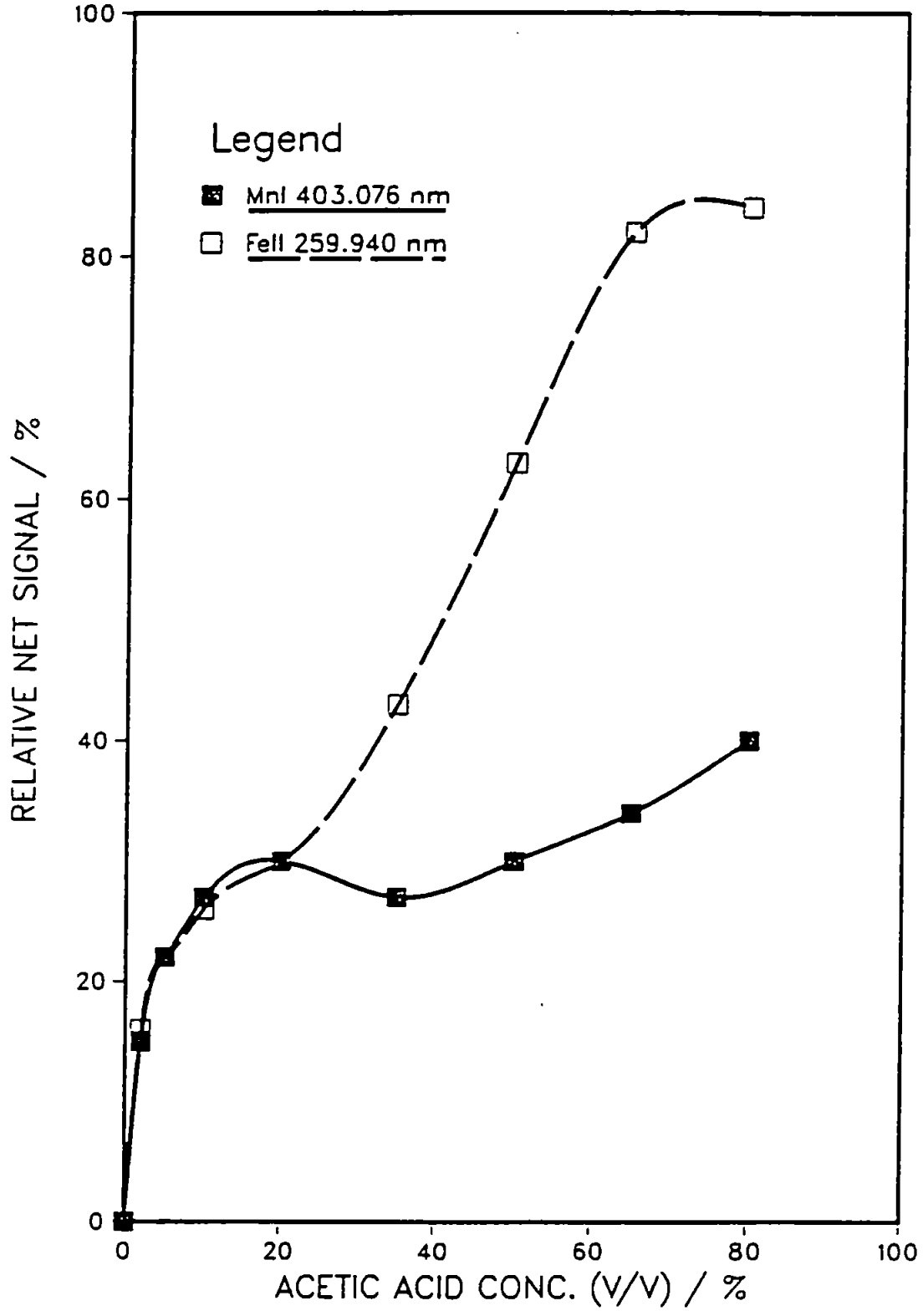

Figure 3.1 Effect of increasing acetic acid concentration on net emission signal for the spectral lines:
—■— Mn I 403.076 nm; _ -□- _ Fe II 259.940 nm

great as to cause significant cooling by transfer of energy to the breakdown of molecular species. Such energy transfer had a more beneficial effect on ion line emission than on atom line emission.

It is clear, however, that matrix matching of standards and samples, or analysis by the method of standard additions is necessary.

Table 3.3 lists the results obtained for trace element determinations in the four samples of acetic acid mother liquor. In general the results obtained using FAAS at Plymouth agree well with those obtained at ICI by FAAS. The results obtained by ICP-AES do not show such good agreement with the exception of Co, excluding sample number 4. The results for Mn and Fe show greater deviation than those for Na and Co. Despite the fact that the standards were matrix matched for acetic acid, the samples were not comprised purely of acetic acid and contained varying amounts of unknown organic constituents. This was especially true for sample 3 which contained a small fraction that was immiscible with water. It is thought that these differences in the sample matrices compared to the standards had a greater effect on the results obtained by ICP-AES and had a proportionally greater effect on the analytes for which ion lines were used for analysis (i.e. Mn and Fe) for the reasons already discussed. This is borne out by the results in Table 3.3, where the deviation of the values for Mn and Fe using ICP-

Table 3.3 Results of the analysis of acetic acid mother liquor by inductively coupled plasma atomic emission spectrometry (ICP-AES) and flame atomic absorption spectrometry (FAAS)

Element	Sample	Concentration found/$\mu g\ ml^{-1}$		
		ICP-AES	FAAS	FAAS*
Mn	1	260	470	430
	2	260	460	401
	3	94	130	118
	4	54	60	79
Fe	1	2.0	2.1	2.5
	2	2.0	2.0	2.5
	3	<1.0	0.3	1.7
	4	6.0	3.4	2.1
Cu	1	<0.2	-	-
	2	<0.2	-	-
	3	<0.2	-	-
	4	<0.2	-	<1.0
Na	1	130	194	186
	2	110	164	157
	3	70	47	43
	4	26	14	11
Co	1	190	206	188
	2	180	200	176
	3	60	58	53
	4	1530	1540	603

* Comparative results obtained from the laboratories of ICI.

AES is greater than for Na and Co compared to those obtained using FAAS.

3.1.3 Conclusions

It has been shown that while the analysis of acetic acid by ICP-AES was possible, matrix matching of standards and samples was a prerequisite. Additionally it has been shown that results obtained using atom lines for analysis by ICP-AES agreed much better with results obtained by FAAS compared to those obtained using ion lines and ICP-AES. When the exact composition of the sample matrix is unknown it is suggested that the method of standard additions may yield better results.

3.2 Analysis of Terephthalic Acid by Slurry Atomisation - ICP - AES

3.2.1 Slurry Introduction

The introduction of solutions of suspended solids, in the form of slurries, into the plasma has been made possible by the development of suitable high solids nebulisers (90). The possibility of slurry introduction into the ICP was first suggested by Greenfield (91). The advantages of slurry introduction are: the elimination of lengthy sample preparation procedures, often involving hazardous acids; the possibility of standardisation using simple aqueous standards; and the minor modifications necessary to existing instrumentation. Fuller (92) has shown that the reliability of analytical results depends to a great extent on the particle size distribution of the slurried

material. Subsequently, it has been demonstrated (88) that grinding of the sample to achieve a particle size distribution of at least less than 8 μm is necessary if the slurry is to model aqueous solutions sufficiently well, after nebulisation, for comparison with aqueous standards.

Furthermore, the internal diameter of the injector tube has been shown to be a critical factor (93), with a relatively large internal diameter of 3 mm being preferable. Slurry atomisation has been employed for the analysis of a wide variety of sample types by ICP-AES, including coals (94, 95), kaolin (96), geological samples (97, 98) and refractory oxide powders (99, 100), with and without grinding the samples. However, a simple and inexpensive bottle and bead grinding method has been developed (101) and successfully used to grind a variety of sample matrices with their subsequent analysis by direct current plasma - atomic emission spectrometry (101), ICP-AES (102) and ICP-MS (103, 104). Additionally, direct current plasma - atomic emission spectrometry has been optimised using simplex optimisation for the analysis of kaolin slurries (105) and temperature measurements have shown that slurry loadings in excess of 12% (m/V) cool the plasma.

With respect to this work the determination of trace elements in terephthalic acid (TA) has presented a problem for some years due to its insolubility in solvents

suitable for use in conventional analyses. Additionally, TA sublimes above 300 ^{o}C, making it difficult to ash and mineralise without sample losses. Therefore, the slurry introduction method looked promising for the analysis of this particular sample providing that a suitable grinding procedure could be developed.

3.2.2 Development of a Suitable Grinding Procedure

The particle size distribution of the TA sample as received is shown in Fig. 3.2A. The addition of a suitable surfactant, in this case 0.1% aerosol-OT (BDH Chemicals Ltd.), reduced the particle size only by a very small degree (Fig. 3.2B), hence it was necessary to grind the sample to reduce the particle size further. The usual grinding procedure adopted is to place an accurately weighed sample into a polypropylene bottle (30 ml capacity) together with 10 - 30 g of blown zirconia spheres and several ml of a surfactant (102). The bottle is then agitated vigorously on a flask shaker for several hours, and the contents quantitatively transferred and made up to volume. This procedure was performed on the TA sample, which was ground for 60 minutes, resulting in the particle size distribution shown in Fig. 3.3A. It is evident that grinding the sample in fact served to increase the particle size. This was probably caused by impaction of the material to form agglomerations. Consequently it was decided to develop a method to grind the sample at a lower temperature than its glass transition temperature. The apparatus developed to grind

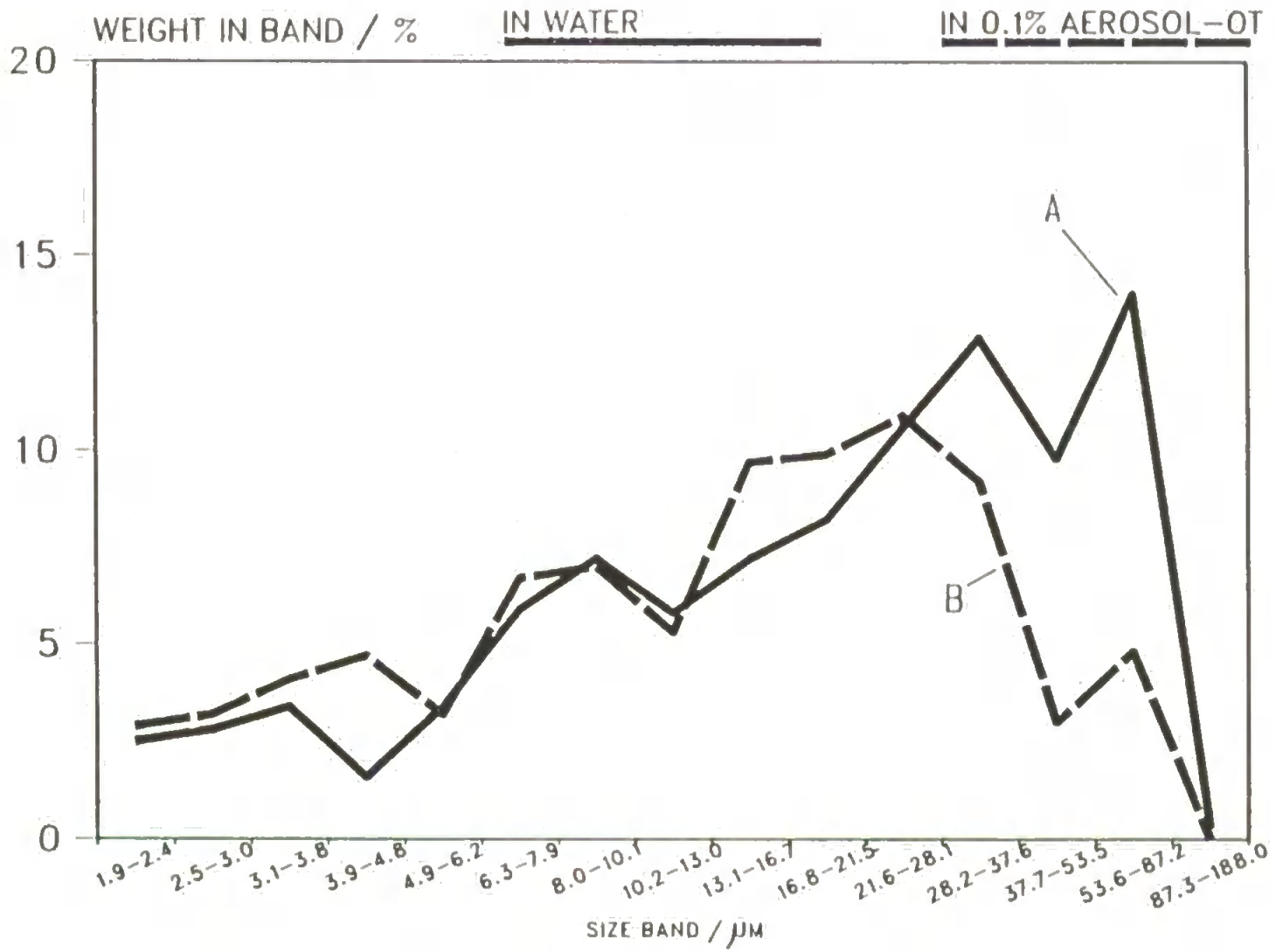

Figure 3.2 Particle size distribution of terephthalic acid as received: A) in water; B) in 0.1% aerosol-OT

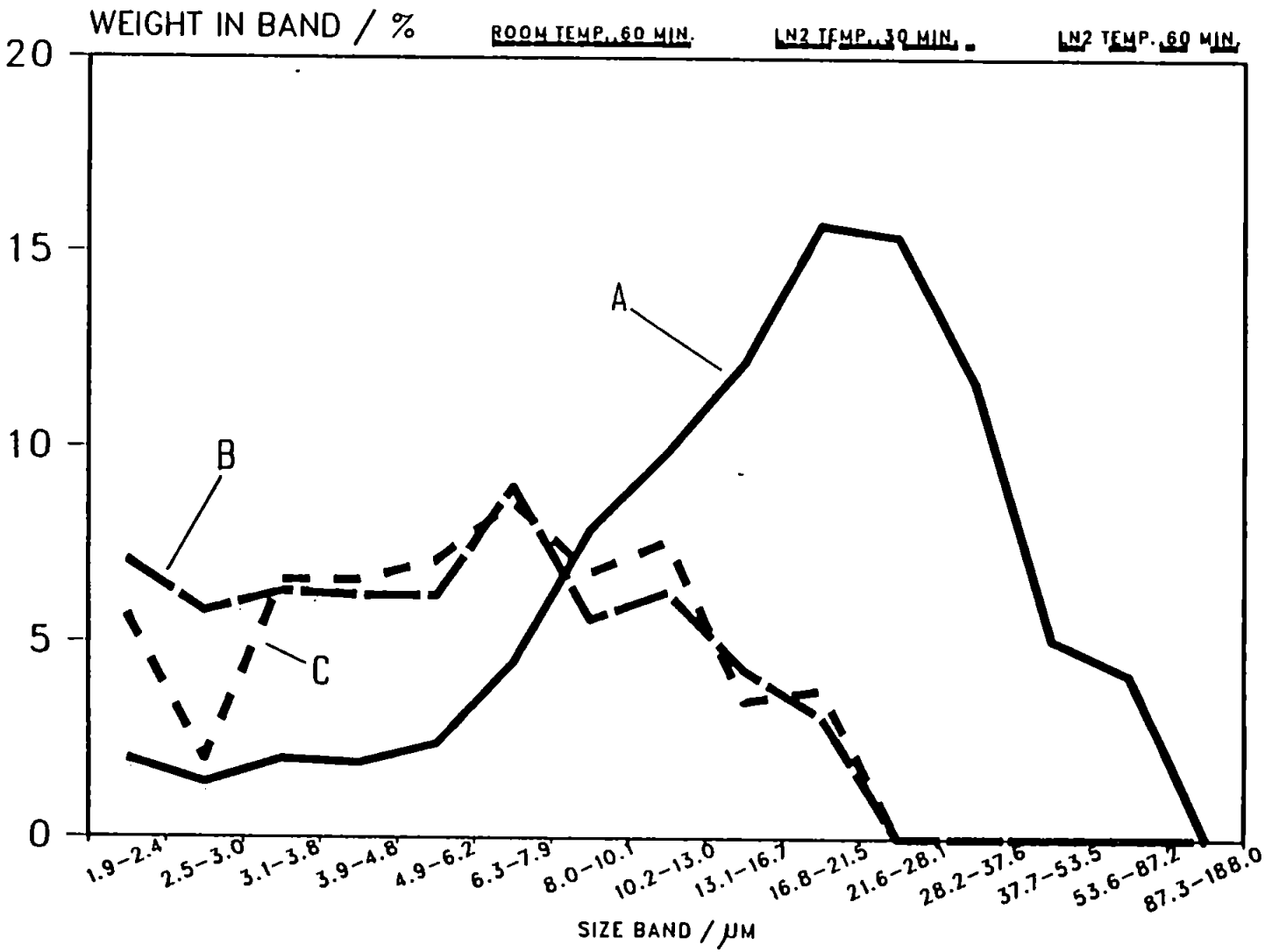

Figure 3.3 Particle size distribution of terephthalic acid after grinding: A) at room temperature for 60 minutes; B) at liquid nitrogen temperature for 30 minutes; C) at liquid nitrogen temperature for 60 minutes; then slurried in 0.1% aerosol-OT

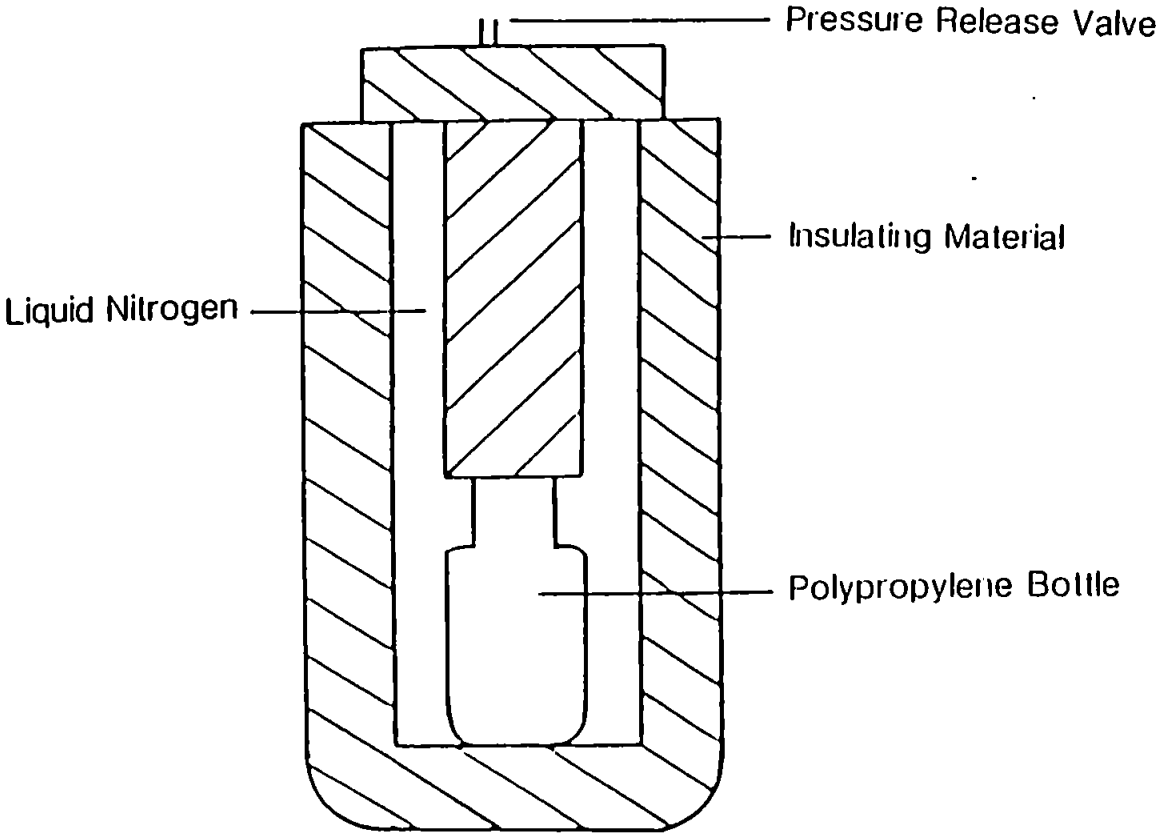

Figure 3.4 The apparatus developed to grind samples at liquid nitrogen temperature

samples at liquid nitrogen temperature is shown in Fig. 3.4. Essentially the grinding method was identical, except that the polypropylene bottle was contained in a liquid nitrogen jacket, and the surfactant solution was excluded during grinding. The particle size distributions after grinding for 30 and 60 minutes using this method are shown in Figures 3.3B and 3.3C respectively. A mean particle size of less than 8 μm was obtained after grinding for 30 minutes, with no significant improvement after 60 minutes. This was considered sufficiently small to attempt analysis by the slurry atomisation method.

3.2.3 Experimental

3.2.3.1 Instrumentation

The inductively coupled plasma - atomic emission spectrometer used is described in Section 2.2.1. Nebulisation of slurried samples was achieved by means of a v-groove, high solids nebuliser (Ebdon nebuliser, PS Analytical Ltd., Sevenoaks, Kent, U.K.), and the injector tube used was of 3 mm internal diameter. Plasma operating conditions and the wavelengths used for analysis are shown in Table 3.4.

A comparative study was undertaken at Plymouth using a direct current plasma (Spectraspan IIIA, ARL, Luton, Beds, U.K.) and slurry atomisation. Additionally, trace elements were determined by an independent analyst after a sulphonated ashing procedure, followed by dissolution in nitric acid, at the laboratory of ICI Materials Research

Table 3.4 Inductively coupled plasma operating conditions and wavelengths used for the analysis of terephthalic acid

Carrier gas/l min^{-1}	1.8
Intermediate gas/l min^{-1}	0.5
Outer gas/l min^{-1}	16
Forward power/kW	1.5
Species and wavelengths monitored /nm	Fe II 259.940 Co I 345.350 Mn II 293.930 Ni II 230.300 Cr II 284.325

Centre, Wilton, Cleveland, U.K., by ICP-AES (Plasma II, Perkin Elmer, Post Office Lane, Beaconsfield, Bucks, U.K.).

3.2.3.2 Sample Preparation

Two separate samples of approximately 2.5 g of TA were accurately weighed into 30 ml capacity polypropylene bottles, together with approximately 30 g of zirconia spheres. Each bottle was placed in an insulated jacket containing liquid nitrogen and agitated on a flask shaker for 60 minutes. Both samples were bulked in 50 ml of 0.1% aerosol-OT to make an approximately 10% m/V slurry. Trace elements were determined by slurry atomisation ICP-AES and DCP-AES using calibration with aqueous standards.

3.2.4 Results and Discussion

The results obtained are shown in Table 3.5. Determinations proved to be extremely difficult due to the very low levels of trace elements in the TA sample. It is also likely that contamination by trace elements in the polypropylene bottles could have contributed to some high results. This may prove to be a persistent problem since the material undergoing analysis is likely to have a similar trace element content as the bottle. Notwithstanding these problems, however, the ICP-AES results, slurry and dissolution, still show quite good agreement, with the exception of Cr which in any case may have been lost during the dissolution procedure. Results obtained by DCP-AES were all higher than those obtained by

Table 3.5 Results for the determination of trace elements in terephthalic acid

Element	Concentration found/$\mu g\ g^{-1}$		
	DCP-AES slurry atomisation	ICP-AES slurry atomisation	ICP-AES* dissolution
Fe	1.1	0.35	0.33 ± 0.007
Co	<0.6	<0.8	0.02 ± 0.01
Mn	0.40	0.10	0.10 ± 0.002
Ni	1.2	<0.8	0.02 ± 0.01
Cr	not determined	1.50	0.04 ± 0.02

* Comparative results obtained from an ICI Laboratory

ICP-AES. This may well have been due to the fact that the DCP-AES analysis was undertaken first, thereby increasing the risk of contamination from polypropylene bottles which had not been conditioned by a previous grinding procedure.

3.3 Analysis of Terephthalic Acid after Dissolution in Sodium Hydroxide Solution

Terephthalic acid dissolves readily in sodium hydroxide solution. However, such a medium is not best suited to the dissolution of samples in which trace elements are to be determined, because of the tendency of the high hydroxide ion concentration to cause precipitation of many trace elements as hydroxides, and ion exchange between metal ions and hydrogen ions on glassware. Despite this, such a method could find application where results are required quickly and only approximate values are necessary.

3.3.1 Experimental

3.3.1.1 Instrumentation

The analysis was performed using an inductively coupled plasma - atomic emission spectrometer (Plasma II, Perkin Elmer, Post Office Lane, Beaconsfield, Bucks, U.K.), described in Table 3.6, equipped with a v-groove high solids nebuliser (Ebdon nebuliser, PS Analytical Ltd.) and a 2.0 mm internal diameter, alumina injector. Operating conditions are given in Table 3.7.

Table 3.6 Details of the Perkin Elmer, Plasma II inductively coupled plasma - atomic emission spectrometer

Nebuliser	A choice of either a cross-flow nebuliser manufactured from Ryton supplied as standard, or a v-groove, high solids nebuliser manufactured from PTFE (Ebdon Nebuliser, PS Analytical Ltd., Sevenoaks, Kent, UK)
Spray chamber	Scott type, double pass, spray chamber manufactured from Ryton
Torch assembly	Fused quartz, Fassel type, demountable torch with a choice of alumina or quartz injector tubes
Power supply	27.12 MHz radio-frequency power supply, with automatic tuning and an output of between 0 - 1800 W under computer control
Monochromator	One meter, Ebert monochromator with a 1800 grooves mm^{-1} grating under computer control and a wavelength range from 160 - 800 nm with 0.018 nm resolution
Photomultiplier	Hammamatsu R-955
Gas flows	All argon gas flows under computer control Carrier gas 0 - 3.0 1 min^{-1} Intermediate gas 0 - 3.0 1 min^{-1} Outer gas 5 - 25 1 min^{-1}
Plasma viewing height	Variable viewing height between 0 - 40 mm above the load coil

Table 3.7 Inductively coupled plasma and spectrometer operating conditions for the analysis of terephthalic acid in sodium hydroxide solution

Spectrometer		
Wavelength	Mn II	257.610 nm
Search window		0.05 nm
Sampling time		100 ms
Plasma		
Carrier gas flow		1.0 l min^{-1}
Intermediate gas flow		1.0 l min^{-1}
Outer gas flow		15 l min^{-1}
Forward power		1000 W
Viewing height		15 mm
Sample uptake rate		2.0 ml min^{-1}

3.3.1.2 Procedure

Ten subsamples of TA, between 2.8 - 3.2 g, were accurately weighed into separate conical flasks. Each sample was dissolved in a 4 + 100 (m/V) solution of sodium hydroxide (AnalaR, BDH Chemicals, Ltd.), made up in deionised, double-distilled water, and then made up to 100 ml in the same solution. Calibration was achieved using aqueous standards matrix matched for NaOH, and the trace element Mn was determined in each of the samples.

3.3.2 Results and Discussion

For each of the ten samples ten replicate measurements of emission intensity were made. The mean and relative standard deviation (RSD) for the determination of Mn in the ten samples of TA is shown below

Mean Mn concentration = 0.82 $\mu g\ g^{-1}$

RSD = 7.3%

The accuracy of the results is open to question, however an acceptable level of precision was obtained considering the nature of the sample matrix. It is anticipated that this method will be adopted as a standard procedure for the determination of Mn in TA samples. The present method employed at ICI involves a sulphonated ashing procedure which results in considerable sample losses due to the partial sublimation of TA at 300°C. The method described above has proved to be rapid and avoids sample losses.

3.4 Conclusions

The determination of trace elements has been undertaken for a particular production stream, i.e. manufacture of terephthalic acid (TA). Problems associated with the analysis of organic samples have been addressed, namely matrix matching of samples and standards, and novel methods of sample preparation such as dissolution of TA in NaOH solution and the analysis of TA in the form of a slurry. These methods were successfully applied to the determination of trace elements in acetic acid and TA.

CHAPTER 4

INTERNAL STANDARDISATION FOR ORGANIC SOLVENTS IN ICP-MS

4.1 Introduction

Many conflicting reports exist on the influence of the sample matrix on the analytical signal in ICP-MS (106-117). In general the most serious matrix effects are those caused by an excess of a heavy easily ionisable element (EIE) or elements in the matrix, which cause suppression of the analyte signal, or in some cases an enhancement. For instance, Tan and Horlick (113) observed suppression of analyte signal in the presence of various EIEs at low nebuliser gas flows, but enhancements at high flows. Gregoire (111, 112) observed only suppression, while Beauchemin et al., (110) mainly observed enhancements. However, several important points can be identified:

(i) Heavy matrix elements with low ionisation potentials cause the most severe effects

(ii) Light analyte elements with high ionisation potentials are most severely affected

(iii) Plasma operating conditions have a great influence on the magnitude of these effects

(iv) The matrix effect is dependent on the absolute amount of matrix element rather than on the molar ratio to analyte, hence the effects can be reduced by dilution of the sample

Several theories have been proposed to account for these effects. The most popular, with respect to the plasma, is that of ionisation suppression in the plasma, whereby the large excess of matrix element with a low first ionisation potential results in a large excess of electrons and positive ions after ionisation. This excess forces the equilibrium for the analyte towards atom formation, resulting in a suppression in the formation of analyte ions. However, this theory lacks credibility considering the overall electron and ion population in the plasma and alone cannot explain the severity of the matrix effects observed in ICP-MS, so further reasons must be sought.

Gregoire (112) has proposed that "ambipolar diffusion" may be a possible explanation. The mechanism is such that the presence of a large excess of a high mass EIE in the plasma gives rise to an electrical field caused by the diffusion of electrons, at a greater rate than ions, out of the central channel. The electrical field results in the diffusion of lighter analyte ions towards the anular region of the plasma, thereby giving rise to a drop in the number of ions that can be sampled from the central channel.

Tan and Horlick (113) have suggested that mass separation effects, in the expansion region and subsequent ion beam, may play a role. They mention two effects, namely pressure diffusion and Mach-number focussing, whereby the heavier ions are focused towards the axis of the beam, and

the lighter ions diffuse away to a greater extent, though the theories were originally developed for neutral molecular beams. The most popular mass separation theory currently is that of space charge effects in the ion beam (113, 115, 117). This is caused by the loss of electrons from the ion beam due to the nature of the ion optics which focus only positively charged species, and results in coulombic repulsion between ions. In the presence of an excess of relatively heavy matrix ions, the lighter analyte ions are repelled from the ion beam to the greatest extent. Mass separation effects are particularly critical in the expansion region since the skimmer cone samples from only a relatively narrow portion of the expansion gases around the axis behind the sampling orifice, and indeed matrix effects have been shown to be less severe when a skimmer with a larger orifice than normal was used (116).

Internal standardisation has been proposed as a possible remedy for matrix effects and instrumental drift. Beauchemin et al., (110) investigated the background species ^{12}C and $^{40}Ar^{40}Ar$ as internal standards to correct for matrix effects, and found some improvement for those elements reasonably close in mass-to-charge ratio (m/z). They subsequently used $^{40}Ar^{40}Ar$ as an internal standard for the analysis of real samples with some success (49, 50). Thompson and Houk (114) have suggested that the internal standard should be close in atomic mass and have a similar first ionisation potential to the analyte if

correction for matrix effects is to be successful. However, Vandecasteele et al. (117) have found that In used as an internal standard corrects adequately for a variety of elements in the presence of a large excess of matrix. Of course for many elements the ideal form of internal standardisation is isotope dilution analysis, which has proved very popular in ICP-MS (42, 45-50).

The analysis of organic compounds, especially organic solvents, is plagued by the problems described in Section 1.4. A particular problem is that of the differences in nebulisation and sample transport caused by the different physical properties of organic solvents. Because of the very rapid sequential mode of operation of the mass spectrometer it might be expected that an internal standard could correct for such transport effects. However, Marshall and Franks (118) have investigated the effect of methacrylic acid on various elements of widely differing atomic mass, and found that enhancements or depressions in analyte signal could be achieved depending on operating conditions. They also found that a single internal standard such as Rh was not suitable for correction.

Evidently, the use of a single internal standard may not be sufficient. Some account must be taken of the effect of an organic sample on ionisation conditions within the plasma and possible perturbation of the ion beam caused by the large amount of carbon in the solvent. Even though

the first ionisation potential of C is quite high and it has a low atomic mass, such will be the excess present due to an organic solvent that some effect might be expected.

In this chapter a novel method of internal standardisation, to compensate for organic solvent matrix effects, is described.

4.2 Experimental

4.2.1 Instrumentation

All experiments were performed using an inductively coupled plasma - mass spectrometer (VG PlasmaQuad 2, VG Elemental, Winsford, Cheshire, U.K.) described in Table 4.1, together with any modifications to the standard instrumentation.

4.2.2 Operating Conditions

Plasma operating conditions are shown in Table 4.2. The mass spectrometer was operated in quantitative scanning mode throughout. Typical data acquisition parameters are shown in Table 4.3.

4.2.3 Reagents and Standards

Multielement standard solutions of Be, Co, La and Pb were prepared by serial dilution of a 10 $\mu g\ ml^{-1}$ multielement stock solution using 2 + 98 (v/v) nitric acid (Aristar, BDH Chemicals Ltd.) in deionised double-distilled water. Corresponding organic samples were prepared by serial dilution of the same multielement stock solution in

Table 4.1 Details of the VG PlasmaQuad 2 inductively coupled plasma - mass spectrometer used in this work

Plasma -	
Forward power	0 - 2000 W
Nebuliser gas	Argon 0 - 2.0 l min^{-1} Oxygen 0 - 0.2 l min^{-1}
Auxilliary gas	Argon 0 - 3.0 l min^{-1}
Coolant gas	Argon 0 - 20 l min^{-1}
Nebuliser	A choice of either the Meinhardt nebuliser supplied as standard or a v-groove high solids nebuliser (Ebdon Nebuliser, PS Analytical Ltd., Sevenoaks, Kent, UK)
Spray chamber	Scott type, double pass spray chamber, jacketed to allow cooling by means of a refrigerated bath (RB-5, Techne, Cambridge, U.K.) containing propan-2-ol and a recirculation pump (TE-8A, Techne)
Torch assembly	A choice of either a fused quartz Fassel type torch supplied as standard or a low-flow torch (Sci-Tek Instruments, Wolverton, Milton Keynes, U.K.)
Ion Sampling -	
Sampling cone	Nickel (Nicone) sampler with a 1.0 mm orifice
Skimmer cone	Nickel skimmer with a 0.75 mm orifice
Sampling distance	8.5 - 14.0 mm from load coil
Vacuum -	
Expansion stage	Commonly between 1.8 - 3.0 m bar
Intermediate	Commnly $< 10^{-4}$ m bar
Analyser	Commonly 1.6×10^{-6} m bar
Spectrometer -	VG SX300 quadropole and D-Tek 402 electron multiplier supplied as standard

Table 4.2 Plasma operating conditions used in this work

Solvent	Propan-2-ol
Torch	Standard
Nebuliser	Meinhard
Nebuliser gas/l min^{-1}	0.720 Argon 0.026 Oxygen
Auxilliary gas/l min^{-1}	1.3
Coolant gas/l min^{-1}	15
Forward power/W	1800
Reflected power/W	45
Spray chamber temperature/^{o}C	-1
Sampling depth/mm	10.5

Table 4.3 Two typical sets of data acquisition prameters used in 'quantitative' scanning mode

	Set A	Set B
Mass range/m/z	8 - 216	8 - 216
No. of channels	2048	2048
No. of scan sweeps	100	50
Dwell time/μs	160	160
Time per scan/s	33	16
No. of scans per run	3	5

propan-2-ol (Aristar, BDH Chemicals Ltd.) by weighing out small volumes of the multielement standard solution into propan-2-ol, then calculating the concentrations in ng ml^{-1}. All standards and samples were spiked either with In (Alfa Chemical Co. Inc., Milwaukee, Wisconsin, USA) or with a mixture of Sc, In and Pt each at 100 ng ml^{-1} as internal standards. All multielement solutions were prepared using Spectrosol standard solutions (BDH Chemicals Ltd.) unless otherwise stated.

4.2.4 Procedure

Several methods of internal standardisation were investigated as described below.

4.2.4.1 Single Sample Uptake

Calibration was achieved using simple aqueous standards, and the organic samples were run as blank subtracted samples in the normal way. Results were calculated by the instrument software with and without In as an internal standard.

4.2.4.2 Dual Sample Uptake I

In this case two sample uptake flows were pumped simultaneously and mixed by means of a T-piece after the peristaltic pump, as shown in Fig. 4.1. During calibration standard solutions were pumped through flow A while a blank solution of propan-2-ol was simultaneously pumped through flow B. Subsequently the organic samples were pumped through flow A while an aqueous blank was

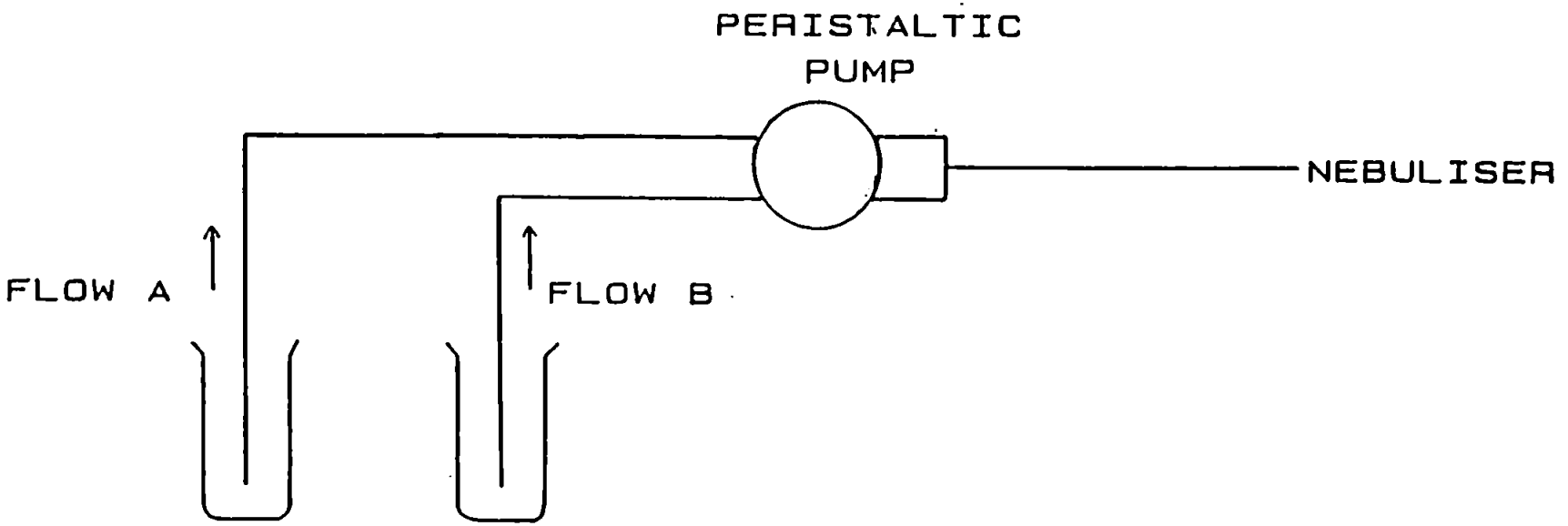

Figure 4.1 Schematic diagram of the pumping arrangement for dual sample uptake I

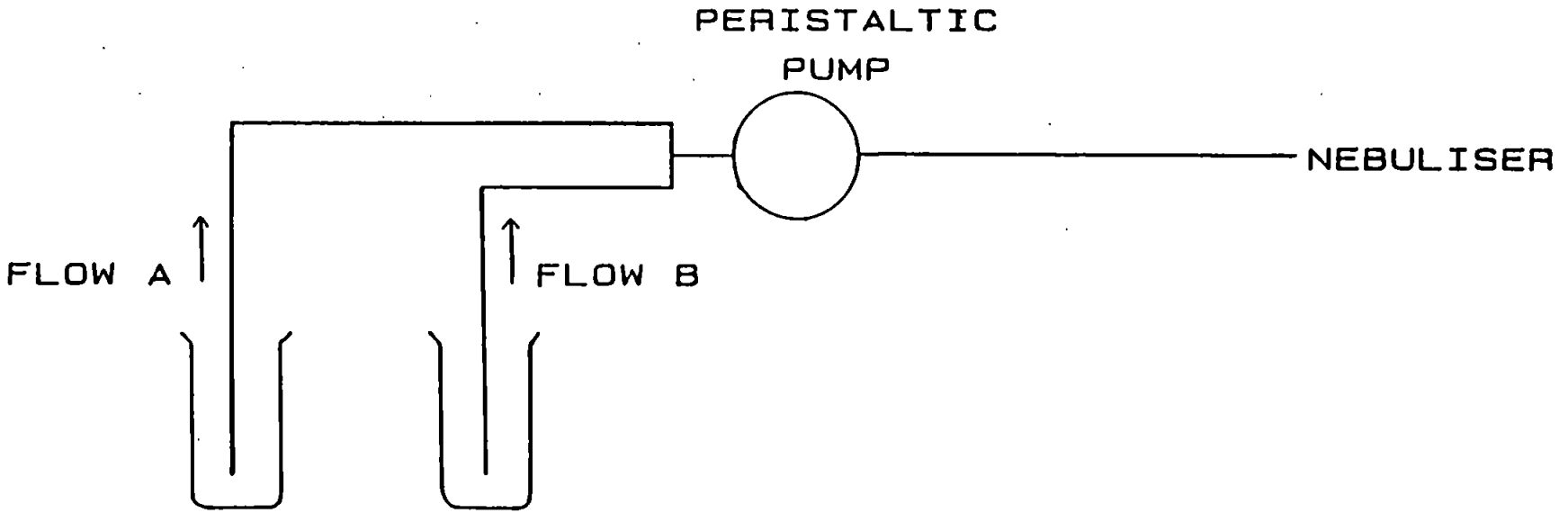

Figure 4.2 Schematic diagram of the pumping arrangement for dual sample uptake II

pumped simultaneously through flow B. Results were calculated by the instrument software with and without In as an internal standard.

4.2.4.3 Dual Sample Uptake II

This procedure was essentially the same as that adopted above except that in this case the two sample uptake flows were mixed prior to the peristaltic pump as shown in Fig. 4.2. Results were calculated by the instrument software using either In, Sc, or Pt, or all three, or none at all as internal standards.

4.2.5 Results and Discussion

4.2.5.1 Single Sample Uptake

Results are shown in Table 4.4 and in Fig. 4.3 in the form of plots of the actual concentrations of the elements in the propan-2-ol samples versus the concentration found compared to the calibration by aqueous solutions. When no internal standard was used the 'found' were lower than the 'actual' concentrations, in the order Pb < La < Co (Fig. 4.3A). Several factors may have contributed to the low recoveries. Firstly, the differences in physical characteristics between standards and samples may have had an effect on their nebulisation efficiencies and transport properties in the spray chamber. However, if this was the only effect then one would expect all elements to behave in a similar manner. A second explanation is that the organic samples affected the ionisation equilibrium in the plasma. Two of these effects have already been discussed

Table 4.4 Mean recovery factors (R) and relative standard deviation (RSD) of five scans for the elements studied in propan-2-ol samples, without (NIS) and with (IS) In as an internal standard, and using the single uptake method

Actual Concentration/ ng ml^{-1}		^{59}Co		^{139}La		^{208}Pb	
		R	RSD/%	R	RSD/%	R	RSD/%
17.5	NIS	0.38	10.6	0.18	9.7	0.15	3.8
	IS	1.69	14.5	0.80	14.9	0.68	8.4
62.1	NIS	0.39	2.5	0.21	2.3	0.17	4.7
	IS	1.74	3.9	0.94	0.3	0.77	4.2
106	NIS	0.39	2.7	0.22	1.7	0.16	2.3
	IS	1.83	2.7	1.03	3.7	0.78	6.0

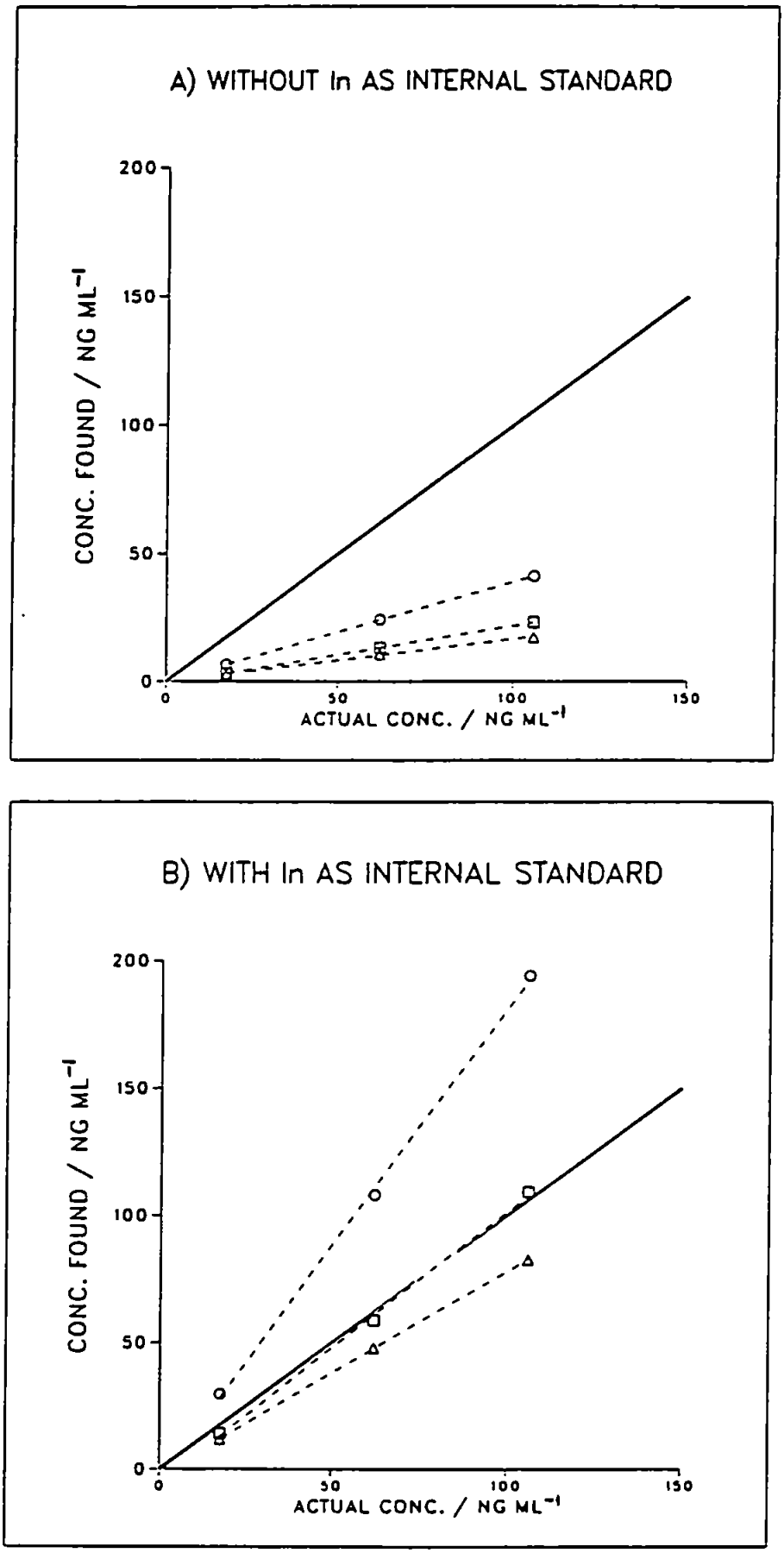

Figure 4.3 Actual concentration vs concentration found in samples of propan-2-ol after calibration with aqueous standards for the elements: ^{59}Co (O); ^{139}La (□); and ^{208}Pb (Δ), with and without In as an internal standard

in Section 4.1 of this chapter, namely ionisation suppression and ambipolar diffusion caused by the large excess of carbon. Additionally the presence of an organic solvent also lowers the ionisation temperature in the plasma due to the energy required for the destruction of organic molecules. The sum of these effects is to reduce the number of analyte ions in the plasma compared to aqueous solution. Thirdly, the large excess of carbon ions which are undoubtedly present may also lead to mass separation in the expansion region and the ion beam, due to pressure diffusion, Mach-number focussing and space charge effects, discussed in Section 4.1 of this chapter. It has been shown (111-114) that in the presence of an excess of an easily ionisable element lighter elements are suppressed to a greater extent than heavier elements, and that those with a high first ionisation potential are suppressed to a greater extent than those with a low first ionisation potential. In this work the major matrix component was carbon which has neither high mass nor a low first ionisation potential. However, it was in such large excess that it undoubtedly played a significant role. The masses of the major isotopes and first ionisation potentials for the elements studied are given in Table 4.5, along with those for Ar and C.

If mass separation effects predominated the expected order of suppression would be Co > La > Pb. A comparison of Table 4.5 and Fig. 4.3A shows that the converse was the case. Similarly if ionisation effects predominated then

Table 4.5 Masses of the major isotopes (M) and first ionisation potentials (I1) for the elements of interest

Element	M	I1(V)
Co	59	7.86
Ba	138	5.21
La	139	5.58
Pb	208	7.42
In	115	5.79
Ar	40	15.76
C	12	11.26

the expected order of suppression would be Co > Pb > La. The difference between La and Pb can be explained on the basis of ionisation suppression, Pb being affected relatively more because of its high first ionisation potential. However, Co shows anomalous behaviour that cannot be explained by the theories mentioned above. The expected result would be for Co to be suppressed to the greatest extent by virtue of a high first ionisation potential and low mass. It would be unwise to postulate a theory based on the limited information presented here, however, it is interesting to note that Long and Bolton (119) observed emission signal enhancements for Y, La, Al and Cr, and emission signal depressions for Ca, Mg, Fe and Cu when investigating the introduction of propane into a pencil plasma for ICP-AES. They put forward the theory that the enhancements were caused by reduction of the metal oxide species by carbon, and that the depressions were caused by the formation of refractory metal carbides. Such reactions may well have played a part in this work, especially since they are thought to be prevalent in the ICP-MS interface region. Additionally, in this study there was the added complication of oxygen introduction in the nebuliser gas flow which might not only cause combustion of the carbon but also the formation of refractory oxides.

The effect of using In as an internal standard is shown in Fig. 4.3B. It is evident that In was only effective as an internal standard for La. This is in agreement with

Thompson and Houk (114) who suggested that the internal standard should match the analyte closely with respect to mass and first ionisation potential. This is certainly the case for In and La (Table 4.5). It seems likely that the internal standard successfully corrected for nebulisation and transport effects, but not for matrix induced enhancements or suppressions. This is borne out by Fig. 4.3B where the effect of the internal standard was to increase recoveries by almost the same factor for all elements (Table 4.4): i.e. 4.7 X for Co; 4.7 X for La; and 4.8 X for Pb; suggesting that it only compensated for nebulisation and transport effects, except in the case of La.

In general the precision achieved for five consecutive scans was better when no internal standard was used (Table 4.4). This is contrary to what might be expected, suggesting again that analyte and internal standard behave differently in the plasma and subsequently in the ion beam.

4.2.5.2 Dual Sample Uptake I

It has been demonstrated in the previous section that the internal standard was capable of correcting only for nebulisation and transport effects caused by the matrix, and not for those prevalent in the plasma, expansion region and ion beam, unless analyte and internal standard were closely matched with respect to mass and first ionisation potential. The obvious way to overcome this is

to matrix-match standards and samples. However, such an approach with regard to organic solvents would require standard solutions made up in the appropriate solvent for the sample of interest. Since many different solvents are used for dilution or dissolution of samples this would entail stocking several sets of standards in the appropriate organic solvents, which are inherently less stable than those in aqueous solution. Hence, the procedure described in Section 4.2.4.2 was employed whereby simultaneous nebulisation of both aqueous and organic phases ensured matrix matching of standards and samples, providing sufficient mixing of the two phases occurred prior to nebulisation. Results are shown in Table 4.6 and in Fig. 4.4 in the same manner as those in Fig. 4.3.

It is evident, from Fig. 4.4A and Table 4.6 that even without internal standardisation recoveries for the elements in propan-2-ol samples were in the range 0.80 - 0.92. When an internal standard was used recoveries were even better, and in the range 0.84 - 1.05 (Fig. 4.4B and Table 4.6). Hence matrix matching of samples and standards was effectively achieved, thereby reducing matrix effects discussed in the previous section. The slightly lower recoveries obtained without internal standardisation are attributable to the difference in uptake rate between organic and aqueous phases, due to slight inconsistencies in pump tubing and the difference in physical properties between water and propan-2-ol. For

Table 4.6 Mean recovery factors (R) and relative standard deviation (RSD) of five scans for the elements studied in propan-2-ol samples, without (NIS) and with (IS) In as an internal standard, and using the dual uptake I method

Actual Concentration/ ng ml^{-1}		^{59}Co		^{139}La		^{208}Pb	
		R	RSD/%	R	RSD/%	R	RSD/%
17.5	NIS	0.85	6.0	0.87	6.6	0.80	10.7
	IS	0.90	7.0	0.92	7.4	0.84	11.6
62.1	NIS	0.86	3.4	0.91	2.5	0.87	10.7
	IS	0.91	6.2	0.96	5.4	0.92	14.2
106	NIS	0.83	1.8	0.92	5.7	0.82	5.1
	IS	0.95	3.5	1.05	5.1	0.94	7.6

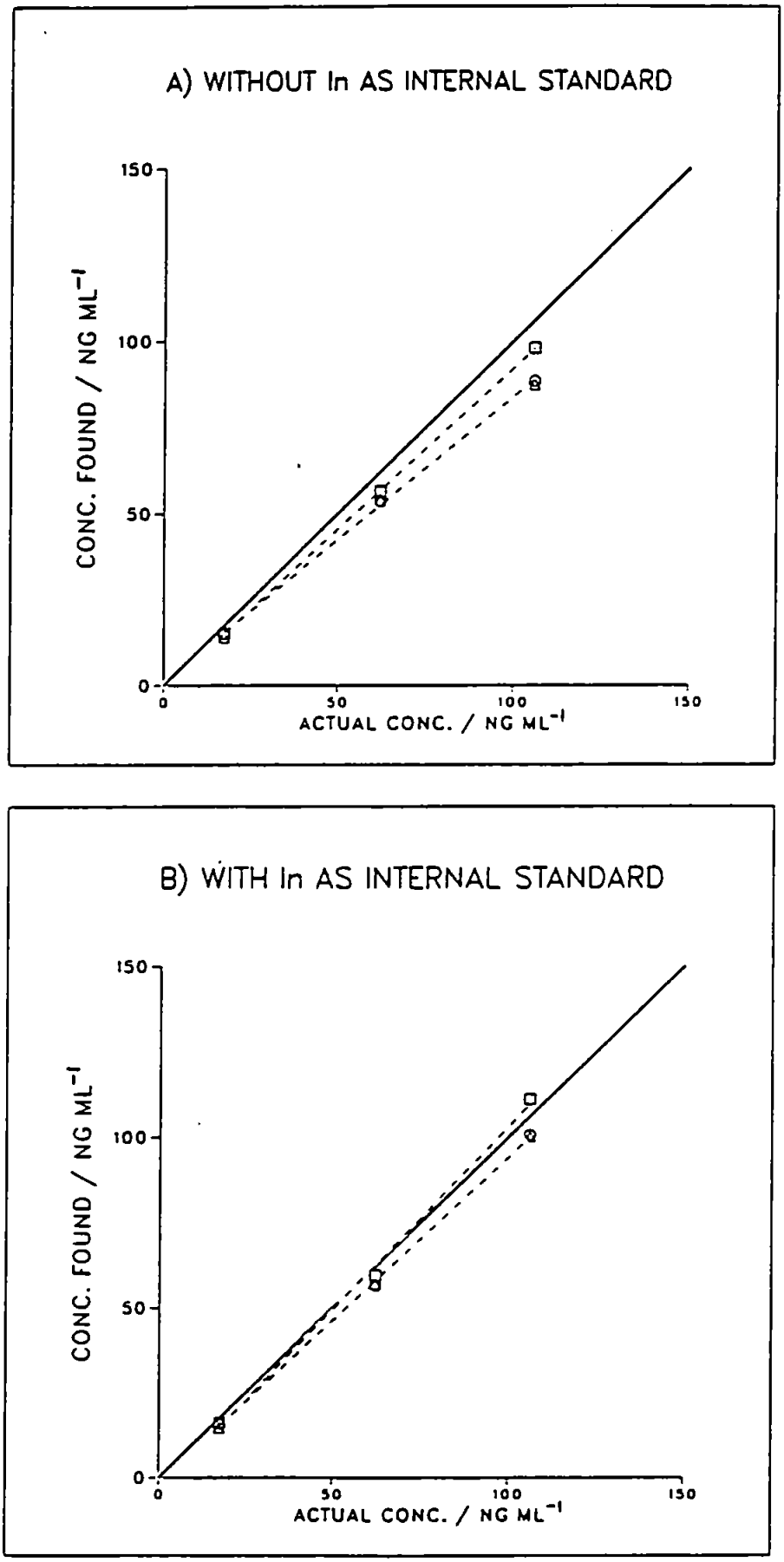

Figure 4.4 Actual concentration vs concentration found in samples of propan-2-ol using the 'dual uptake I' method for the elements: ^{59}Co (O); ^{139}La (□); and ^{208}Pb (Δ), with and without In as an internal standard

propan-2-ol samples the difference in uptake rate compared to water was not great, however, for other organic solvents uptake rates can vary considerably. This problem may be overcome by using an internal standard.

The advantage of this technique is that only a blank solution of the organic solvent is necessary, aqueous standards being used for calibration.

The precision achieved for five consecutive scans was worse when the internal standard was employed (Table 4.6), contrary to what might be expected. One possible explanation is that because the aspiration of an organic solvent necessarily results in worse precision, due to its destabilising effect on the plasma, compared to the introduction of aqueous solution only, then the multiplicative effect of analyte and internal standard signal noise becomes significant. Another contributing factor may have been the excessive pump noise caused by pumping two streams simultaneously and then merging them.

4.2.5.3 Dual Sample Uptake II

This procedure was basically a refinement of that described in the previous section, the main difference being that aqueous and organic phases were mixed prior to the peristaltic pump in an effort to reduce the pump noise caused by pumping two streams simultaneously. Additionally, the use of three internal standards at the same time was investigated, namely Sc, In and Pt, which

effectively covered the mass range. Results are shown in Table 4.7 and Figs. 4.5 - 4.6 in the same format as before.

When no internal standard was used element recoveries were in the range 0.39 - 0.49 (Table 4.7 and Fig. 4.5A). The reason for this is that the uptake rates of the organic and aqueous phases were substantially different (0.40 ml min^{-1} for propan-2-ol and 0.87 ml min^{-1} for the aqueous phase) due to physical differences between solvents, exacerbated by the fact that they were mixed prior to the pump. However, when a correction was made for this recoveries were raised to between 0.85 - 1.06 indicated by the values in parentheses in Table 4.7.

An easier option was to use an internal standard. This worked well, and recoveries of between 0.91 - 1.02 were obtained using In as an internal standard (Table 4.7 and Fig. 4.5B).

The precision achieved for three consecutive scans was slightly improved in most cases when the internal standard was used (Table 4.7). This improvement, as opposed to the degradation observed using the method described in the previous section, may be attributable to the reduction in pump noise caused by pumping only one solvent stream, and hence a reduction in the multiplicative noise of analyte and internal standard.

Table 4.7 Mean recovery factors (R) and relative standard deviation (RSD) of five scans for the elements studied in propan-2-ol samples, without (NIS) and with (IS) In as an internal standard, and using the dual uptake II method

Actual Concentration/ ng ml^{-1}		^{59}Co		^{139}La		^{208}Pb	
		R	RSD/%	R	RSD/%	R	RSD/%
11.9	NIS	0.44(0.96)	4.3	0.39(0.85)	15.6	0.46(1.0)	7.2
(5.5)	IS	0.91	5.8	0.92	13.4	0.99	5.8
58.8	NIS	0.48(1.04)	9.6	0.46(1.0)	5.1	0.49(1.06)	16.4
(27.0)	IS	0.99	7.3	0.98	5.4	1.02	12.0
107	NIS	0.47(1.02)	9.3	0.46(1.0)	3.5	0.46(1.0)	5.4
(49.2)	IS	0.98	7.5	0.99	3.7	0.99	8.9

NB Values in parentheses refer to the actual concentrations and mean recovery factors when the difference in uptake rate between organic and aqueous phases is taken into account.

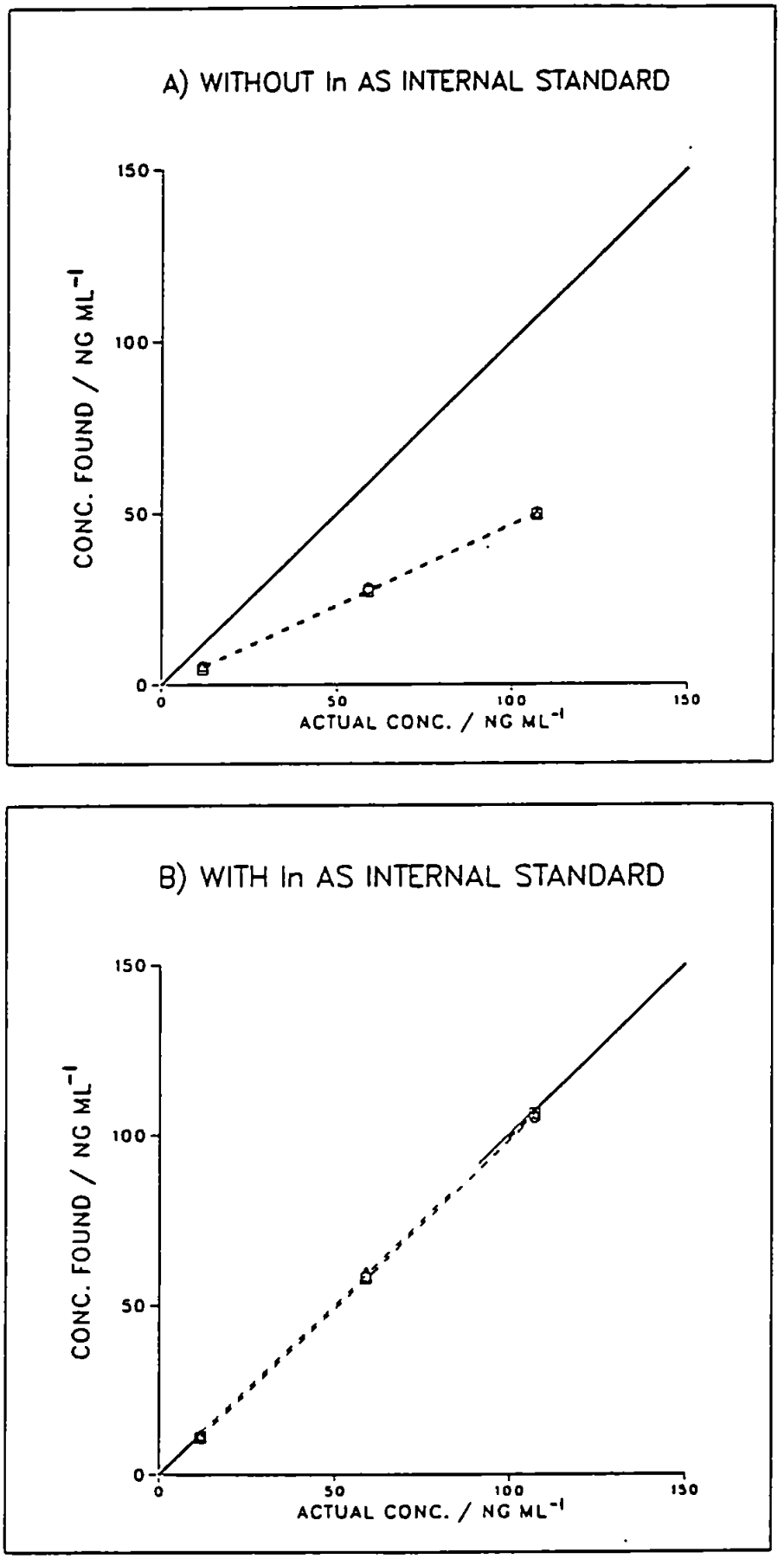

Figure 4.5 Actual concentration vs concentration found in samples of propan-2-ol using the 'dual uptake II' method for the elements: ^{59}Co (O); ^{139}La (□); and ^{208}Pb (Δ), with and without In as an internal standard

The instrument software also facilitated the use of more than one internal standard. The mode of operation was much like that employed for semi-quantitative calibration. For instance if the internal standards Sc, In and Pt are used, a semi-quantitative calibration can be plotted for the signals of the major isotopes at 45, 115 and 195 m/z units respectively. It is then possible to extrapolate from the curve to effectively obtain an internal standard signal for the analyte isotope of interest and ratio this to the analyte signal, thereby achieving internal standardisation at any specific m/z unit. The disadvantage of this approach is that it takes no account of first ionisation potential, only mass. Results are shown in Fig. 4.6 as plots of 'actual' versus 'found' concentration as before, using Sc, In and Pt as internal standards using the isotopes at 45, 115 and 195 m/z units respectively. Fig. 4.6 indicates that La and Pb showed good recoveries, even though a little high, while the recovery for Co was very low. The reason for the low Co recovery is that at 45 m/z units a large signal also arises from the polyatomic species $^{12}CO_2H^+$ and/or $^{13}CO_2^+$, which swamps that due to $^{45}Sc^+$ and results in the Sc internal standard being rendered ineffectual. Recoveries for La and Pb were less affected because there were no interferences at 115 and 195 m/z units, corresponding to ^{115}In and ^{195}Pt, which primarily influence the portion of the semi-quantitative curve from which extrapolations are made for internal standardisation of ^{139}La and ^{208}Pb isotopes. However, the skewing of the curve caused by the

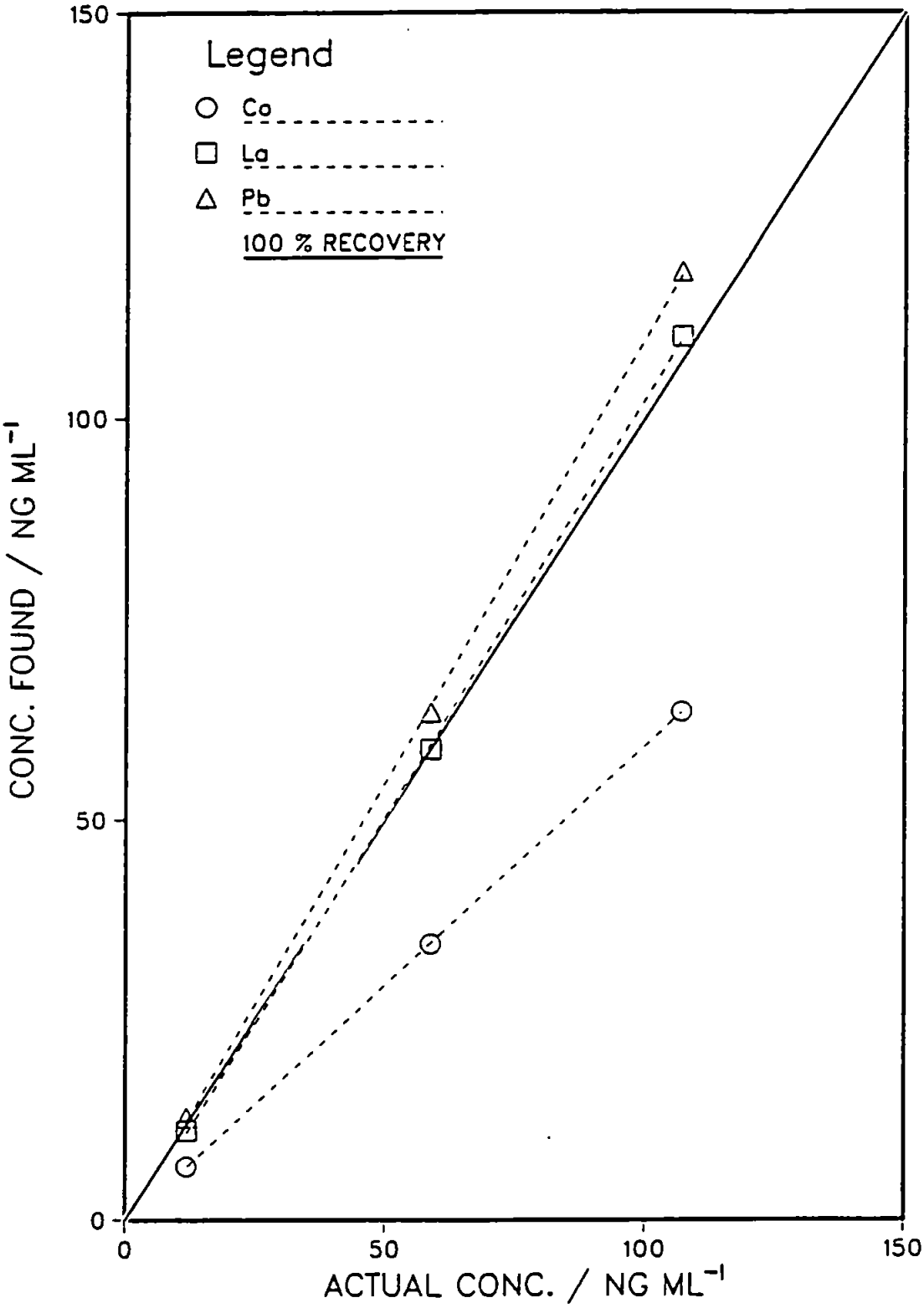

Figure 4.6 Actual concentration vs concentration found in samples of propan-2-ol using the 'dual uptake II' method for the elements: ^{59}Co (O); ^{139}La (□); and ^{208}Pb (Δ), with Sc, In and Pt as internal standards

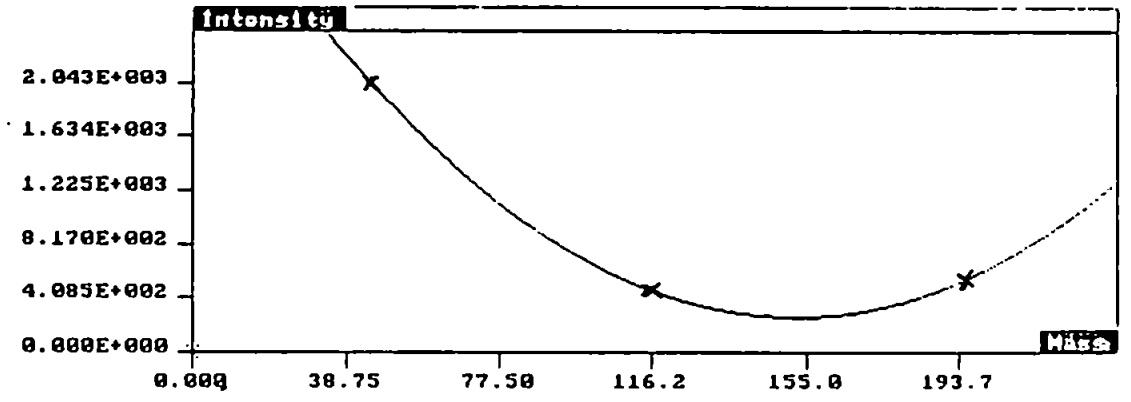

Figure 4.7 Semi-quantitative calibration curve calculated using the 'dual uptake II' method and the elements ^{45}Sc, ^{115}In, ^{195}Pt

interference at 45 m/z units does have some effect (Fig. 4.7) resulting in a relatively poor performance when using Sc, In and Pt as internal standards compared to In alone. Unfortunately the choice of internal standard is limited at the low mass range, Sc being the only element not likely to be present in most samples. However, the performance of In as the sole internal standard has been shown to be adequate.

4.2.6 Conclusions

Matrix effects caused by an organic solvent were compensated for by internal standardisation provided the external standard and analyte elements were closely matched with respect to mass and first ionisation potential. These matrix effects were eliminated by employing a novel method of sample introduction,and by using In as an internal standard to compensate for the difference in uptake rates between aqueous and organic phases. The most effective method was to mix the two phases prior to the peristaltic pump, thereby achieving matrix matching of standards and samples and a slight improvement in precision when using an internal standard.

CHAPTER 5

SIMPLEX OPTIMISATION OF PLASMA OPERATING CONDITIONS FOR ICP-MS USING TWO TYPES OF TORCH

5.1 Introduction

Reports of "optimisation" studies for ICP-MS (39, 40, 120, 121) have been confined to investigations of various individual operating parameters on performance. Whereas "optimisation" studies for ICP-AES generally use either signal-to-background or signal-to-noise ratio as the criterion of merit, due to the relatively large variations in continuum background with operating conditions, "optimisation" studies for ICP-MS generally use maximum signal counts as the criterion of merit due to the very low continuum background signals associated with the technique. More importantly, from the point of view of ICP-MS, is the need to optimise the instrument for maximum signal while at the same time minimising potential interferences such as doubly charged, oxide and various other polyatomic ions.

Several sets of workers have "optimised" plasma operating conditions, and even ion lense voltages, for the two main commercially available systems, namely the Sciex Elan (39, 121) and the VG PlasmaQuad (40, 120). They "optimised" the systems for maximum analyte signal using univariate "optimisation" techniques, and subsequently chose operating conditions which gave large analyte signals but also minimal signals due to doubly charged and polyatomic

ions. In general it was found that the same set of operating conditions could be used for different elements with widely differing masses, ionisation potentials and chemistries, and that the operating conditions which yielded best analyte signals almost always coincided with the conditions at which doubly charged and oxide ions were at relatively low levels. The trends observed for the two different instruments were broadly similar, however, differences have been noted in the behaviour of doubly charged ions (120), probably due to important differences in design of the load coil, interface and ion lenses. All workers identified the most important parameters to be nebuliser gas flow, foward power and sampling depth.

The "optimisation" studies mentioned above have been applied to ICP-MS systems operating with standard components, and the preferred "optimisation" technique has been to carry out a series of univariate searches. As has already been shown for ICP-AES, in Chapter 2, a more rigorous optimisation regime is necessary for instrumental systems that have operating parameters which are interdependent variables. In comparison to ICP-AES little is known about the response surfaces of various criteria of merit for ICP-MS since it is a relatively new technique. This is especially true when modifications are made to standard components. Since a comparison between ICP-MS systems with modifications can only be valid if each system is operating under optimum conditions, a multivariate optimisation technique such as simplex

optimisation is necessary to locate the true optima. In this work simplex optimisation was used to optimise the plasma operating conditions of an ICP-MS instrument using both a standard Fassel torch and a low-flow torch. Low-flow torches have been shown to allow more stable plasma operation for ICP-AES (70). It has been observed in this laboratory (122) that stable operation of the plasma is more difficult for ICP-MS compared to ICP-AES on introduction of an organic solvent, probably because of the close association between the plasma and sampling interface in the former instrument. Therefore, a low flow torch may have certain advantages over the standard torch in ICP-MS for the introduction of organic solvents.

Gordon et al. (123) have "optimised" a water cooled low-flow torch for ICP-MS using a univariate "optimisation" technique, and arrived at "optimum" operating conditions of: plasma gas, 2.1 l min^{-1}; nebuliser gas 0.20 l min^{-1}; forward power 1100 W. Using this torch they observed analyte signals comparable with the standard torch, a reduction in metal oxides and the argon dimer, and an increase in doubly charged ions and plasma potential in comparison with the standard torch. However, since their optimisation took no account of the dependent nature of the variables such conclusions may or may not be rigorously valid.

Simplex optimisation has so far not been applied to ICP-MS except for the optimisation of ion optics (124). Hence,

it was considered that a more rigorous multivariate optimisation of plasma operating conditions was long overdue. In this work plasma operating conditions, using both a standard torch and a low-flow torch, have been optimised using simplex optimisation, and the two torches subsequently evaluated with regard to plasma stability for the introduction of volatile organic solvents.

5.2 Experimental

5.2.1 Instrumentation

All experiments were performed using an inductively coupled plasma - mass spectrometer (VG PlasmaQuad 2, VG Elemental, Winsford, Cheshire, U.K.) described in Section 4.2.1. Torch dimensions are given in Table 5.1. The low-flow torch differed from the standard torch in that the spacing between the intermediate and outer tubes, and the internal diameter of the injector tube were smaller in the former. Additionally, the inlet tubes for the auxilliary (intermediate) and coolant (outer) gases were constricted in the low-flow torch, thereby increasing the velocity of these gases through the intermediate and outer tubes respectively. A standard Meinhardt nebuliser was used in conjunction with the low-flow torch, and a v-groove nebuliser (Ebdon nebuliser, PS Analytical, Sevenoaks, Kent, U.K.) with the standard torch.

5.2.2 Simplex Optimisation Parameters

The parameters which were optimised are listed in Table 5.2, with the ranges over which optimisation experiments

Table 5.1 Dimensions of the standard and low-flow torches used in this work

		Standard torch	Low-flow torch
Injector tube	i.d./mm	1.6	1.0
Intermediate tube	o.d./mm	15.6	16.6
Outer tube	i.d./mm	20.4	20.4
	o.d./mm	18.0	18.0
Configuration factor		0.77	0.81
Gas inlets	i.d./mm	6	2

Table 5.2 Boundary limits of parameters studied during the simplex optimisation

Parameter	Range	
	Standard torch	Low-flow torch
Nebuliser gas/l min^{-1}	0.200 - 1.250	0 - 0.800
Auxilliary gas/l min^{-1}	0 - 2.5	0 - 2.0
Coolant gas/l min^{-1}	11 - 18	6 - 10
Forward power/W	900 - 1800	500 - 900

were conducted. The sampling depth was not included because adjustment of this parameter caused arcing between the torch box and sampling cone. The sampling depth was maintained at 10.75 and 11.50 mm for the standard and low-flow torches respectively, and the spray chamber was maintained at +2°C.

Simplex optimisation experiments were performed using a software package developed previously (88) and run on a microcomputer (Apple IIe, Apple Computer Inc., Cupertino, California, USA). The signal for In^+, in area counts s^{-1}, at 115 m/z units was taken as the criterion of merit. Whenever operating conditions were altered the ion lenses, namely the extraction, collector, L1, L2, L3, L4, and the pole bias were re-adjusted to obtain the maximum signal. Additionally, the position of the torch in the x, y and z axes was re-adjusted to obtain maximum signal. This was particularly critical for the low-flow torch due to the small internal diameter of the injector tube.

After each optimisation univariate searches were performed for each parameter in turn while holding the others at the optimum established by the simplex procedure.

5.2.3 Mass Spectrometer Operating Conditions

The mass spectrometer was operated in survey scanning mode throughout. Data acquisition parameters are listed in Table 5.3.

Table 5.3 Data acquisition parameters used in survey scanning mode

Mass range/m/z	8.0 - 215.5
No. of channels	2048
No. of scan sweeps	100
Dwell time/μs	320
Time per scan/s	65.5
No. of scans	1

5.2.4 Reagents and Standards

A multielement standard solution of Be, Co, In, Ba and Pb, 100 ng ml^{-1}, was prepared by dilution of a 10 μg ml^{-1} multielement stock solution using 2 + 98 (v/v) nitric acid (Aristar, BDH Chemicals Ltd.) in deionised double-distilled water. All multielement stock solutions were made up using single element standard solutions (Spectrosol, BDH Chemicals Ltd. or Alfa Chemical Co. Inc.).

A semi-quantitative determination of trace elements in organic samples diluted in xylene was also performed. For semi-quantitative calibration a multielement solution of Li, Co, In, Ba and Pb, 100 ng ml^{-1}, was prepared by dilution of a 10 μg ml^{-1} multielement stock solution using xylene (Aristar, BDH Chemicals Ltd.). The multielement stock solution was prepared by diluting single element standard solution of the cyclohexylbutyrate salts of the metals (BDH Chemicals Ltd.) in xylene for Li, Co, Ba and Pb, and a 1000 μg ml^{-1} solution of In in xylene (Alfa Chemical Co. Inc.).

5.3 Results and Discussion

Optimisation experiments were completed in between 25 - 30 steps. The only problem encountered was that caused by extreme sets of operating conditions at the boundary limits, which made tuning of the ion lenses unreproducible. Table 5.4 shows the optimum conditions established for the standard and low-flow torches.

Table 5.4 Optimum operating conditions established for the standard and low-flow torches

	Optimum conditions	
	Standard torch	Low-flow torch
Nebuliser gas/l min^{-1}	0.842	0.670
Auxilliary gas/l min^{-1}	0.8	1.6
Coolant gas/l min^{-1}	11.5	6.8
Forward power/W	1583	865

Univariate searches at the established optimum conditions for analyte signal, Ba^{2+}/Ba^{+} ratio, BaO^{+}/Ba^{+} ratio, ArO^{+}, ArN^{+} and $ArAr^{+}$ are shown in Figs. 5.1 - 5.15.

The vertical arrows on the figures indicate the optima determined by the simplex procedure, and the error bars represent the range of the final simplex. The effects of the different operating parameters on various criteria are discussed below.

5.3.1 Effect of Operating Parameters

5.3.1.1 Nebuliser Gas

The effect of nebuliser gas flow on analyte signal for the elements Be, Co, In, Ba, and Pb using the isotopes at 9, 59, 115, 138 and 208 m/z units respectively is shown in Fig. 5.1A for the standard torch and Fig. 5.1B for the low-flow torch. It should be remembered that the optimisation was performed using In^{+} response as the criterion of merit, hence the vertical arrows indicate the optimum conditions for this element only. The simplex procedure located the optimum successfully for both torches. However, in the case of the standard torch (Fig. 5.1A) Be^{+} and Co^{+} signals peaked at higher nebuliser gas flow rates than In^{+}, and Ba^{+} and Pb^{+} signals peaked at slightly lower flow rates, the trend being that the lower the mass the higher the nebuliser gas flow that was required for maximum signal. Gray and co-workers (40, 125) have shown that plasma potential and ion energies for elements of different mass are dependent on the nebuliser

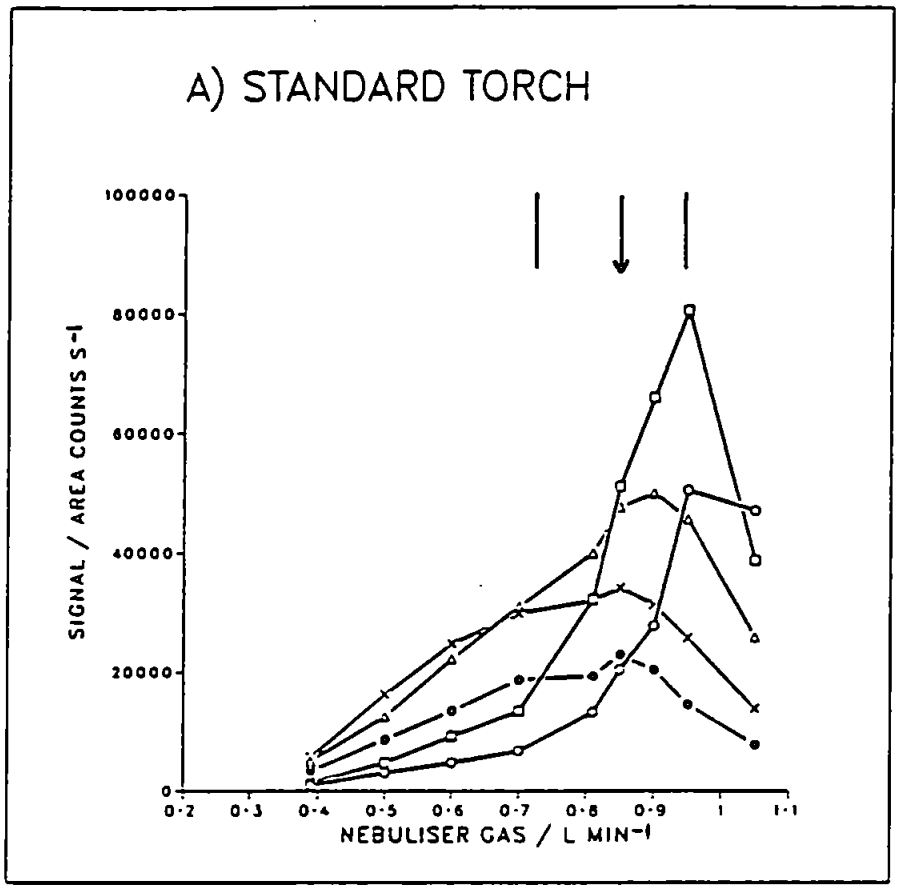

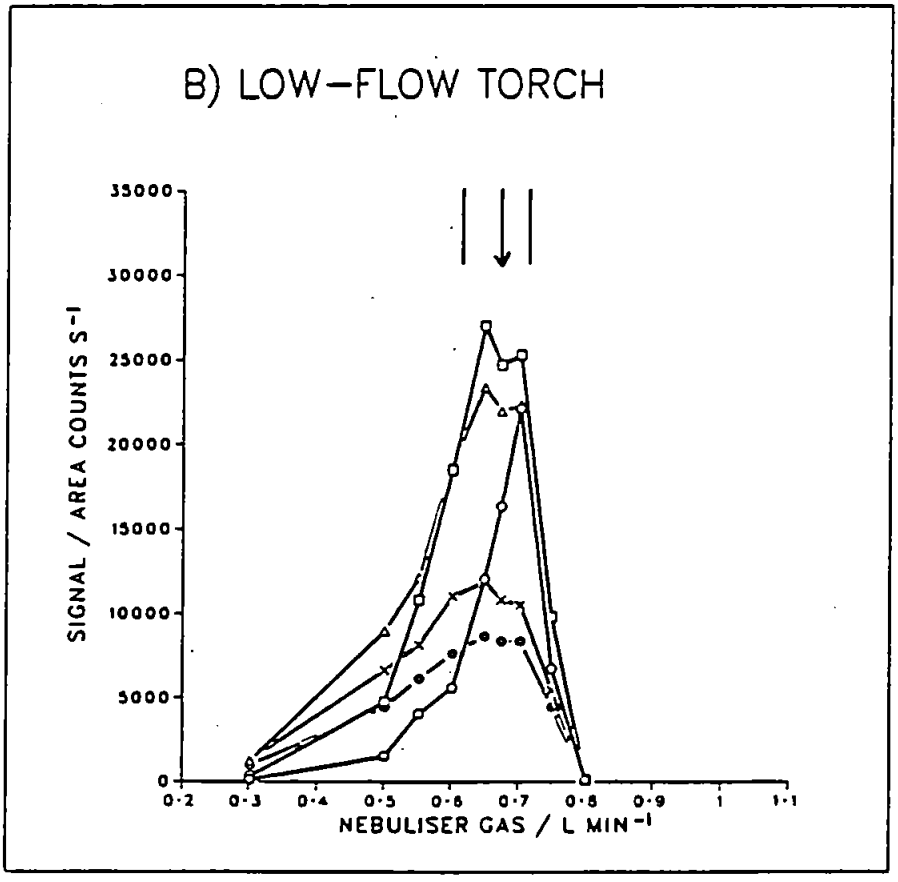

Figure 5.1 Effect of nebuliser gas flow on signals for: $^{9}Be^{+}$ (O); $^{59}Co^{+}$ (□); $^{115}In^{+}$ (Δ); $^{138}Ba^{+}$ (X); and $^{208}Pb^{+}$ (O), using the standard and low-flow torches

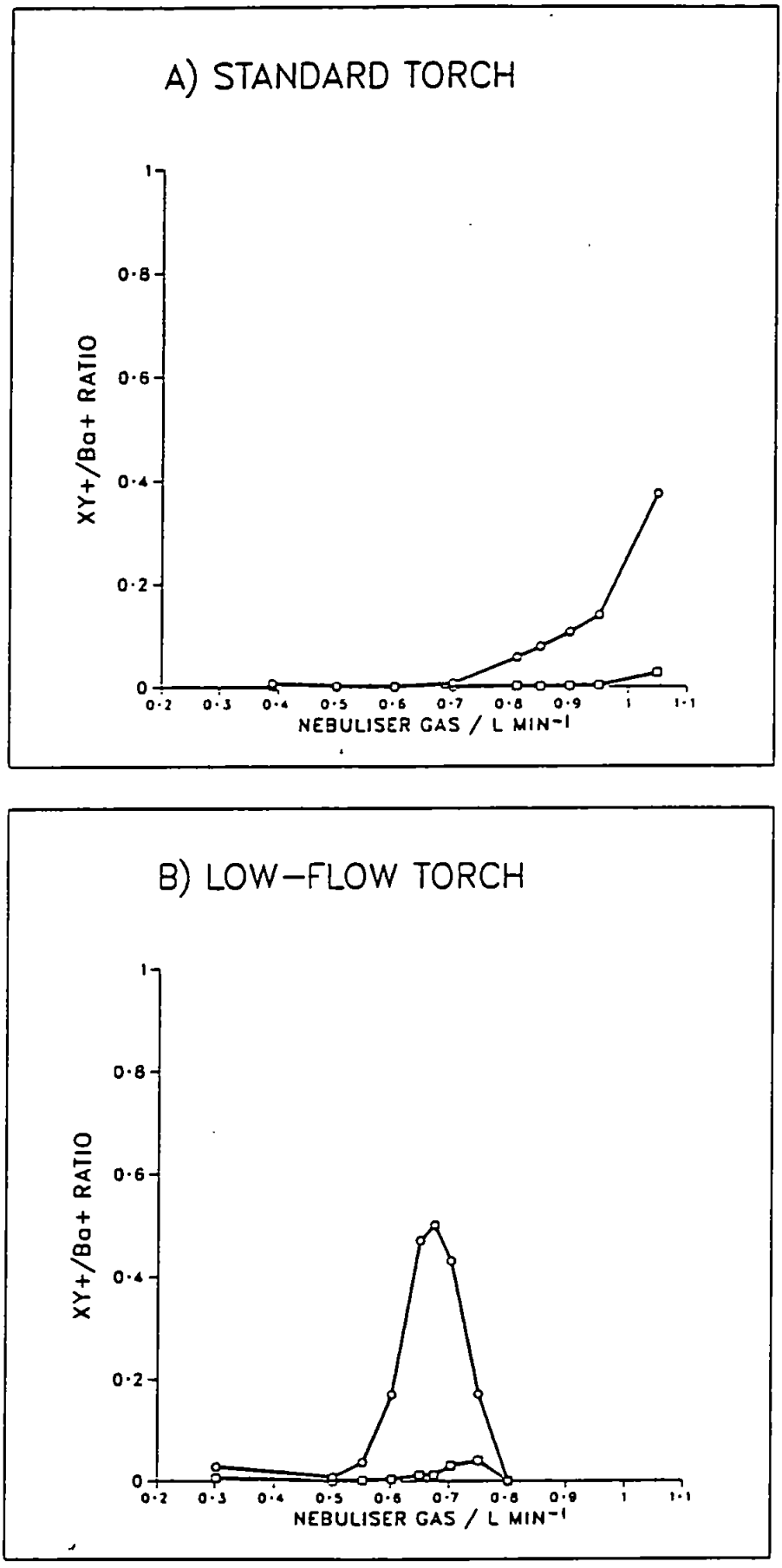

Figure 5.2 Effect of nebuliser gas flow on the ratios for: Ba^{2+}/Ba^{+} (O); and BaO^{+}/Ba^{+} (□), using the standard and low-flow torches

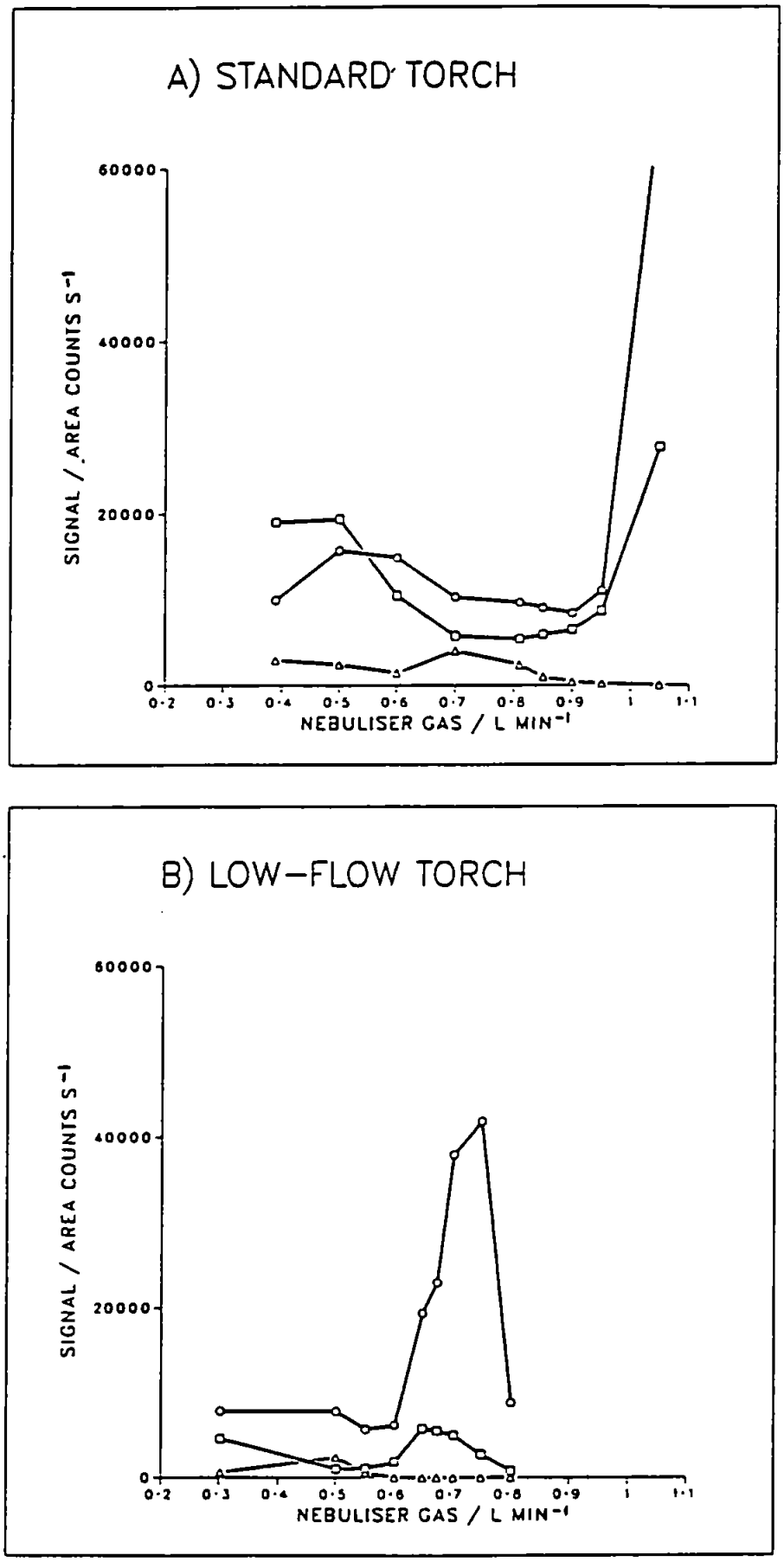

Figure 5.3 Effect of nebuliser gas flow on the signals for: ArO^+ (O); ArN^+ (□); and $ArAr^+$ (Δ), using the standard and low-flow torches

gas flow and forward power, at least in the VG PlasmaQuad instrument for which plasma potentials between +5 to +20V are common. A consequence of this is that certain sets of operating conditions may result in ion energies which vary across the mass range, making it difficult to optimise the ion lenses to achieve uniform response for elements of different mass. This may be the cause of the trends observed and shown in Fig. 5.1A since the ion optics were optimised for In^+ only. These results differ from those of Gray and Williams (40) who found that one nebuliser gas flow was optimum for elements of different mass. One explanation for this may be that they performed experiments at 1300 W forward power whereas this work was performed at 1583 W forward power found as optimum. Douglas and French (126) have suggested that ion energies vary considerably more than those reported by Gray and Williams due to an artifact caused by measuring the energies of the ions after the ion optics, which act as a filter for ions of the same energy.

For the low-flow torch, with the exception of Be, all elements exhibited maximum signals at more or less the same nebuliser gas flow (Fig. 5.1B). Gordon et al. (123) have postulated that the plasma potential is greater in plasmas operated at low flows, with a consequent increase in ion energies. However, as long as the spread in ion energies for elements of different masses is small, then one set of ion lens conditions, such as those for In^+, should be optimum for all ions. This seems to be the case

for the low-flow plasma studied in this work, with the exception of Be.

The major effect of a high plasma potential is to increase the amount of doubly charged ions (123, 125). This was the case for the low-flow torch studied in this work, the Ba^{2+}/Ba^{+} ratio showing a peak which coincided with the peaks in analyte signals, and having the high value of about 0.5 at its maximum (Fig. 5.2B). During operation of the low-flow torch what looked like a glow discharge or boundary layer was visible at the sampler orifice. This would also cause large amounts of doubly charged ions to be formed, and might explain why the peak in Ba^{2+}/Ba^{+} ratio closely matched that of analyte signal.

For the standard torch the Ba^{2+}/Ba^{+} ratio was much lower at the optimum nebuliser gas flow (Fig. 5.2A) in comparison with the low-flow torch, but increased as gas flow increased. These results are consistent with those obtained by other workers (40, 120) using a PlasmaQuad instrument with an assymetrically grounded load coil. Gray et al. (125) have shown that as nebuliser gas flow increases so does the plasma potential, resulting in an increase in the amount of doubly charged ions, a decrease in ArO^{+}/Co^{+} and $ArAr^{+}/Co^{+}$ ratios and a slight decrease in CeO^{+}. For the Elan instrument with a centre tapped load coil the Ba^{2+}/Ba^{+} ratio decreases with nebuliser gas flow (39). The behaviour is different in this instrument because the plasma potential is relatively low (127), i.e.

+0.5 to -3.5 V, and less dependent on operating conditions.

For both torches the BaO^+/Ba^+ ratios were low at optimum nebuliser gas flows (Fig. 5.2A and B) and therefore present no problems. The BaO^+/Ba^+ ratio increased slightly at high gas flow for the standard torch (Fig. 5.2A) in agreement with Gray and Williams (40), and the ratio showed a small peak at 0.75 l min^{-1} for the low-flow torch (Fig. 5.2B) which could have been due to an increase in the amount of O^+ at this gas flow.

The effect of nebuliser gas flow on ArO^+, ArN^+ and $ArAr^+$ is shown in Fig. 5.3. For the standard torch the trends exhibited in Fig. 5.3A agree with those reported by Gray and Williams (40), and show minima at the optimum nebuliser gas flow, though the response for $ArAr^+$ was much lower in this study. In contrast, for the low-flow torch, the ArN^+ and ArO^+ signals peaked at nebuliser gas flows which were the same as and 0.01 l min^{-1} higher respectively than the optimum for In^+ signal (Fig. 5.3B). It is likely that the presence of the O^+ and N^+ precursors influenced the formation of the polyatomic species to the greatest extent, their concentration in the plasma being determined by nebuliser gas flow. However, Douglas and French (126) have calculated that for low-flow argon plasmas a greater proportion of the plasma gas will be sampled through the sampler orifice, possibly leading to greater entrainment of atmospheric gases, which will also

influence ArO^+ and ArN^+ formation. Whatever the case, more work is necessary to determine the mechanisms of formation of these species in a low-flow, low power plasma with a consequently high plasma potential.

The low-flow torch gave rise to a smaller signal for $ArAr^+$ in comparison with the standard torch(Fig. 5.3), though the difference was not great.

5.3.1.2 Forward Power

The effect of forward power on analyte signal is shown in Fig. 5.4 for both torches. With regard to the standard torch (Fig. 5.4A) the simplex procedure has successfully located the optimum forward power for maximum In^+ signal. However, the maximum signals for Be^+ and Co^+ were at lower power, while those for Ba^+ and Pb^+ were at higher power. As observed for nebuliser gas flow the optima were mass dependent, though in this case the order was reversed, i.e. higher masses required higher power for maximum signal. A correlation between power and first ionisation potential can not be made as one would expect those elements with a high first ionisation potential to require higher power, whereas this was not the case (Table 5.5).

A disparity in ion energies for elements of different masses may again be the cause, as discussed in the previous section, since the ion optics were optimised only for In^+. Gray et al. (125) found that plasma potential, and hence ion energies, increase as nebuliser gas flow is

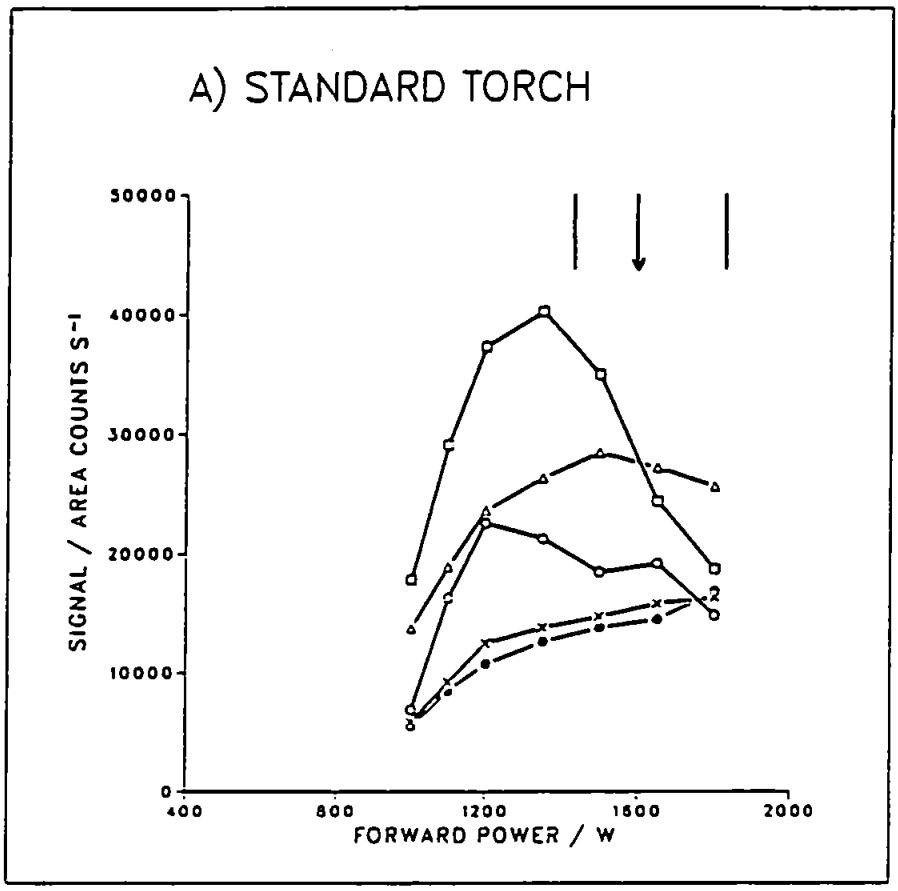

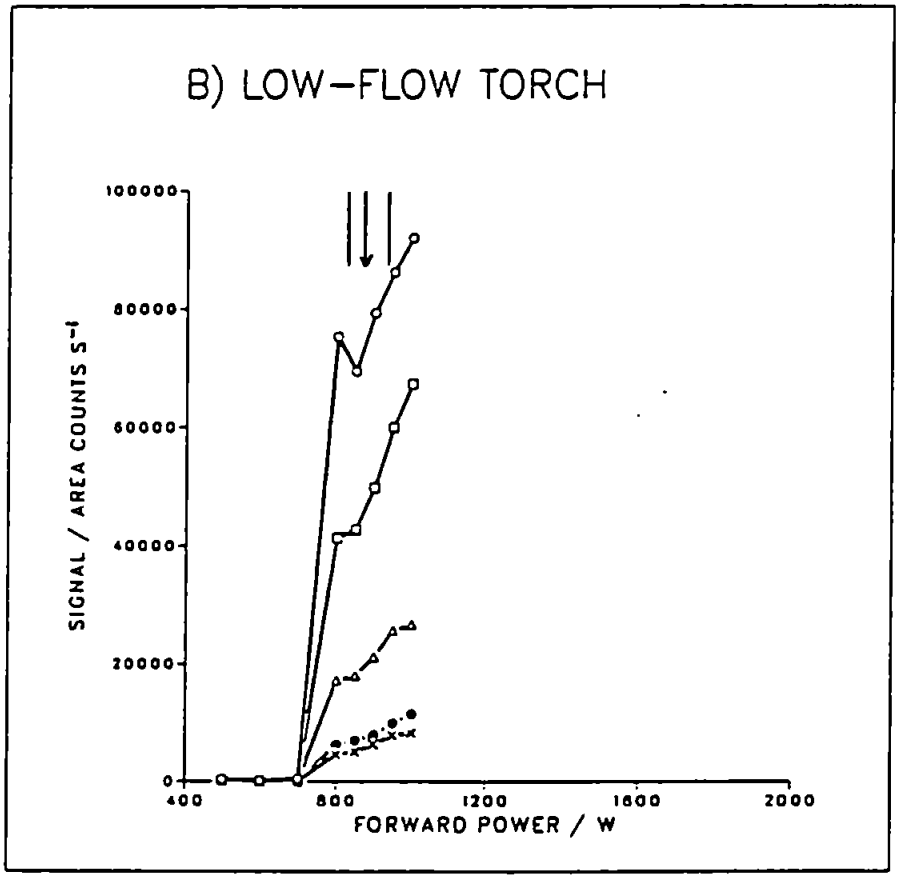

Figure 5.4 Effect of forward power on the signals for: $^{9}Be^{+}$ (O); $^{59}Co^{+}$ (□); $^{115}In^{+}$ (Δ); $^{138}Ba^{+}$ (X); and $^{208}Pb^{+}$ (●), using the standard and low-flow torches

Table 5.5 Masses of the major isotopes (M), first ionisation potentials (I1) and apparent optimum powers (P_{opt}) for the elements studied

Element	M	I1/V	P_{opt}/W
Be	9	9.32	1300
Co	59	7.86	1350
In	115	5.79	1583
Ba	138	5.21	>1800
Pb	208	7.42	>1800

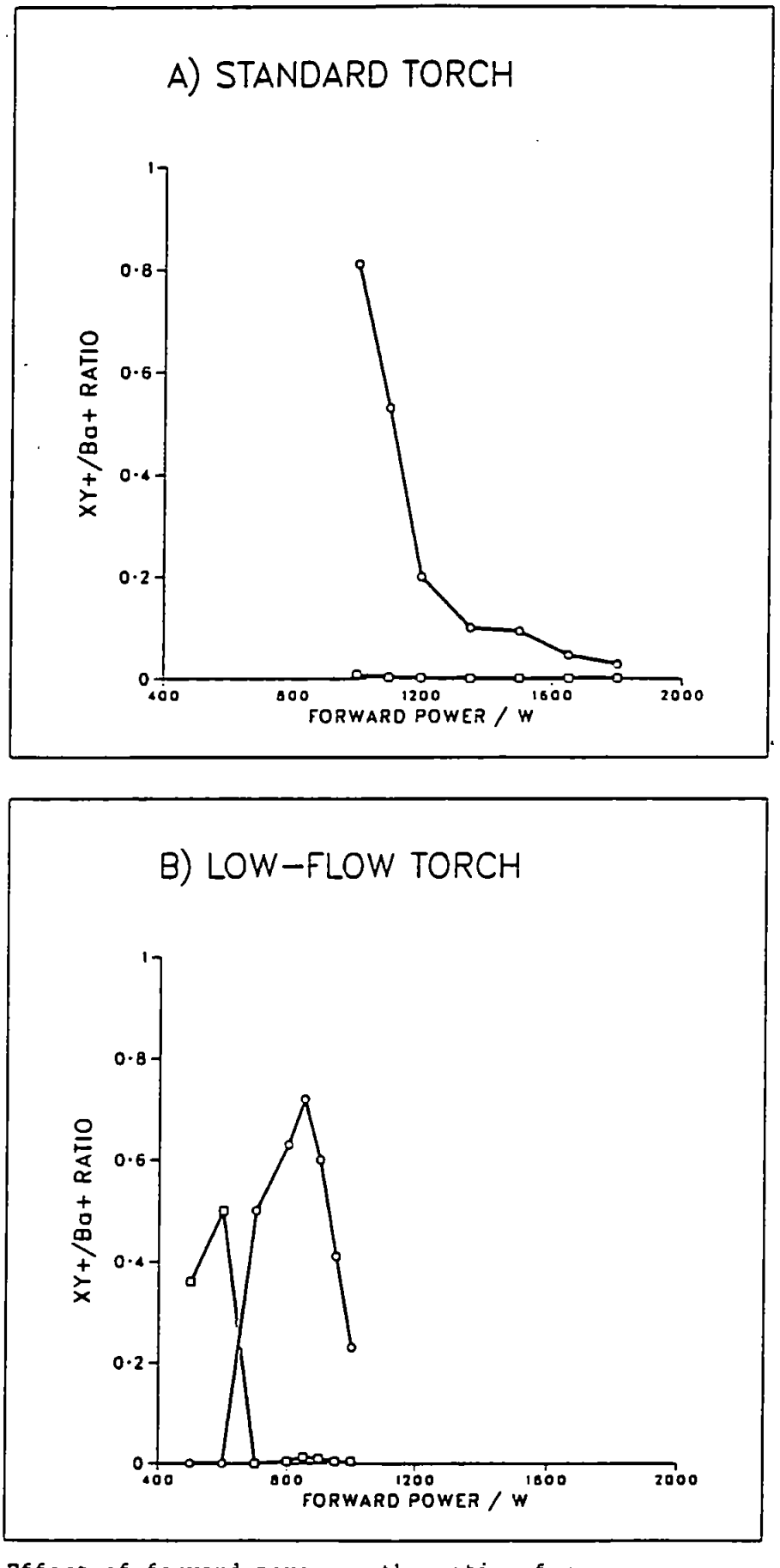

Figure 5.5 Effect of forward power on the ratios for: Ba^{2+}/Ba^{+} (O); and BaO^{+}/Ba^{+} (□), using the standard and low-flow torches

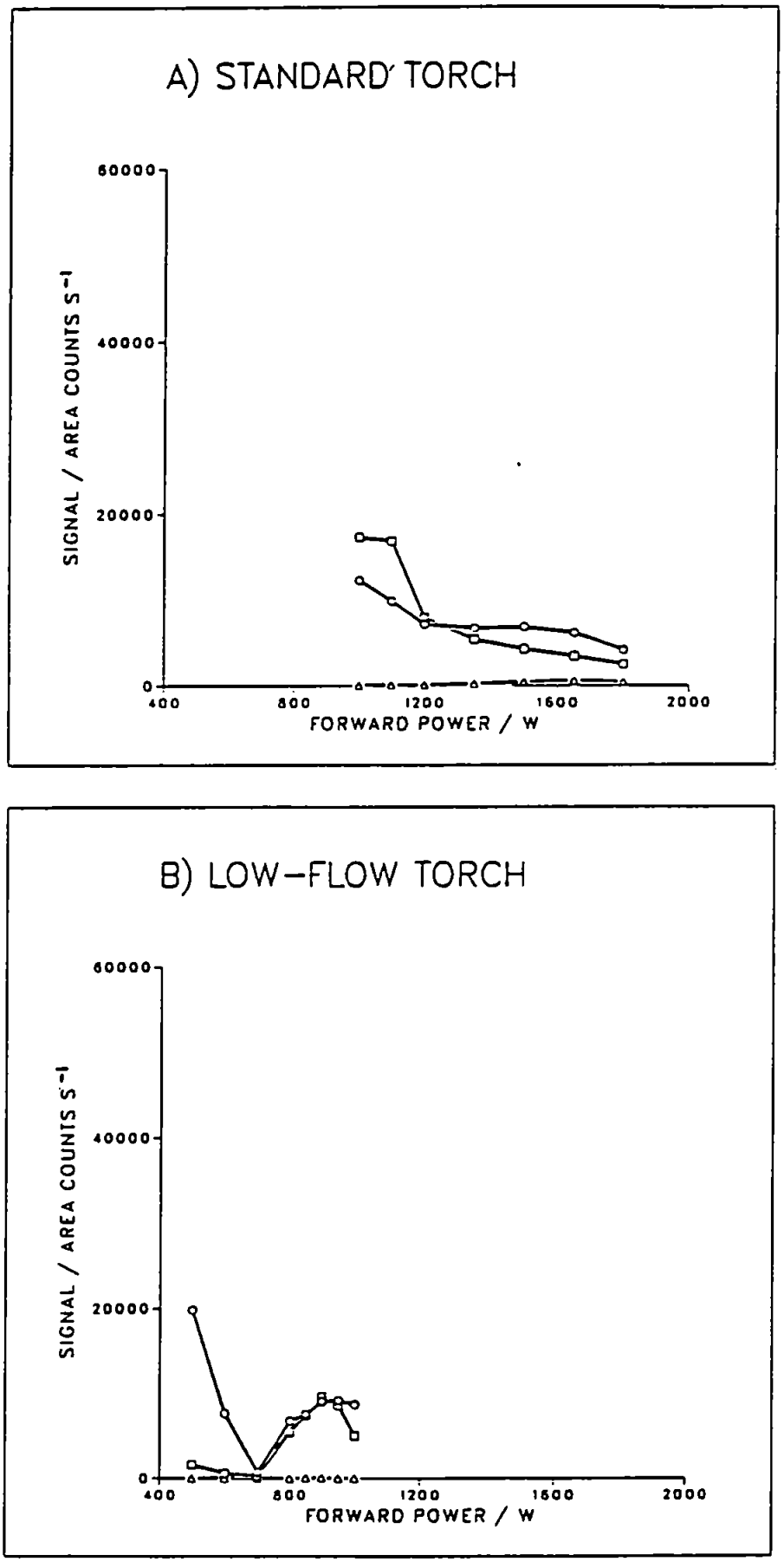

Figure 5.6 Effect of forward power on the signals for: ArO^+ (O); ArN^+ (□); and $ArAr^+$ (Δ), using the standard and low-flow torches

increased but decrease as power is increased. Bearing this in mind the trends in mass dependent optima for nebuliser gas flow and power support each other. Taking Pb as an example, for one particular nebuliser gas flow or forward power Pb^+ ions will have a greater energy than In^+ ions due to the mass dependent acquisition of kinetic energy in the expansion region. Hence Pb^+ ions with energies required for maximum transmission through ion optics optimised for In^+ will be most prevalent at a lower nebuliser gas flow or a higher power than is optimal for In^+. Such an effect was observed in this work, however since no measurements of ion energy were made such an explanation remains tentative.

In comparison, for the low-flow torch, maximum signal was not obtained for any of the elements, even at the highest power studied (Fig. 5.4B). The simplex procedure located the 'optimum' power for In^+ signal at a lower value than would be regarded as optimum, i.e. the optimisation failed. This was because at a power greater than 1000 W the torch started to melt, requiring a false low response to be input to the computer whenever such a condition arose. This had the effect of causing the simplex to locate an 'optimum' at a lower power. However, the trends exhibited show a similar pattern for all elements, indicating that the discrepancy in ion energies was less pronounced in the low-flow plasma compared to that for the standard torch. The increase in analyte response with increasing power is probably due to a corresponding

increase in ionisation temperature.

For the standard torch the Ba^{2+}/Ba^{+} ratio decreased with increasing power to less than 0.1 at the optimum (Fig. 5.5A) in agreement with the results of Long and Brown (120), and possibly due to a corresponding decrease in plasma potential. The BaO^{+}/Ba^{+} ratio was less than 0.01 at all powers studied.

For the low-flow torch the Ba^{2+}/Ba^{+} ratio exhibited different behaviour, showing a maximum at 825 W (Fig. 5.5B) which coincided with the optimum power for In^{+} signal. The subsequent decrease in the ratio above 825 W could have been due to a corresponding decrease in plasma potential, though this seems unlikely. As mentioned in the previous section a boundary layer or discharge was visible in the sampler orifice during operation, and this may well have had an effect. Gordon et al. (123) observed Ce^{2+}/Ce^{+} ratios of up to 1.0 and a much broader peak profile between 900 - 1400 W using their water cooled low-flow torch, though it was operated at much lower gas flows and was different in design. Evidently it is desirable to operate this particular torch at the maximum power possible to reduce the Ba^{2+}/Ba^{+} ratio, while at the same time improving analyte signals. The BaO^{+}/Ba^{+} ratio was of the order of 0.01 between 800 - 1000 W (Fig. 5.5B), which was the analytically useful power range, and therefore presented fewer problems.

The ArO^+ and ArN^+ signals exhibited contrasting behaviour for the two torches (Fig. 5.6). Whereas for the standard torch the signals for these species decreased with increasing forward power (Fig. 5.6A), for the low-flow torch they decreased to a minimum at 700 W, increased to maxima at 950 W and 900 W respectively, then decreased again (Fig. 5.6B). In the latter case the initial decrease in polyatomic ions may have been due to a reduction in the entrainment of atmospheric gases as the plasma increased in size with increasing power. Subsequently O^+ and N^+ precursors in the nebuliser gas predominated, and the polyatomic ions increased as ionisation temperature increased with power, until the point at which other factors such as ion energy or decomposition had a greater influence. The $ArAr^+$ signal varied very little for both torches over the power ranges studied.

5.3.1.3 Sampling Depth

This parameter was not included in the simplex optimisation but was held constant at 10.75 and 11.5 mm for the standard and low-flow torches respectively. However, univariate searches were undertaken to ascertain whether this parameter had a significant effect on the criteria already mentioned.

Sampling depth had very little effect on analyte signals for either torch (Fig. 5.7), and the trends indicate that the range investigated was well within the zone in the

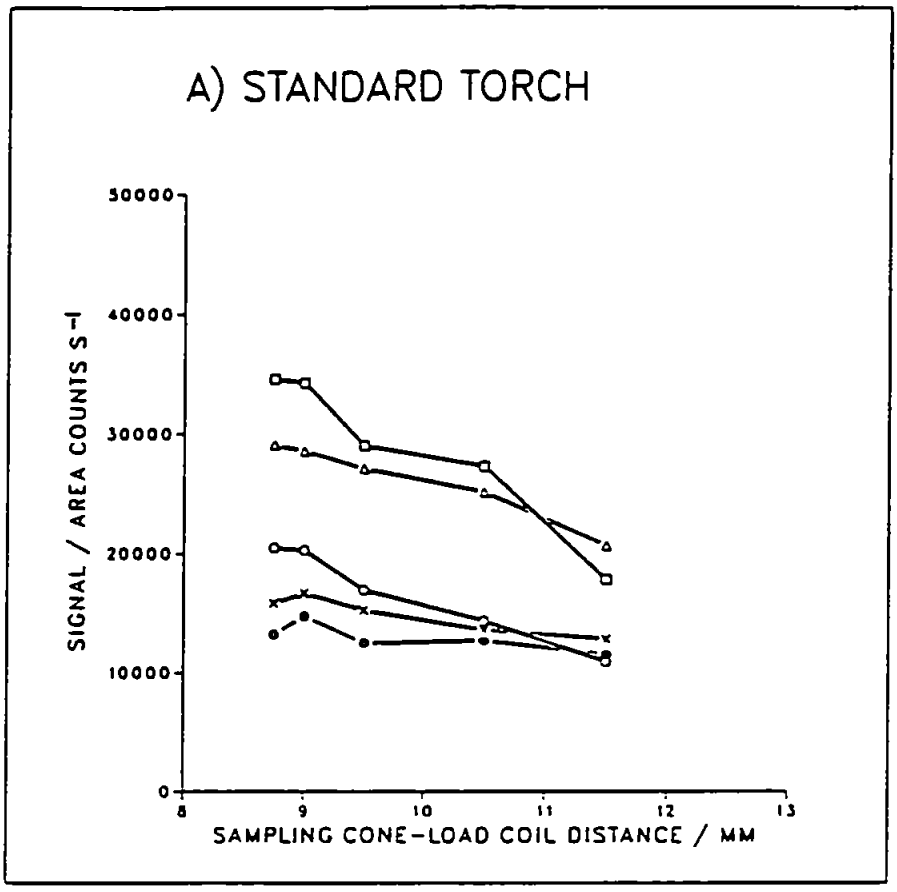

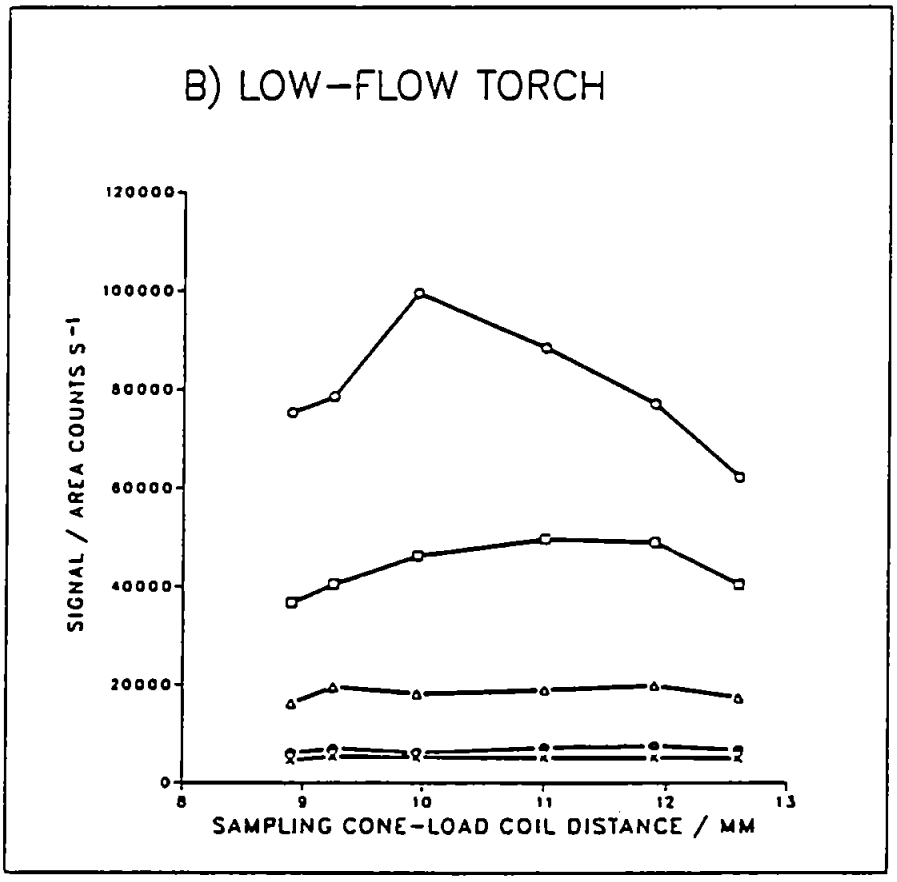

Figure 5.7 Effect of sampling depth on the signals for: $^{9}Be^{+}$ (O); $^{59}Co^{+}$ (□); $^{115}In^{+}$ (Δ); $^{138}Ba^{+}$ (X); and $^{208}Pb^{+}$ (O), using the standard and low-flow torches

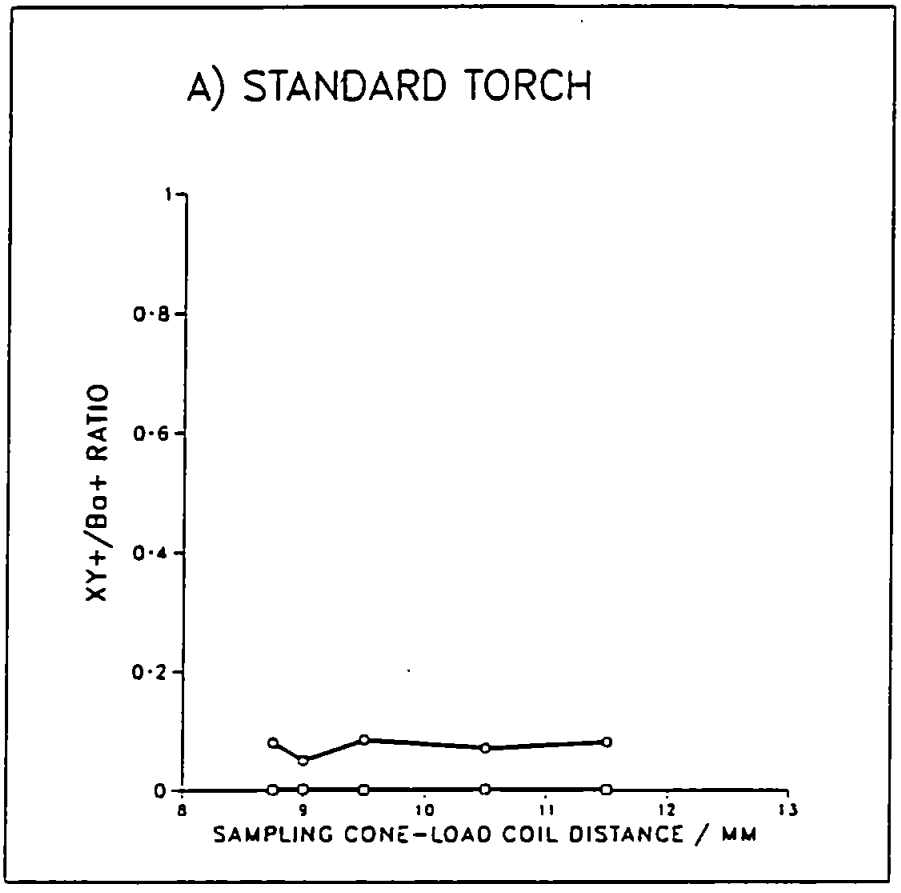

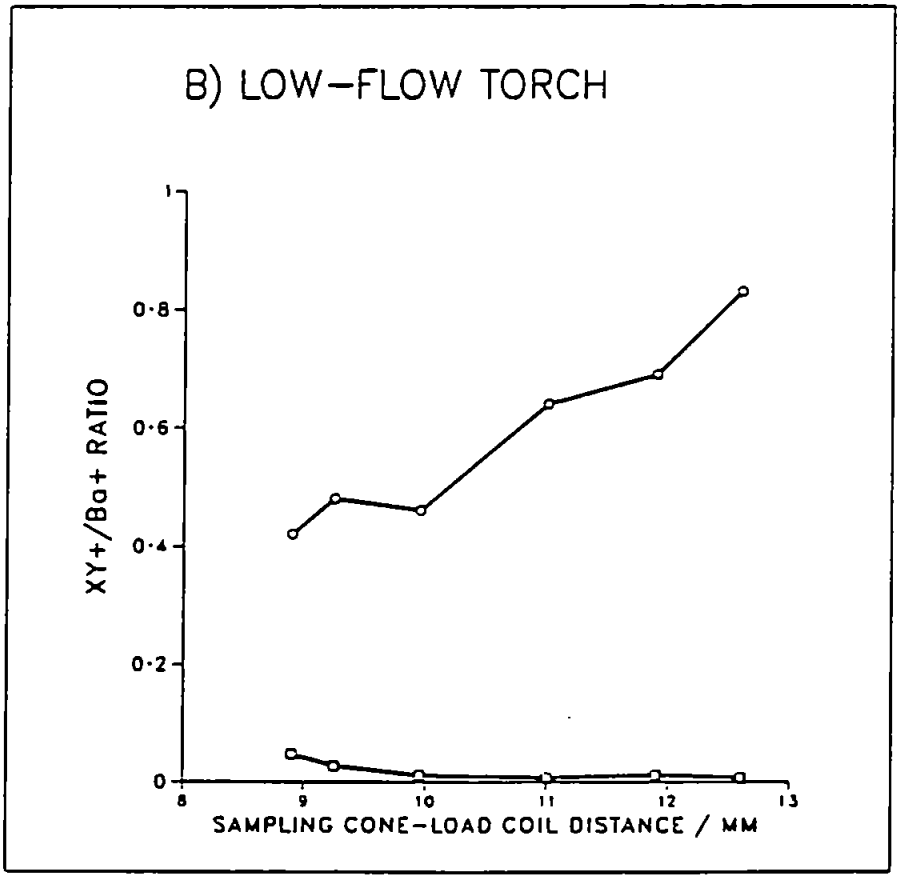

Figure 5.8 Effect of sampling depth on the ratios for: Ba^{2+}/Ba^{+} (O); and BaO^{+}/Ba^{+} (□), using the standard and low-flow torches

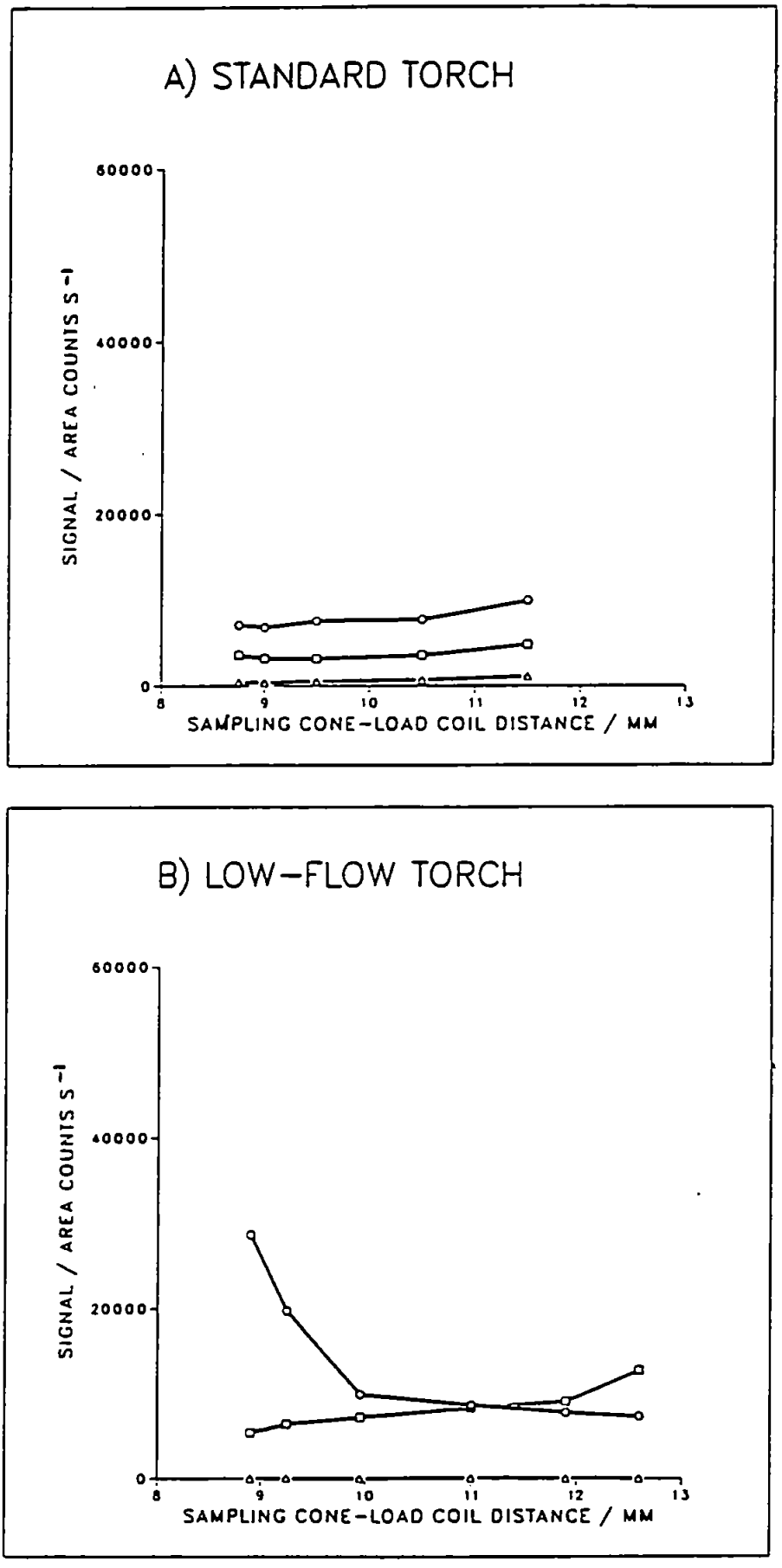

Figure 5.9 Effect of sampling depth on the signals for: ArO^+ (O); ArN^+ (□); and $ArAr^+$ (Δ), using the standard and low-flow torches

plasma between the initial radiation and normal analytical zones where singly charged ion populations are greatest.

Similarly very little change was observed in the Ba^{2+}/Ba^{+} and BaO^{+}/Ba^{+} ratios for either torch (Fig. 5.8), though a steady increase in the $Ba2^{+}/Ba^{+}$ ratio was observed using the low-flow torch as the distance between the sampling cone and the load coil was increased (Fig. 5.8B). This was probably linked to the discharge in the sampler orifice which increased in intensity as the sampling position moved further away from the load coil.

A gradual increase in the signals for ArO^{+}, ArN^{+} and $ArAr^{+}$ was observed as sampling distance from the load coil increased for the standard torch (Fig. 5.9A), probably because ions were sampled from a cooler region of the plasma. The trends exhibited by these ions when using the low-flow torch contrasted greatly (Fig. 5.9B). The signal for ArO^{+} decreased, that for ArN^{+} increased slightly and that for $ArAr^{+}$ remained constant. The contrasting trends for ArO^{+} and ArN^{+} suggest that these ions may be formed by precursors from different sources in the low-flow plasma, O^{+} ions from the nebuliser gas contributing to ArO^{+}, and N^{+} ions from entrained atmospheric gases contributing to ArN^{+}.

5.3.1.4 Auxilliary Gas

The simplex optimisation successfully located the optimum gas flows for both torches. The trends in analyte signals

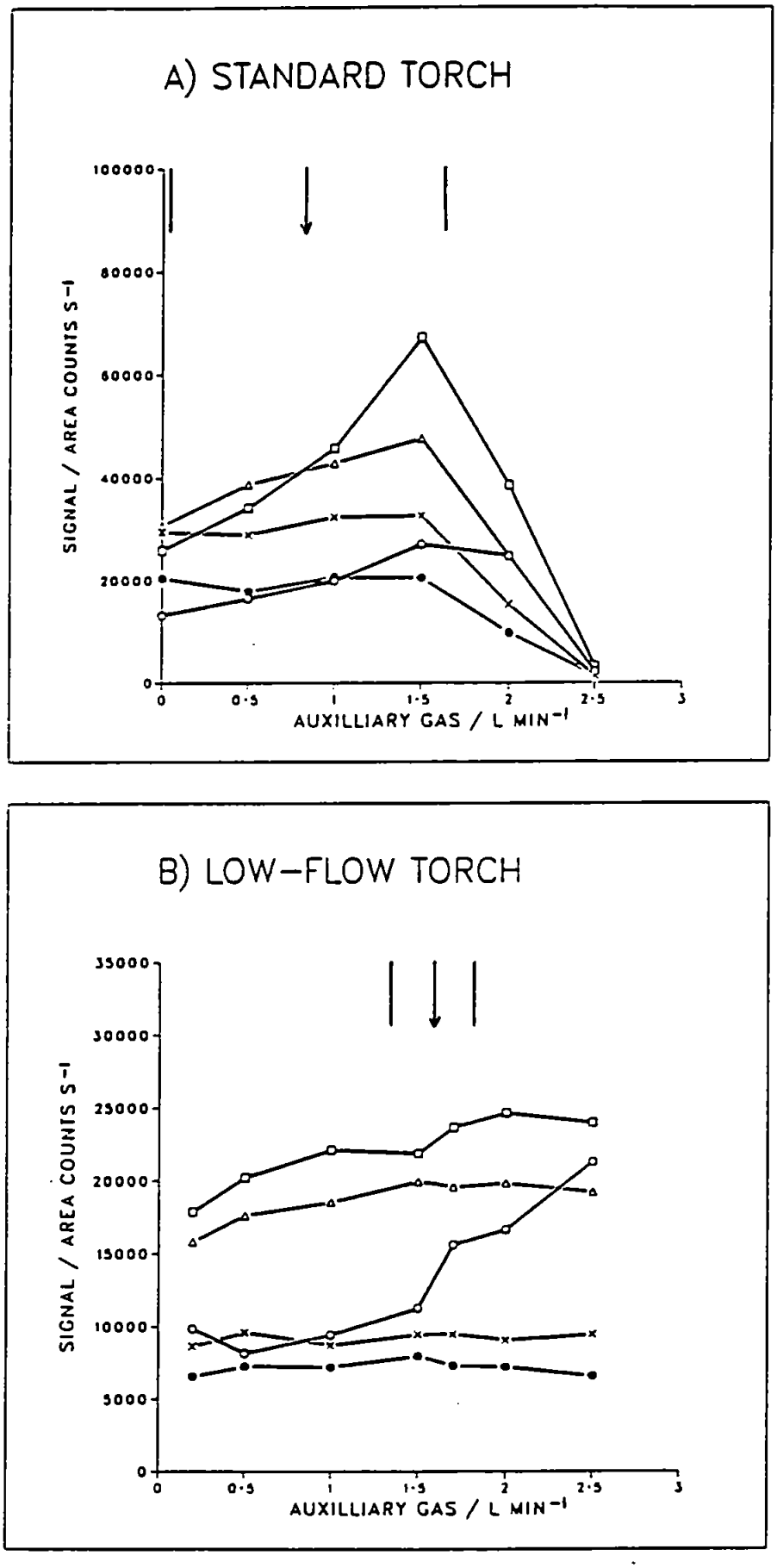

Figure 5.10 Effect of auxilliary gas flow on the signals for: $^{9}Be^{+}$ (O); $^{59}Co^{+}$ (□); $^{115}In^{+}$ (Δ); $^{138}Ba^{+}$ (X); and $^{208}Pb^{+}$ (●), using the standard and low-flow torches

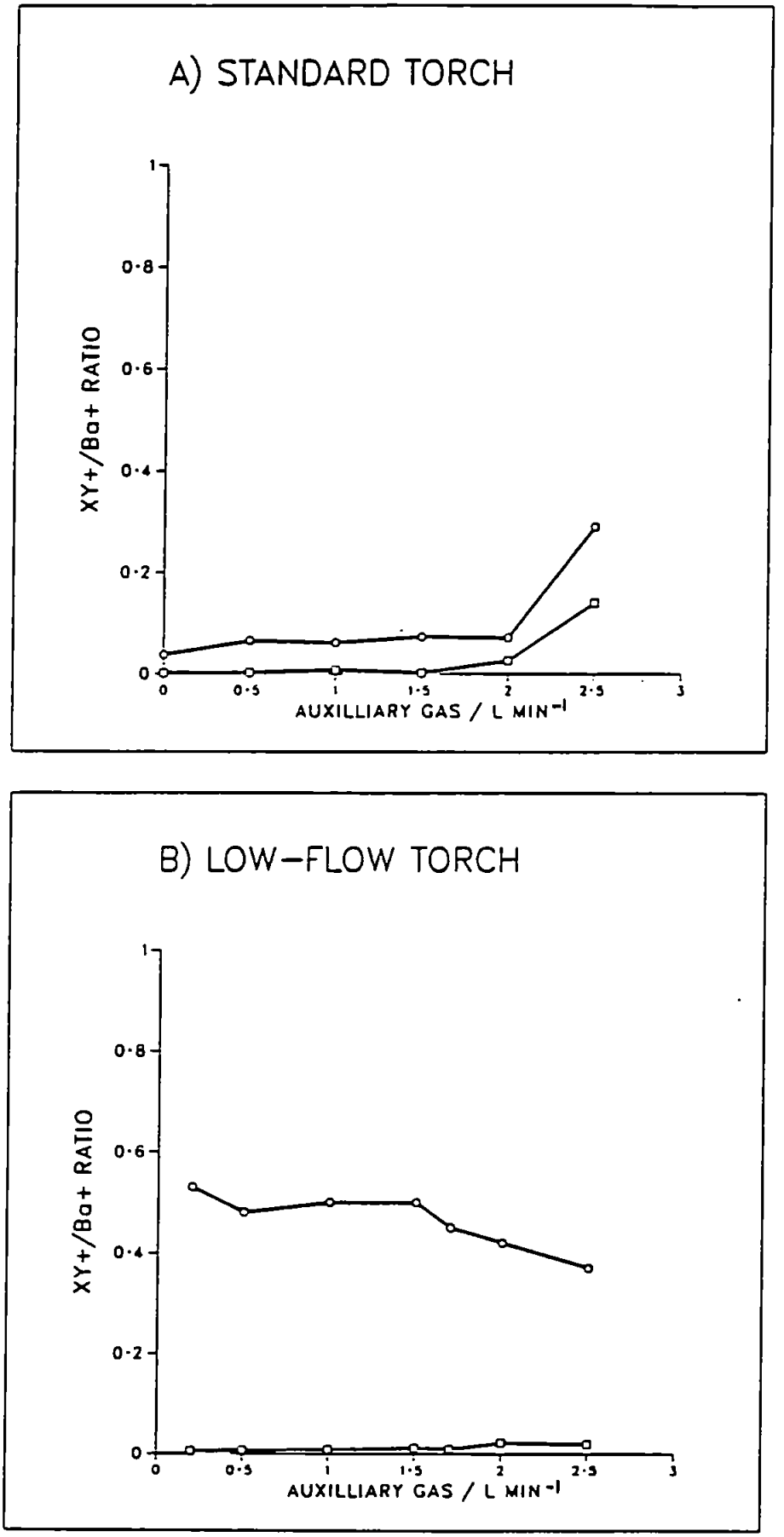

Figure 5.11 Effect of auxilliary gas flow on the ratios for: Ba^{2+}/Ba^{+} (O); and BaO^{+}/Ba^{+} (□), using the standard and low-flow torches

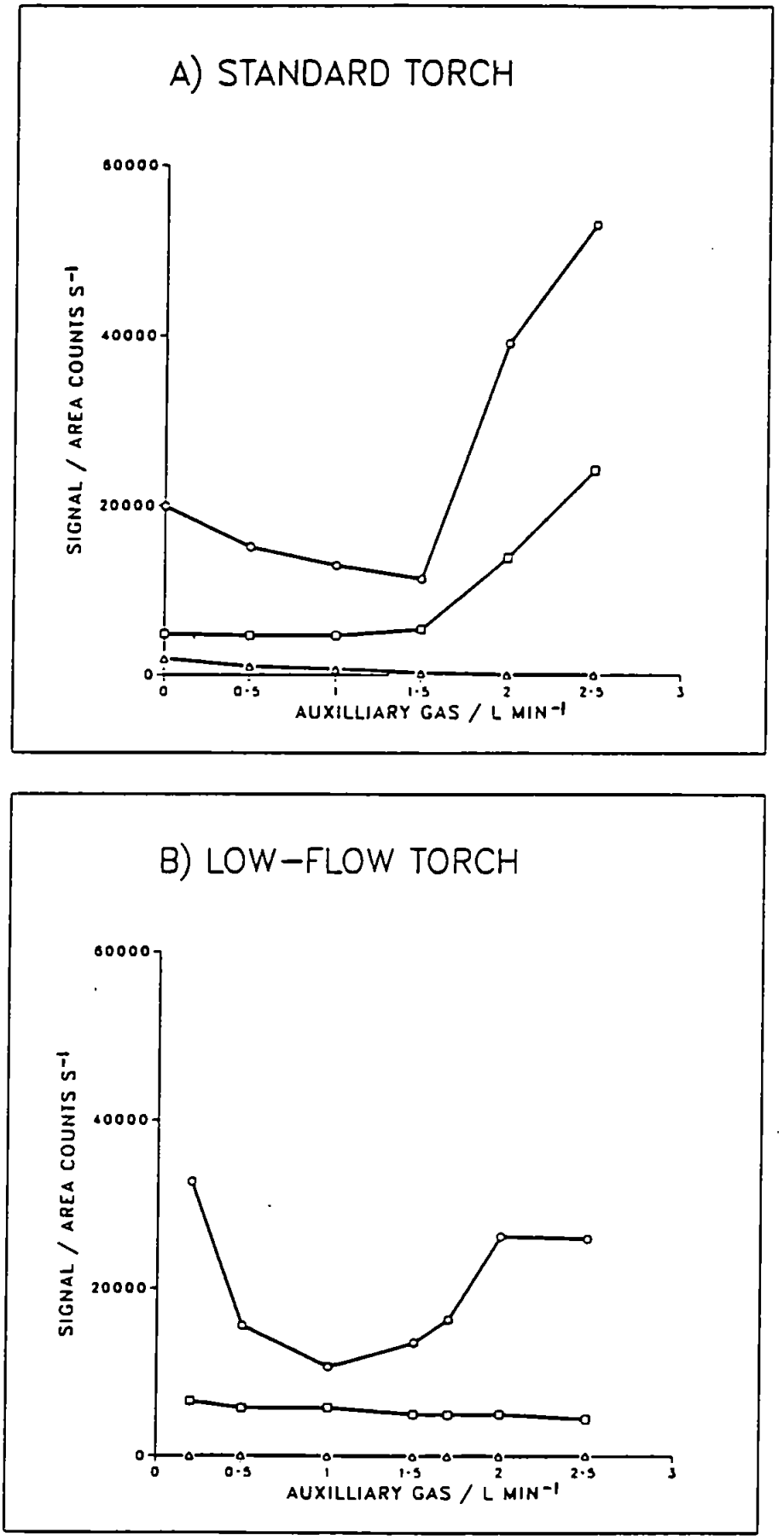

Figure 5.12 Effect of auxilliary gas flow on the signals for: ArO^+ (O); ArN^+ (□); and $ArAr^+$ (Δ), using the standard and low-flow torches

observed for the standard torch (Fig. 5.10A) agree with the results of Long and Brown (120) who observed an identical pattern, albeit at lower gas flows. For the low-flow torch auxilliary gas flow had little effect on analyte signals (Fig. 5.10B). Likewise Ba^{2+}/Ba^{+} and BaO^{+}/Ba^{+} ratios were relatively unaffected (Fig. 5.11) for both torches.

ArO^{+} and ArN^{+} signals exhibited similar behaviour for the standard torch (Fig. 5.12A), though contrasting behaviour for the low-flow torch (Fig. 5.12B) suggesting again that these ions were formed by precursors from different sources with this torch. For both torches the optimum gas flows determined for In coincided with signals close to the minima observed for these ions. The $ArAr^{+}$ signal varied very little over the ranges studied for either torch (Fig. 5.12).

5.3.1.5 Coolant Gas

The simplex optimisation located the'optimum' coolant gas flow to be close to the lower boundary limit for both torches (Fig. 5.13). Evidently the true optima were below the boundary limits for coolant gas flow at 11 l min^{-1} and 6 l min^{-1} for the standard and low-flow torches respectively. The torches could not be operated below these flows because of the danger of melting. Analyte signals varied in a similar manner for both torches, i.e. decreasing as coolant gas flow increased, however, a coolant gas flow of 10 l min^{-1} would be necessary for the

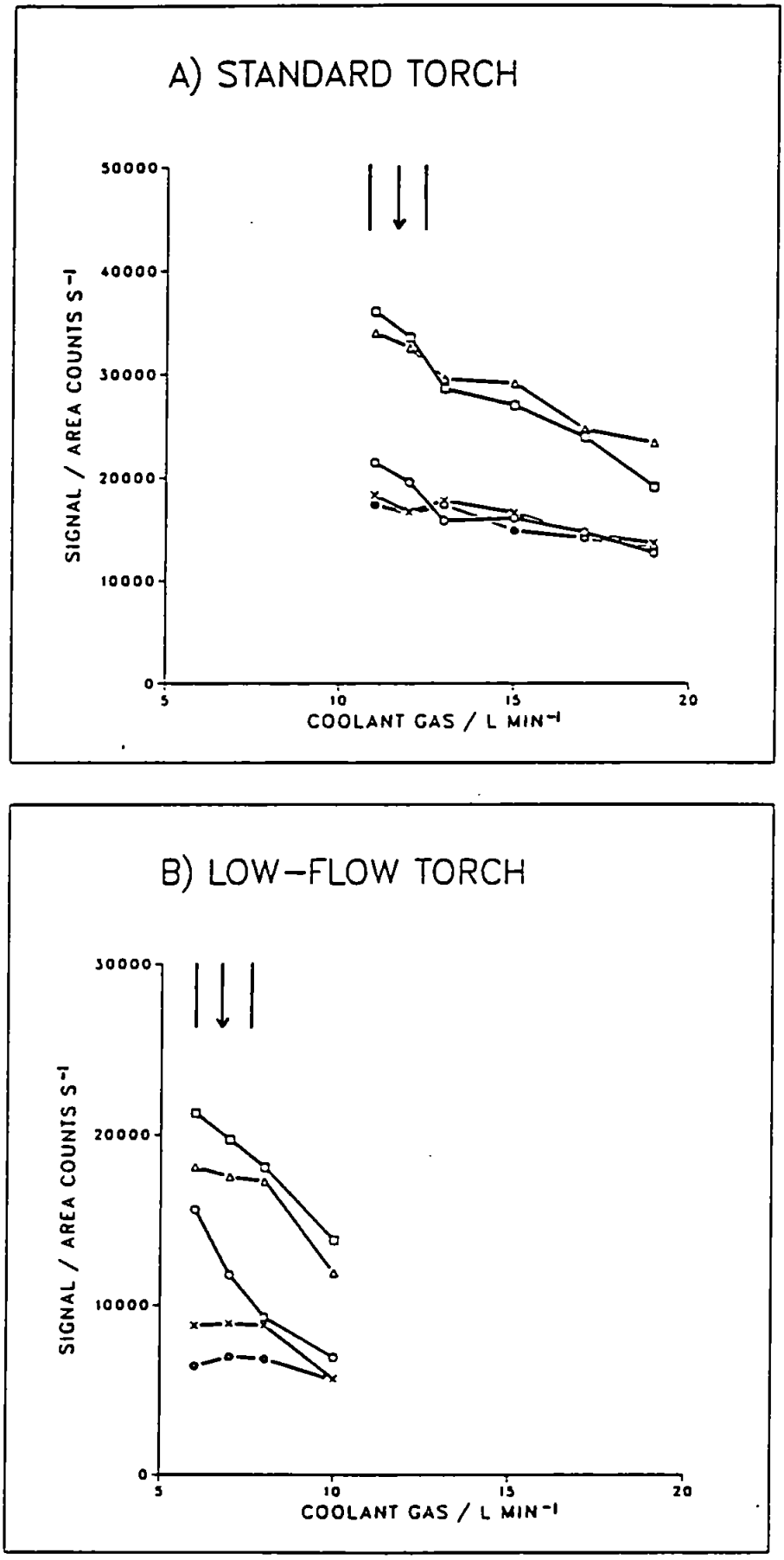

Figure 5.13 Effect of coolant gas flow on the signals for: $^{9}Be^{+}$ (O); $^{59}Co^{+}$ (□); $^{115}In^{+}$ (Δ); $^{138}Ba^{+}$ (X); and $^{208}Pb^{+}$ (O), using the standard and low-flow torches

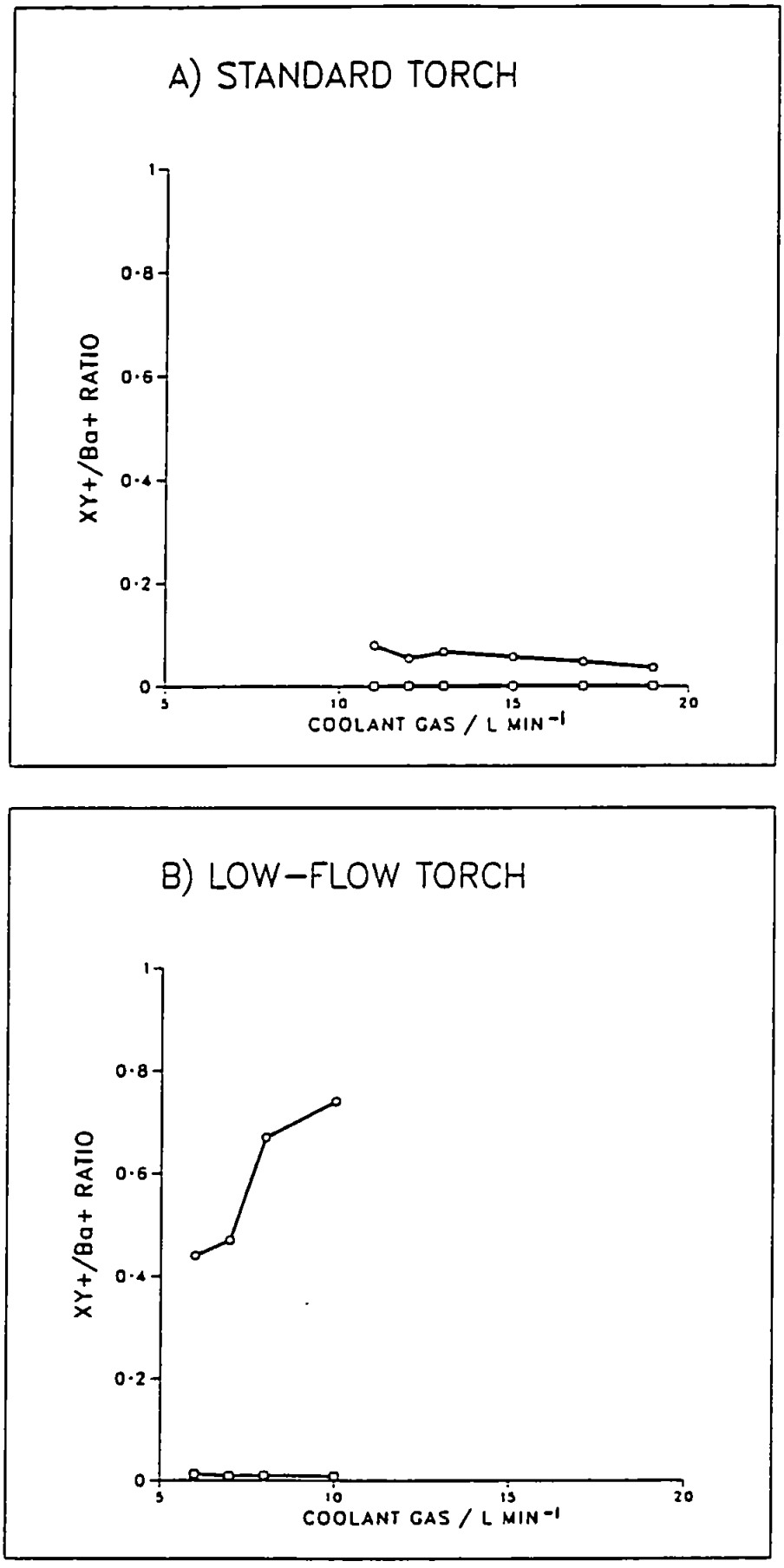

Figure 5.14 Effect of coolant gas flow on the ratios for: Ba^{2+}/Ba^{+} (O); and BaO^{+}/Ba^{+} (□), using the standard and low-flow torches

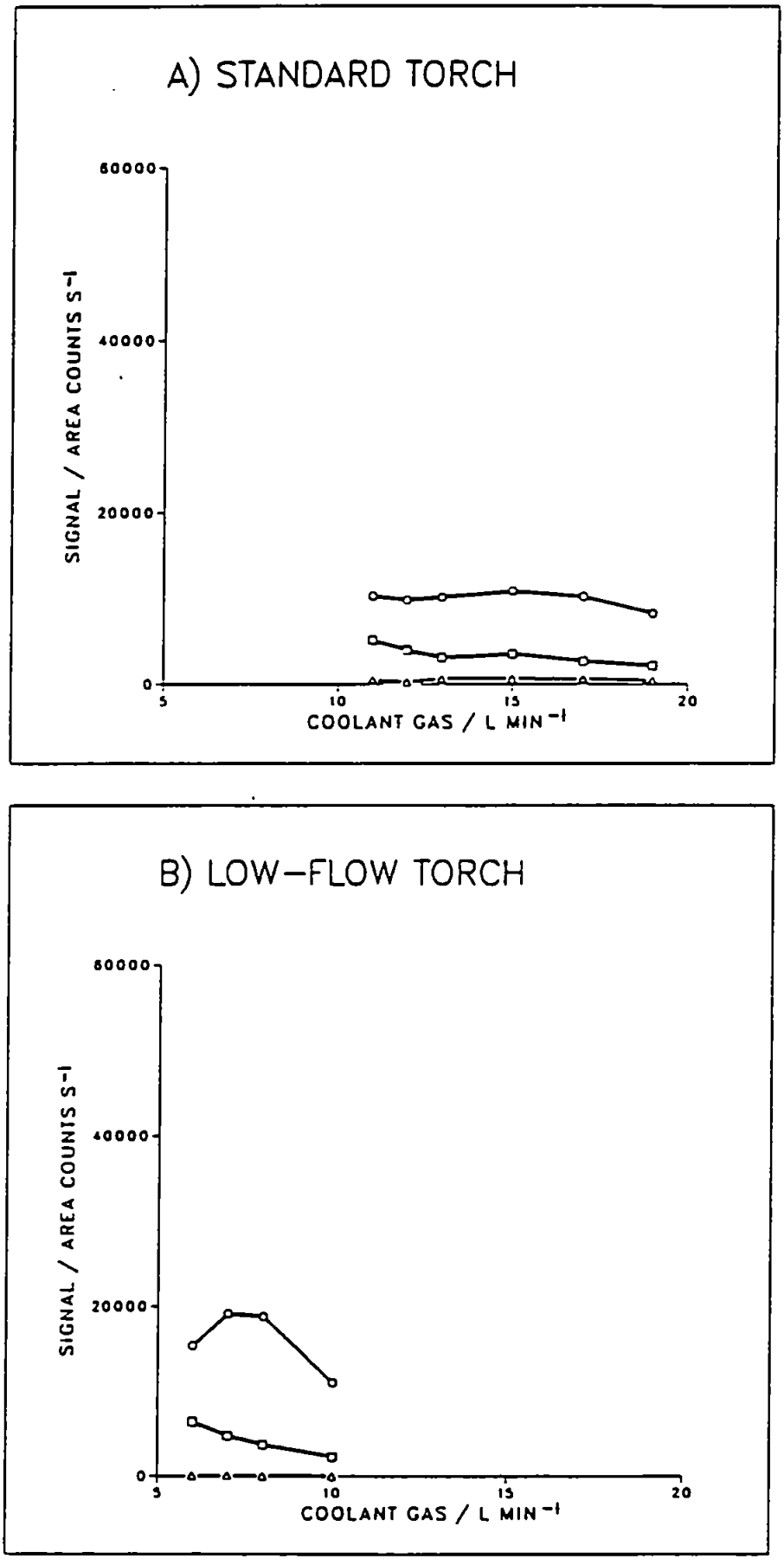

Figure 5.15 Effect of coolant gas flow on the signals for: ArO^+ (O); ArN^+ (□); and $ArAr^+$ (Δ), using the standard and low-flow torches

low-flow torch if it was operated at the maximum possible power, for the reasons mentioned in Section 5.3.1.2.

BaO^+/Ba^+ ratios remained constant throughout the range of coolant gas flow studied (Fig. 5.14) for both torches. Ba^{2+}/Ba^+ ratios exhibited contrasting behaviour for the two torches with respect to gas flow (Fig. 5.14). It is difficult to assess the influence of this parameter on the formation of Ba^{2+} ions in the plasma. It may be that it caused plasma cooling, and hence lowered the ionisation temperature in both cases, but also had an influence on the discharge/boundary layer for the low-flow torch, thereby in effect slightly increasing the Ba^{2+} level.

The signals for ArO^+, ArN^+ and $ArAr^+$ showed very little change with respect to coolant gas for the standard torch (Fig. 5.15A). However, once again the ArO^+ and ArN^+ signals exhibited dissimilar trends for the low-flow torch (Fig. 5.15B). This lends further strength to the argument that these species were formed by precursors from different sources in the low-flow plasma. More significantly, such species were more prevalent in the low-flow plasma, and were more sensitive to coolant gas flow than for the standard torch.

5.3.1.6 Summary

A comparison of various figures of merit can be made for the two torches operating at conditions found to be optimum for In^+ signal by reference to Table 5.6.

Table 5.6 Figures of merit for the standard and low-flow torches operated at optimum conditions

Figure of Merit	Standard torch	Low-flow torch
$^{115}In^+$ signal/area counts s^{-1}	47,591	17,508
Ba^{2+}/Ba^+ ratio	0.078	0.510
BaO^+/Ba^+ ratio	0.001	0.008
ArO^+/In^+ ratio	0.19	1.12
ArN^+/In^+ ratio	0.12	0.27
$ArAr^+/In^+$ ratio	0.020	0.003

In general, signals for a number of elements covering the mass range were lower with the low-flow torch compared to the standard torch, though considerable variation in the magnitude of signals for the low mass elements Be and Co was noted for the low-flow torch. The Ba^{2+}/Ba^{+} ratio was much greater and was influenced differently by operating parameters for the low-flow compared to the standard torch, probably because of a greater plasma potential in the low-flow plasma. BaO^{+}/Ba^{+} ratios were low for both torches with no significant variations with respect to operating parameters. ArO^{+}/In^{+} and ArN^{+}/In^{+} ratios were higher for the low-flow compared to the standard torch, and results suggested that the ArO^{+} and ArN^{+} species were formed by precursors from different sources in the low-flow plasma but not in the plasma formed with the standard torch. The $ArAr^{+}/In^{+}$ ratio was lower for the low-flow torch than the standard torch.

5.3.2 Effect of Organic Solvents

Several organic solvents of differing volatility were introduced into plasmas formed with the low-flow torch and the standard torch, and their effects on plasma stability and reflected power noted for each. The torches were operated using the conditions shown in Table 5.7.

It was necessary to introduce oxygen into the nebuliser gas to prevent carbon deposition on the cones. The amount varied depending on the solvent used. Also the sample uptake rate was reduced considerably for the more volatile

Table 5.7 Operating conditions for the low-flow and standard torches for organic solvent introduction

Condition	Standard torch	Low-flow torch
Ar Nebuliser gas/l min^{-1}	0.802	0.655
O_2 Nebuliser gas/l min^{-1}	0.025 - 0.071	0.025 - 0.115
Auxilliary gas/l min^{-1}	1.3	1.0
Coolant gas/l min^{-1}	15	10
Forward power/W	1800	1000
Sampling depth/mm	10.5	10.5
Spray chamber temperature/^{o}C	-2	-2
Sample uptake rate/ml min^{-1}	0.12 - 1.46	0.12 - 1.46

solvents namely acetone, cyclohexane and hexane, though in general a greater sample uptake rate could be tolerated by the low-flow torch. The performance of the two torches with respect to reflected power and plasma stability is shown in Table 5.8.

It is evident from Table 5.8 that the low-flow torch was much more tolerant of organic solvents, especially the more volatile solvents, than the standard torch. This may be an advantage in several applications such as the analysis of high purity organic solvents and coupled HPLC/ICP-MS studies where the mobile phases may well contain organic solvents.

5.3.3 Semi-Quantitative Analysis of Organic Samples using the Low-Flow Torch

A semi-quantitative calibration was performed using a 100 ng ml^{-1} solution of Li, Co, In, Ba, and Pb in xylene. The calibration curve is shown in Fig. 5.16 both with and without Ba included in the calibration. As can be seen, when Ba was included the curve was biased (Fig. 5.16A) due to the low Ba^{+} response caused by the propensity for Ba^{2+} ions to form using this torch. However, when Ba was excluded a useable calibration curve was obtained (Fig. 5.16B), and this was used for subsequent calculations. Because of this effect it may be necessary to perform a separate calibration using elements of low second ionisation potential if such elements are to be determined semi-quantitatively, though Ba is the worst case having

Table 5.8 Reflected power and plasma stability (S = stable; U = unstable and VU = very unstable) compared for the low-flow and standard torches during organic solvent introduction

	Standard torch		Low-flow torch	
	Reflected power/W	Plasma Stability	Reflected power/W	Plasma Stability
Propan-2-ol	45	S	10	S
Ethanol	42	S	10	S
Methanol	60	S	12	S
Acetone	80	VU	25	S
Cyclohexane	65	VU	20	S
Hexane	67	VU	45	U

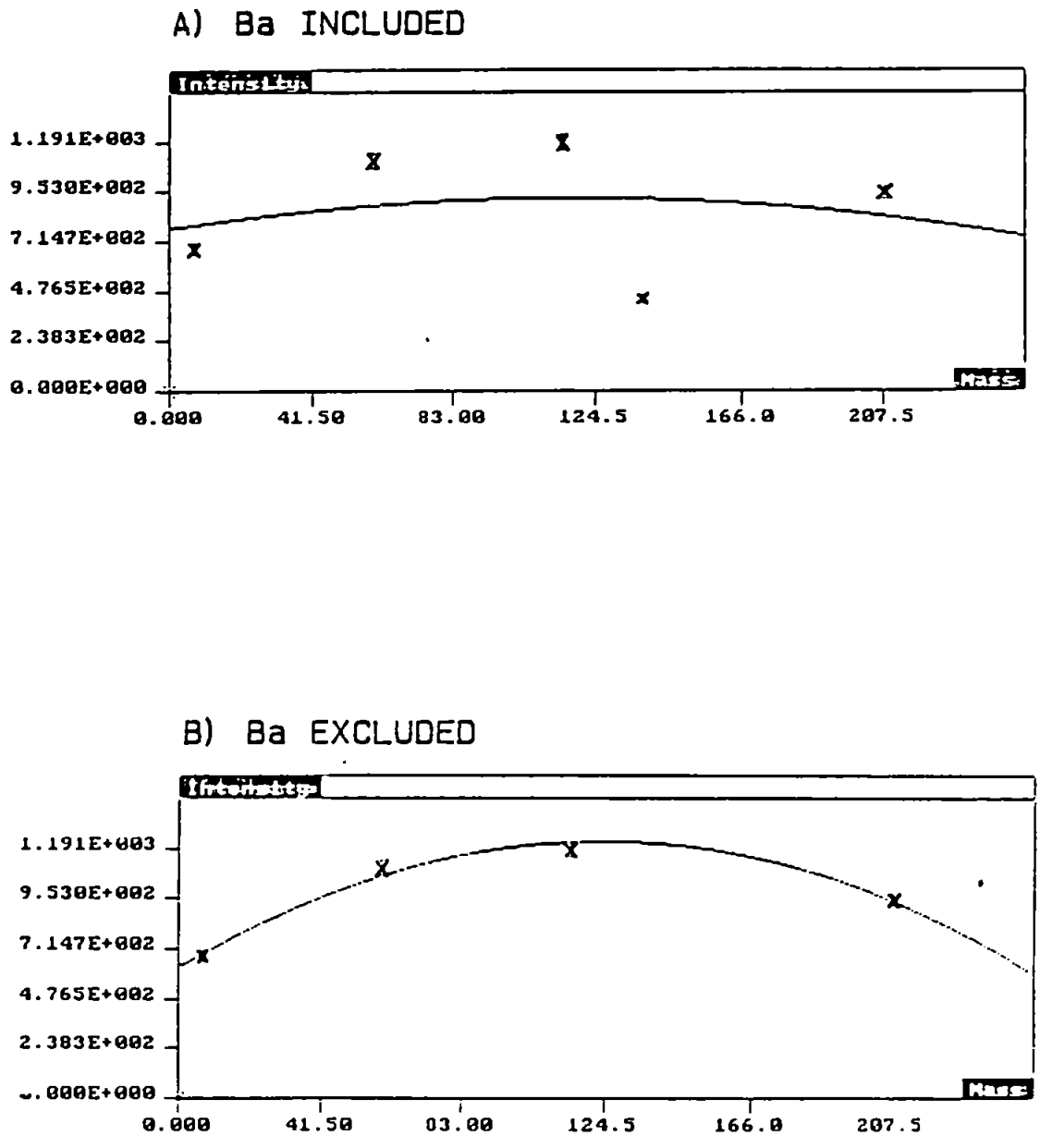

Figure 5.16 Semi-quantitative calibration curves calculated with: A) ^{138}Ba included; B) ^{138}Ba excluded, and using the low-flow torch

the lowest second ionisation potential. In any case semi-quantitative determinations are usually regarded as not being more accurate than within a factor of 3, so such precautions may be overzealous.

Four organic samples were analysed. Heavy and light distillation fractions of liquid petroleum and an iso-octanol sample were spiked with In as an internal standard at 100 ng ml^{-1}. A fuel oil sample was diluted in xylene to 1% (m/v) and spiked with In as an internal standard as before. Plasma operating conditions for the low-flow torch are shown in Table 5.9. The nebuliser gas flow was adjusted to give maximum In response while aspirating xylene.

Results are shown in Table 5.10 for a number of selected elements that require monitoring in the petrochemicals industry. Sodium, V and Ni levels must be controlled because they may act as catalyst poisons or cause corrosion, especially V which catalyses the oxidation of SO_2 to SO_3 resulting in sulphuric acid formation.

Lead, Cu and Zn need to be monitored as they can cause oxidative decomposition of oils. Barium is monitored as a marker for various additives. The results clearly show the distribution of trace elements in oils throughout the refinement process, some metals being lost through successive refinements, or fluctuations in composition due to contributions from components used in plant

Table 5.9 Plasma operating conditions for the semi-quantitative analysis of organic samples using the low-flow torch

Ar Nebuliser gas/l min^{-1}	0.375
O_2 Nebuliser gas/l min^{-1}	0.034
Auxilliary gas/l min^{-1}	1.5
Coolant gas/l min^{-1}	9
Forward power/W	900
Sampling depth/mm	10.5
Spray chamber temperature/^{o}C	-2

Table 5.10 Results for selected elements in the organic samples liquid petroleum (LPL for the light fraction and LPH for the heavy fraction) fuel oil (FO) and iso-octanol (ISO)

		Concentration in sample/$\mu g\ g^{-1}$			
Element	Mass	FO	LPH	LPL	ISO
Na	23	100	5.8	4.7	3.3
V	51	13	3.2	0.24	0.22
Ni	60	10	42	0.033	0.15
Cu	65	0.14	<0.001	<0.001	0.004
Zn	66	0.84	<0.001	0.003	0.006
Pb	208	0.20	<0.001	0.001	0.002
Ba	138	0.65	<0.001	0.003	<0.001

construction or additives. Also demonstrated are the low detection limits achievable using ICP-MS (i.e. 0.001 $\mu g\ g^{-1}$) and the number of elements which can be determined simultaneously, even though only a few elements were selected and shown here. Evidently the technique can be applied to the monitoring of ultra-trace elements in many other solvents, particularly more volatile solvents when using the low-flow torch.

5.4 Conclusions

Both standard and low-flow torches have been optimised by simplex optimisation with respect to operating conditions. The two torches have been shown to differ significantly in performance with regard to various criteria of merit. The main advantages of the low-flow torch compared to the standard torch may be its greater tolerance of volatile organic solvents, and in certain cases doubly charged species may be used for analysis where an interference at the m/z for the singly charged species exists.

CHAPTER 6

THE EFFECT OF ORGANIC SOLVENTS AND MOLECULAR GASES ON POLYATOMIC ION INTERFERENCES IN ICP-MS

6.1 Introduction

One of the major problems associated with ICP-MS has been its susceptibility to polyatomic ion interferences (38, 39, 109, 128, 129), particularly below 80 m/z units. Gray (109) has suggested that such interferences are caused by condensation reactions in the expansion region of the interface or collisions close to the walls of the first stage. Precursors for the formation of polyatomic ions originate from the plasma gas and entrained atmospheric gases (*i.e.* Ar, N and O), water, the sample matrix and acids used for dissolution of the sample. Polyatomic ions such as ArO^+, ArN^+, $ArAr^+$, O_2^+, N_2^+ and various other combinations arising from the plasma and atmospheric gases can be minimised by judicious choice of operating conditions (39, 40), though they cannot be entirely eliminated and still cause major interferences. Polyatomic ions formed from O^+ and OH^+ precursors from water can be reduced by cooling the spray chamber and hence reducing the amount of water vapour reaching the plasma (130, 131). Interfering ions formed from precursors in the sample matrix and acids used for dissolution have been minimised by a variety of methods including chromatographic separation (132-135), hydride generation (135, 136), electrothermal vaporisation (137), mathematical correction (128, 129) and the use of

alternative sample preparation procedures (104, 128, 138).

A particular problem has been the interferences caused by $^{40}Ar^{35}Cl^{+}$ on $^{75}As^{+}$, $^{40}Ar^{36}Ar^{+}$ on $^{76}Se^{+}$, $^{40}Ar^{37}Cl^{+}$ on $^{77}Se^{+}$ and $^{40}Ar^{38}Ar^{+}$ on $^{78}Se^{+}$, in matrices with a high chloride content (139) or where chloride containing acids have been used for sample dissolution (128). These interferences are particularly troublesome as As is mono-isotopic and masses 77 and 78 would be the Se isotopes of choice given other isobaric interferences. The problem has been overcome to some extent by the methods mentioned above, in particular co-precipitation of chloride with silver (133), alternative sample preparation procedures (104, 128, 138) and mathematical correction (128, 129). However, no simple, robust and reliable technique has yet been devised to address the problem, short of employing an entirely different plasma gas such as helium (140-142).

In this work the effect of introducing an organic solvent or molecular gas into the central channel of the ICP has been studied, with particular reference to the elimination of interferences on As and Se as well as the effect on other polyatomic ions prevalent in ICP-MS.

6.2 Instrumentation

The instrument used in this work was an inductively coupled plasma - mass spectrometer (VG PlasmaQuad 2, VG Elemental, Winsford, Cheshire, UK) described in Section 4.2.1. The only modification was the use of a high solids

v-groove nebuliser (Ebdon nebuliser, PS Analytical, Sevenoaks, Kent, UK).

6.3 Preliminary Experiments

6.3.1 Procedure

Preliminary experiments were performed to assess the effect of nebuliser gas flow on the severity of a number of polyatomic ion interferents. In practice a standard solution of In (100 ng ml^{-1}) was spiked with hydrochloric acid (Aristar grade, BDH Chemicals Ltd.) to a concentration of 3 + 97 (v/v) in deionised, double-distilled water. Four different protocols were used, and the influence of nebuliser gas flow on the polyatomic interferents compared. Firstly experiments were performed without any modification to the standard solution and secondly it was spiked with propan-2-ol to a concentration of 10% (v/v). Thirdly and fourthly experiments were performed without modification to the standard solution but with the addition of O_2 and N_2 respectively into the nebuliser gas flow. Operating conditions are shown in Table 6.1.

Additionally, studies were performed to investigate the effect of increasing propan-2-ol and N_2 at fixed nebuliser gas flow rate, and the effect of N_2 at different powers.

6.3.2 Results and Discussion

The effect of nebuliser gas flow on In^+ response at 115 m/z units is shown in Fig. 6.1 for the four methods

Table 6.1 Operating conditions for the various methods to assess the effect of nebuliser gas flow on polyatomic ion interferences

Parameter	Method Modification*			
	None	Propan-2-ol spike	O_2 Introduction	N_2 Introduction
Ar Nebuliser gas flow/l min^{-1}	0.5 - 1.0	0.5 - 1.0	0.5 - 1.0	0.5 - 1.0
O_2 Nebuliser gas flow/l min^{-1}	0	0.03	0.03	0
N_2 Nebuliser gas flow/l min^{-1}	0	0	0	0.03
Auxilliary gas flow/l min^{-1}	1.0	1.0	1.0	1.0
Coolant gas flow/l min^{-1}	15	15	15	15
Forward power/W	1800	1800	1800	1800
Sampling depth/mm	10.5	10.5	10.5	10.5
Spray chamber temperature/^{o}C	+5	+5	+5	+5

* For full description of method see text

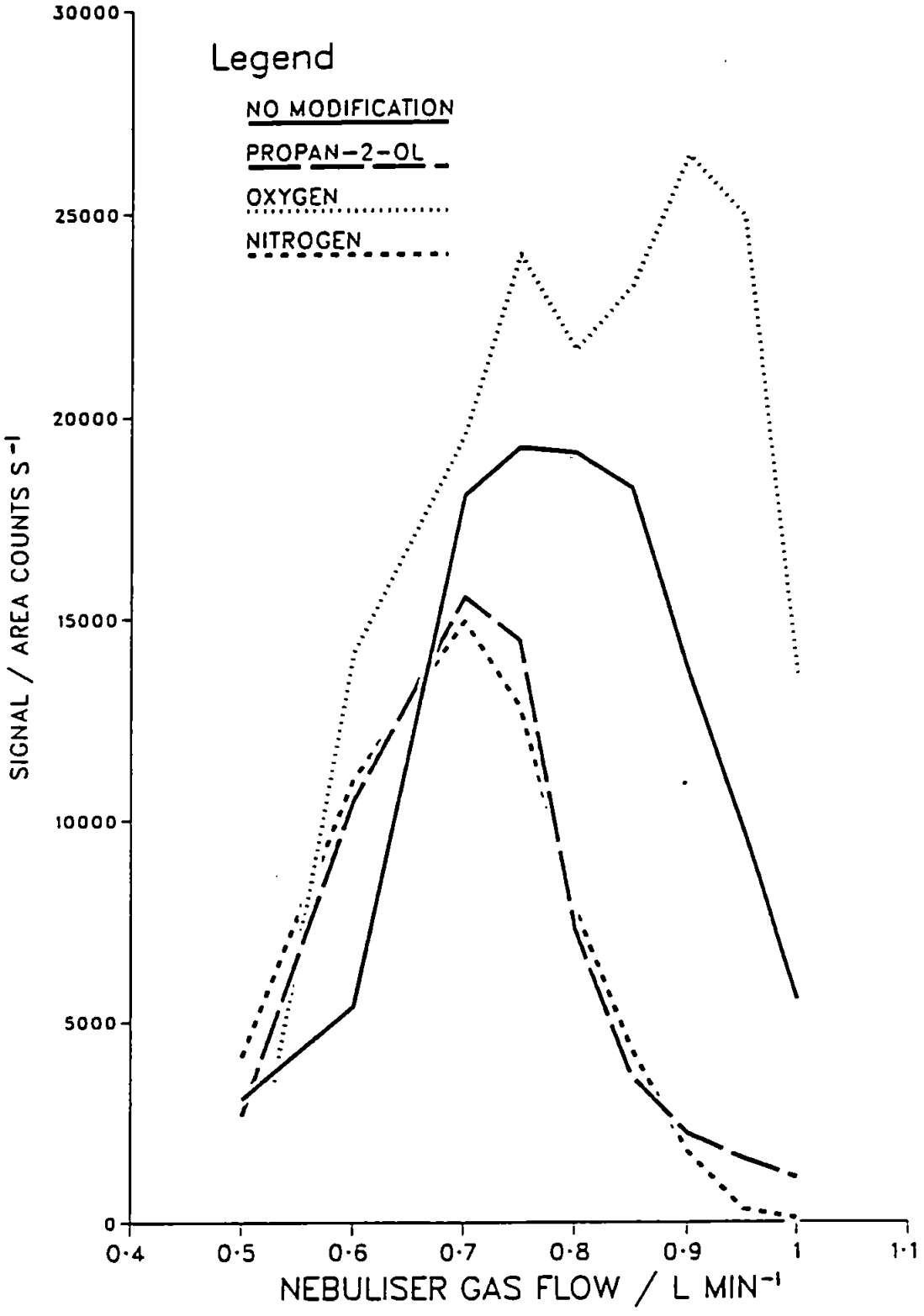

Figure 6.1 Effect of nebuliser gas flow on the signal for $^{115}In^{+}$ using the various method modifications

employed. The effect of N_2 and propan-2-ol was to shift the optimum gas flow to a lower flow compared to no modification. This was probably due to a reduction in the ionisation temperature in the plasma caused by the molecular gas and organic solvent. However, O_2 introduction had the opposite effect, causing an increase in the optimum nebuliser gas flow compared to no modification. The reasons for this are unclear as one would also expect O_2 to reduce the ionisation temperature, however, it may be that O_2 contributes to the ionisation processes in the plasma.

The effect of nebuliser gas flow on the responses for $ArCl^+$ and $ArAr^+$ at 75 and 76 m/z units respectively and the In^+/xy^+ ratios (where xy^+ indicates a polyatomic ion species) is shown in Figs. 6.2 and 6.3 for the four methods. For a particular nebuliser gas flow O_2, N_2 and propan-2-ol introduction resulted in a startling decrease in $ArCl^+$ response (Fig. 6.2A) and a corresponding increase in the $In^+/ArCl^+$ ratio (Fig. 6.2B) compared to no modification. The magnitude of the decrease in $ArCl^+$ response is in the order N_2 > propan-2-ol > O_2 > no modification. Similarly at flow rates above 0.75 l min^{-1} a large decrease in $ArAr^+$ response (Fig. 6.3A) and an increase in the $In^+/ArAr^+$ ratio (Fig. 6.3B) was also evident when introducing O_2, N_2 and propan-2-ol. At flow rates below 0.75 l min^{-1} no great change, or an increase in, $ArAr^+$ response was observed. The slightly different behaviour of the $ArAr^+$ ion compared to the $ArCl^+$ ion

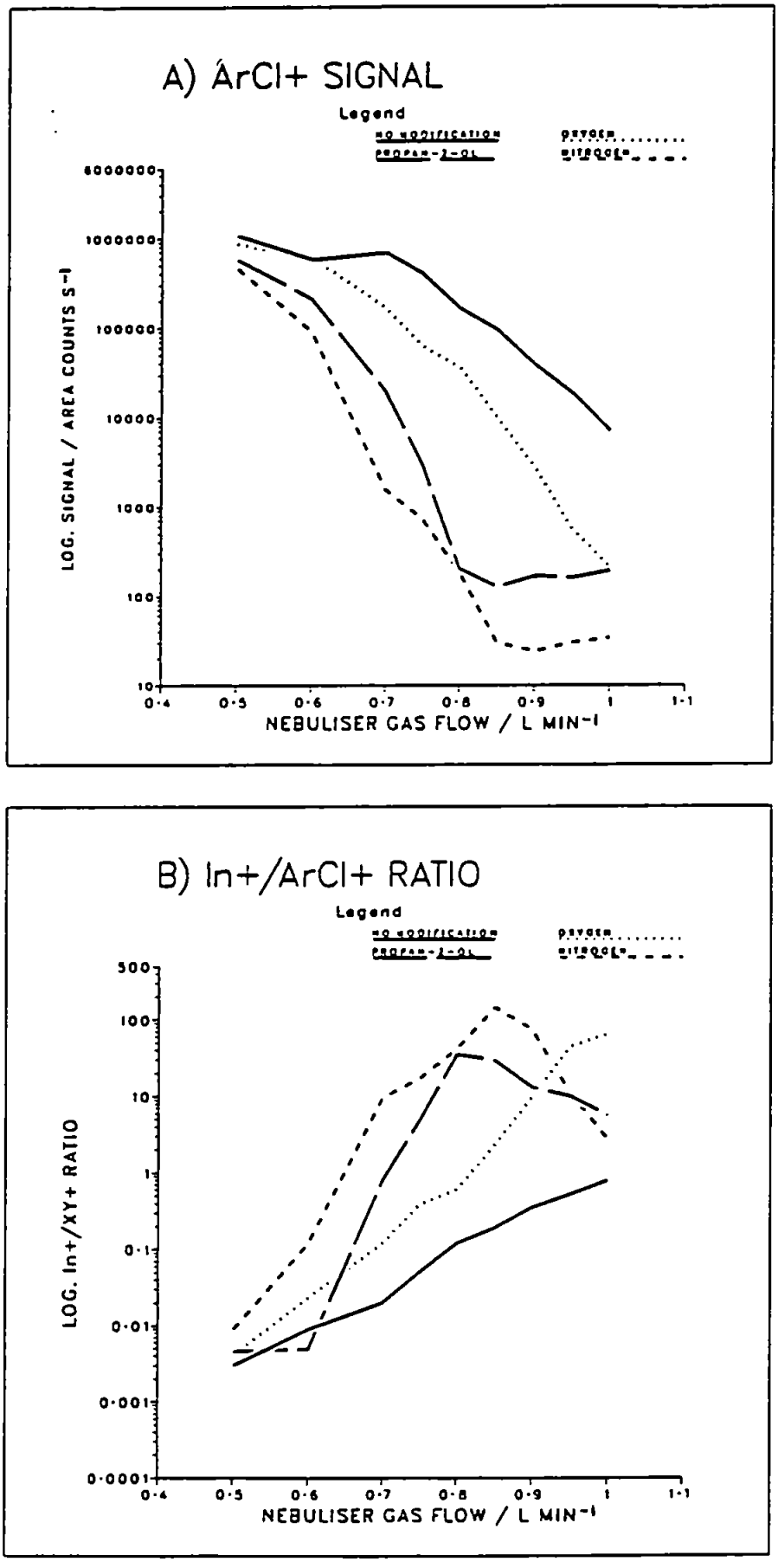

Figure 6.2 Effect of nebuliser gas flow on: A) $ArCl^+$ signal; and B) $In^+/ArCl^+$ ratio, using the various method modifications

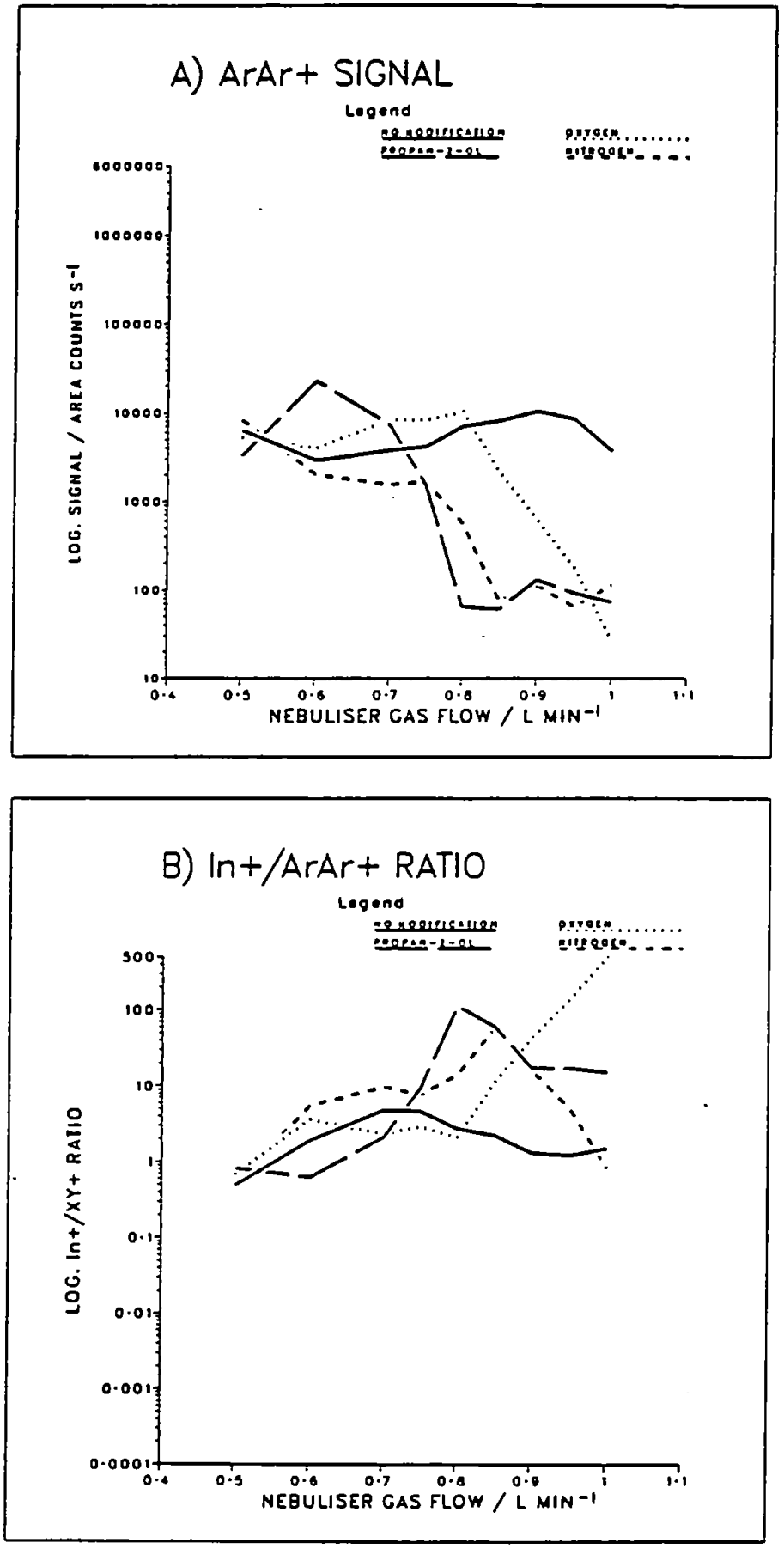

Figure 6.3 Effect of nebuliser gas flow on: A) $ArAr^+$ signal; and B) $In^+/ArAr^+$ ratio, using the various method modifications

suggests that their mechanism of formation and/or ionisation are different. The results are summarised in Table 6.2 for a nebuliser flow rate of 0.85 l min^{-1}.

As can be seen from Table 6.2 improvements of up to 1000 and 20 times in the $In^+/ArCl^+$ and $In^+/ArAr^+$ ratios respectively were achieved using the method modifications. Three mechanisms may account for the reduction in these polyatomic ions. Firstly, the introduction of an organic solvent or molecular gas may reduce the ionisation temperature in the plasma whilst at the same time increasing the kinetic temperature. This may result in the suppression of ionisation of some polyatomic species and also increase their rate of decomposition. However, as most polyatomic ions are thought to be formed in the expansion region and at the surface of the cones (109) other explanations may be that competitive formation of ArC^+, ArN^+ and ArO^+ or alternatively CCl^+, NCl^+ and OCl^+ occurs.

The effect of nebuliser gas flow on the responses for ArC^+, ArN^+ and ArO^+, at 52, 54 and 56 m/z units respectively, and the corresponding In^+/xy^+ ratios, is shown in Figs. 6.4 - 6.6 for the four different methods.

Taking ArC^+ first, in general the effects of O_2 and N_2 introduction were to decrease the ArC^+ signal (Fig. 6.4A) and increase the In^+/ArC^+ ratio (Fig. 6.4B). Conversely, the effect of the propan-2-ol spike was to increase the

Table 6.2 In^+ response and In^+/xy^+ ratios using the four methods and a nebuliser gas flow of 0.85 l min^{-1}

Method Modification	In^+ response/ area counts s^{-1}	In^+/xy^+ ratios	
		$In^+/ArCl^+$	$In^+/ArAr^+$
None	18,213	0.19	2.2
Propan-2-ol spike	3,646	29	60
O_2 introduction	23,198	2.3	11
N_2 introduction	4,333	144	58

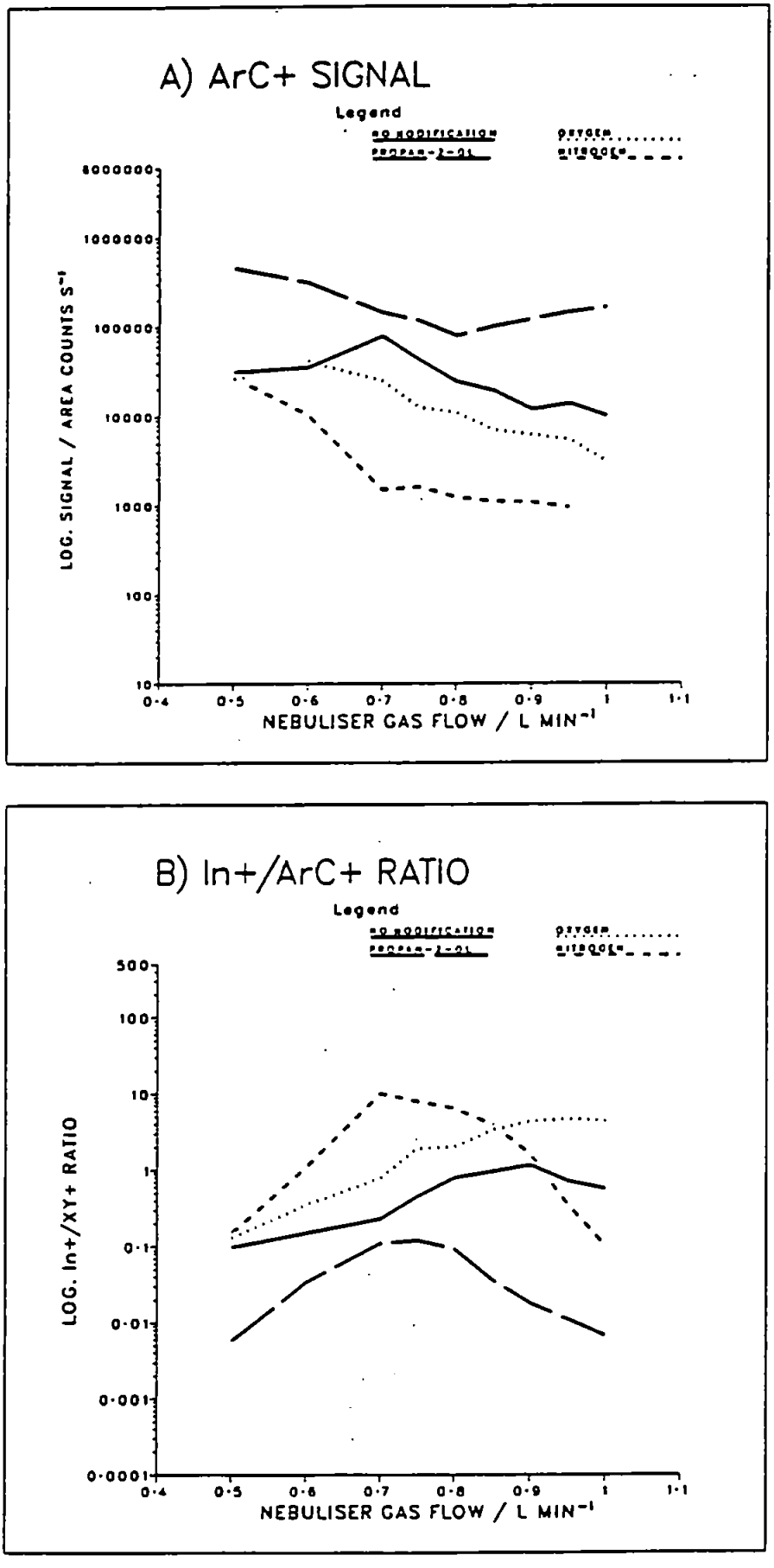

Figure 6.4 Effect of nebuliser gas flow on: A) ArC^+ signal; and B) In^+/ArC^+ ratio, using the various method modifications

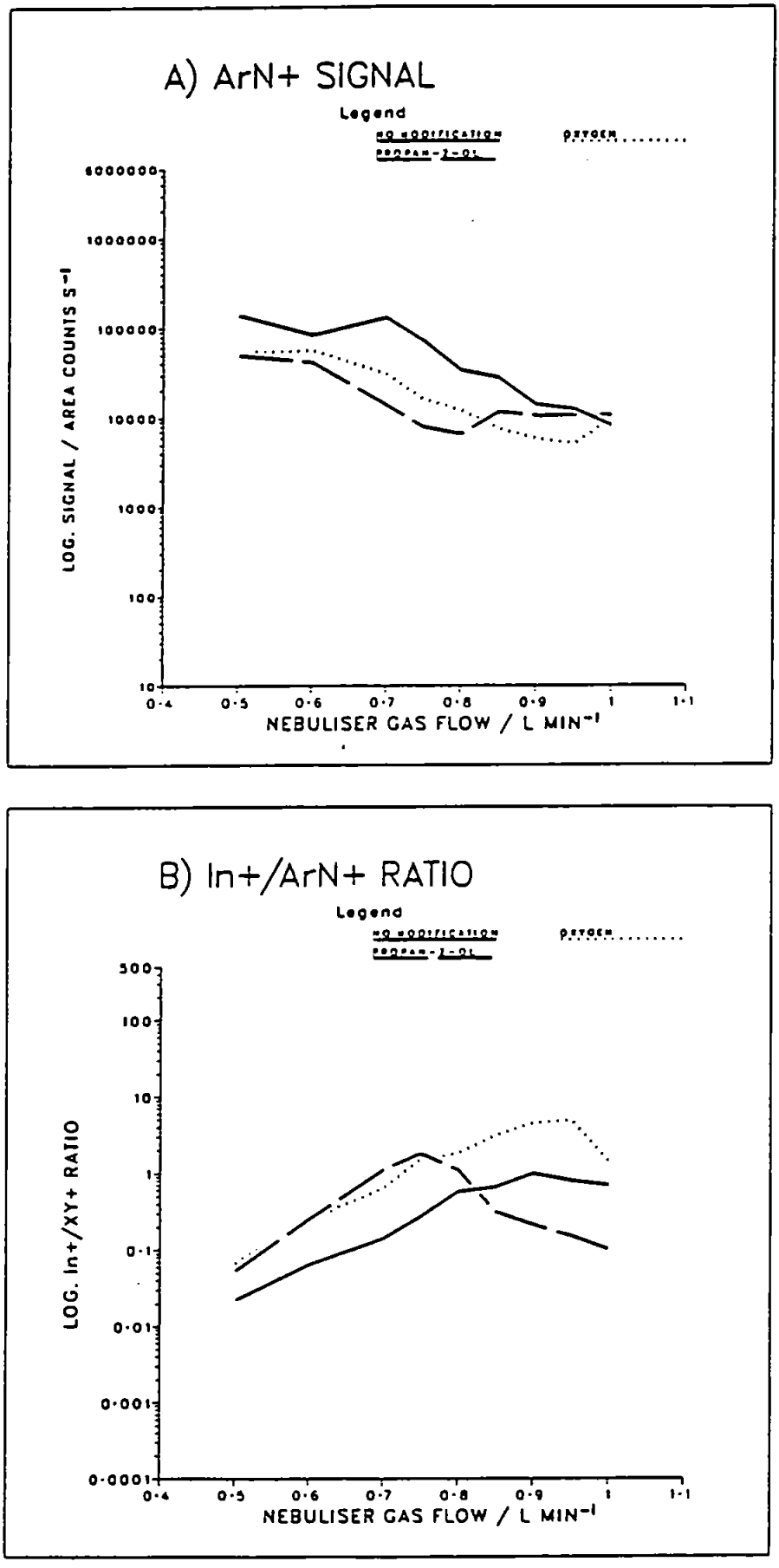

Figure 6.5 Effect of nebuliser gas flow on: A) ArN^+ signal; and B) In^+/ArN^+ ratio, using the various method modifications

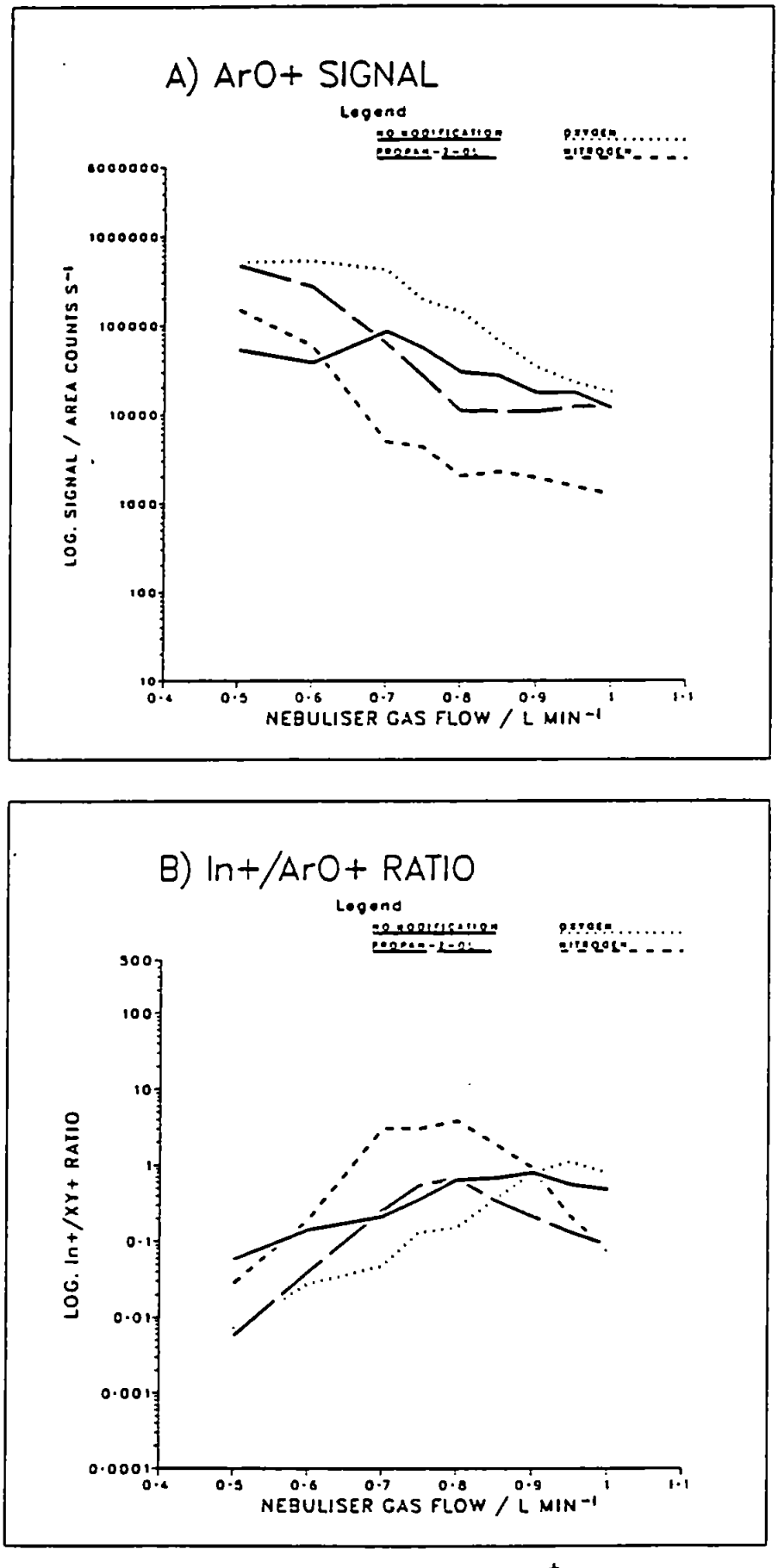

Figure 6.6 Effect of nebuliser gas flow on: A) ArO^+ signal; and B) In^+/ArO^+ ratio, using the various method modifications

ArC^+ signal and decrease the In^+/ArC^+ ratio, suggesting that competitive formation of ArC^+ over $ArCl^+$ and $ArAr^+$ took place to some extent when propan-2-ol was introduced.

Similarly, the effects of O_2 introduction and the propan-2-ol spike were to decrease the ArN^+ signal (Fig. 6.5A) and increase the In^+/ArN^+ ratio (Fig. 6.5B) at most gas flows. The effect of N_2 introduction is not shown since the ArN^+ signal increased to such an extent that saturation of the electron-multiplier occurred and the region of the spectrum at 54 m/z units was 'skip-scanned' to prolong multiplier life. However, these results also suggest that competitive formation of ArN^+ over $ArCl^+$ and $ArAr^+$ was a possibility when N_2 was introduced.

Finally, the effect of N_2 introduction was to decrease the ArO^+ signal (Fig. 6.6A) and increase the In^+/ArO^+ ratio (Fig. 6.6B) while O_2 introduction had the opposite effect. The effect of the propan-2-ol spike depended on the nebuliser gas flow, causing either an increase or decrease in ArO^+ signal and In^+/ArO^+ ratio (Fig. 6.6). This was probably due to the necessity to introduce O_2 simultaneously to prevent carbon deposition on the cones, which complicates interpretation of the results. However, the competitive formation of ArO^+ over $ArCl^+$ and $ArAr^+$ may again be indicated when O_2 was introduced.

The effect of nebuliser gas flow on the responses for CCl^+, NCl^+ and OCl^+ at 47, 49 and 51 m/z units

respectively, and the corresponding In^+/xy^+ ratios is shown in Figs. 6.7 - 6.9 for the four different methods.

The effect of the propan-2-ol spike was to increase the CCl^+ signal by a reasonably large extent (Fig. 6.7A) with a corresponding decrease in the In^+/CCl^+ ratio (Fig. 6.7B). Nitrogen and O_2 introduction caused a decrease in the CCl^+ signal by a small amount (Fig. 6.7A) and an increase in the In^+/CCl^+ ratio (Fig. 6.7B), though this trend reversed at high gas flows for N_2 introduction due to the decrease in In^+ signal. This evidence suggests that CCl^+ may have been formed in competition with $ArCl^+$.

The effects of the method modifications on NCl^+ were less pronounced. Oxygen introduction caused a decrease in NCl^+ signal (Fig. 6.8A) and an increase in the In^+/NCl^+ ratio (Fig. 6.8B). The propan-2-ol spike caused a decrease in NCl^+ signal up to 0.90 l min^{-1} nebuliser gas flow, then an increase, and a reduction in the In^+/NCl^+ ratio. Nitrogen introduction had a variable effect dependent on gas flow, and the only significant decrease in the In^+/NCl^+ ratio occurred at a nebuliser gas flow greater than 0.80 l min^{-1} (Fig. 6.8B). This suggests that the competitive formation of NCl^+ was less important than the formation of ArN^+ in preference to $ArCl^+$.

Both N_2 introduction and the propan-2-ol spike caused a reduction in the OCl^+ signal (Fig. 6.9A) and an increase in the In^+/OCl^+ ratio (Fig. 6.9B), while O_2 introduction

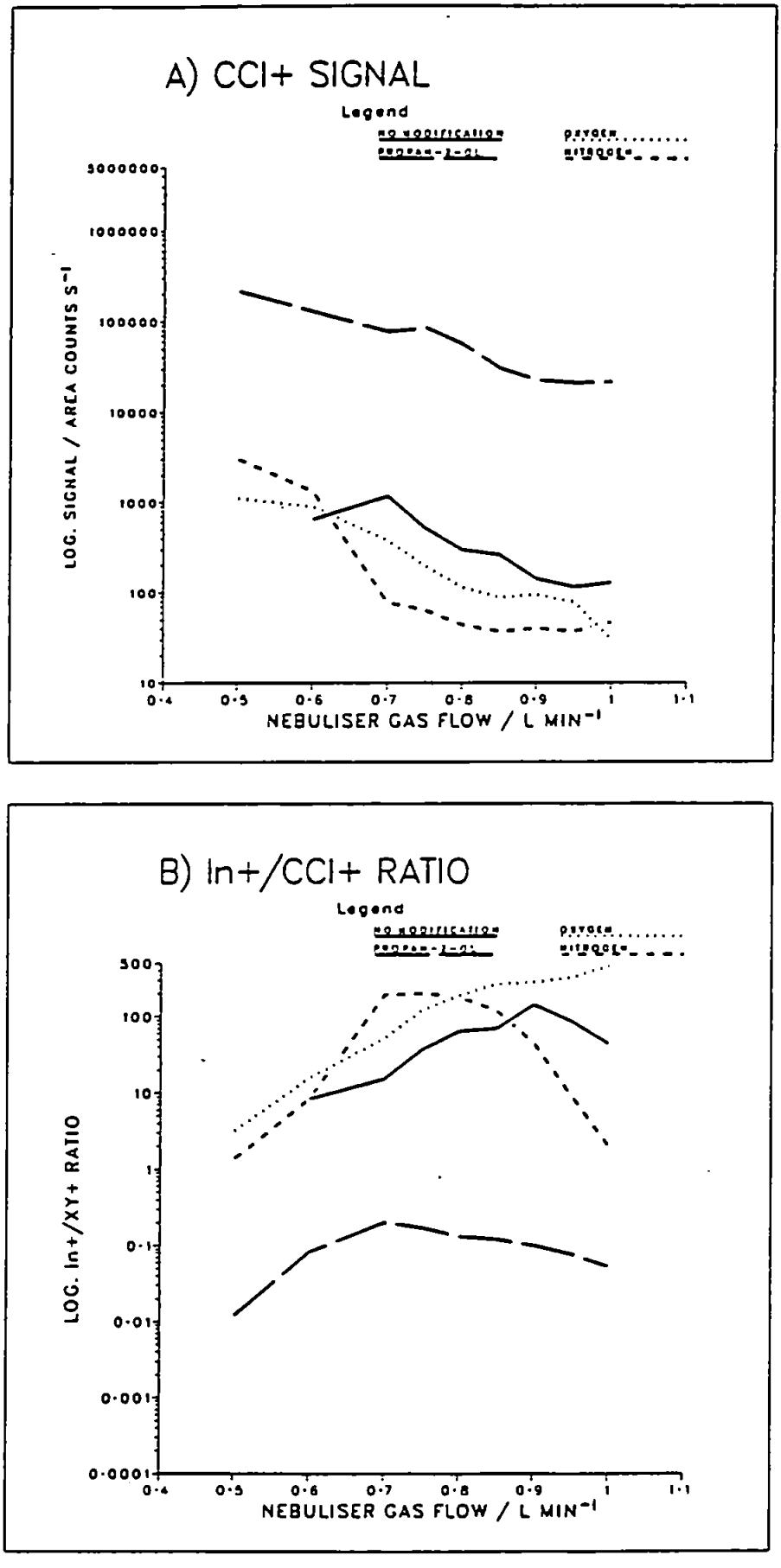

Figure 6.7 Effect of nebuliser gas flow on: A) CCl^+ signal; and B) In^+/CCl^+ ratio, using the various method modifications

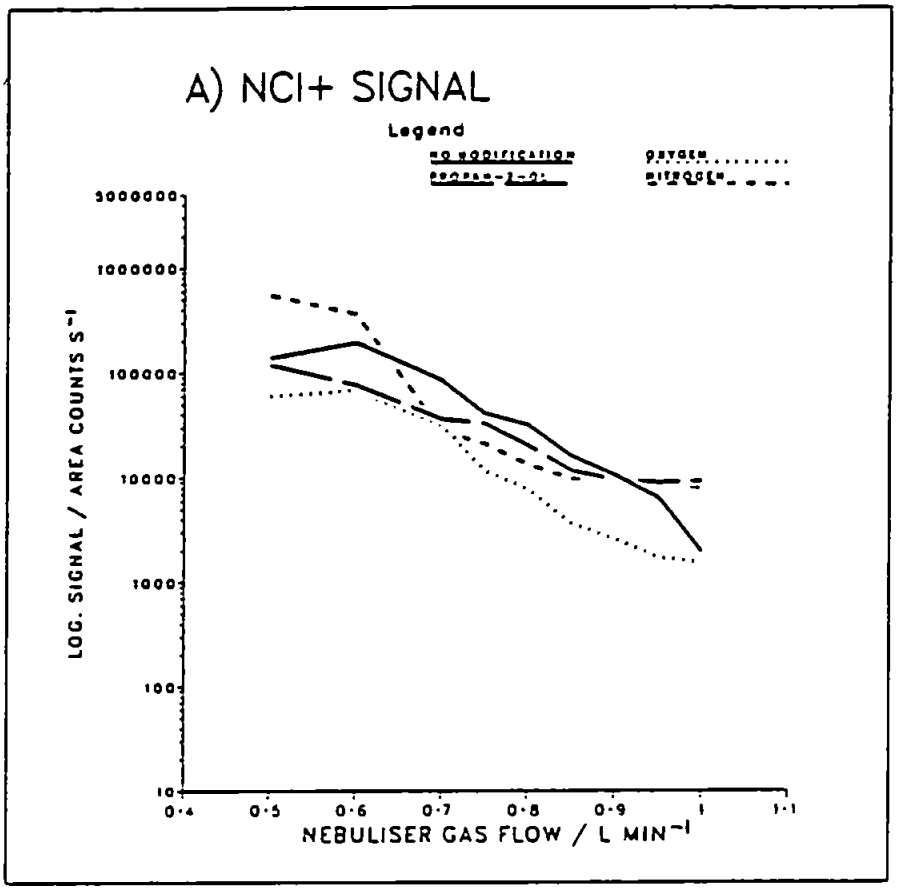

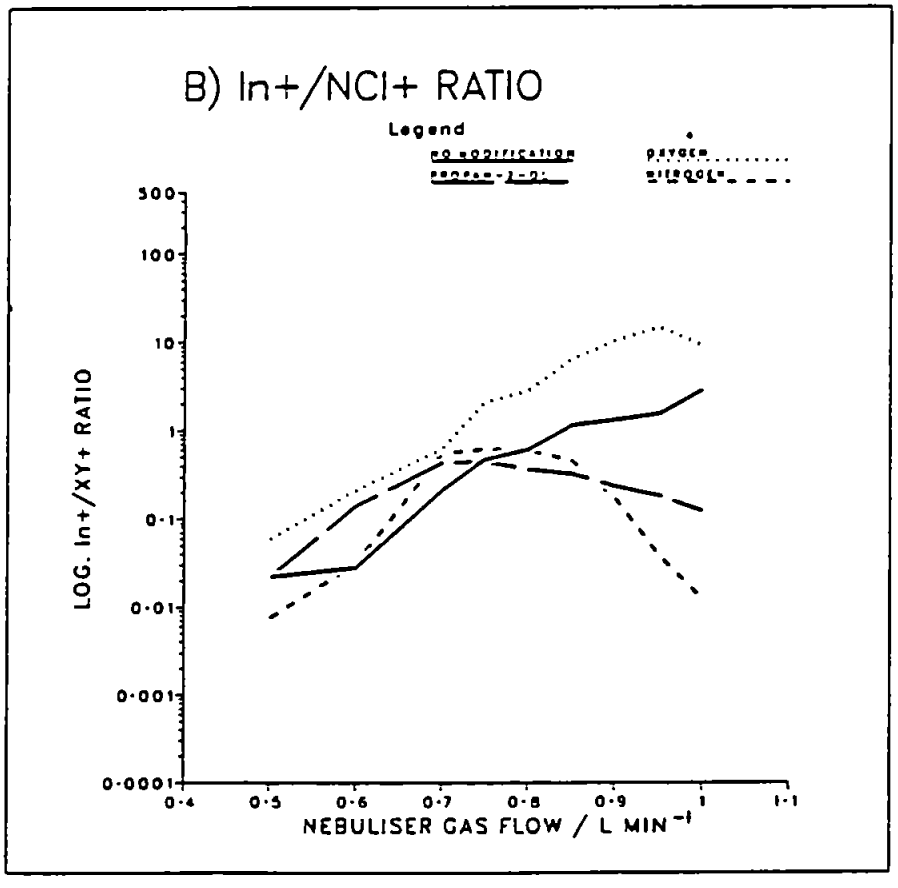

Figure 6.8 Effect of nebuliser gas flow on: A) NCl^+ signal; and B) In^+/NCl^+ ratio, using the various method modifications

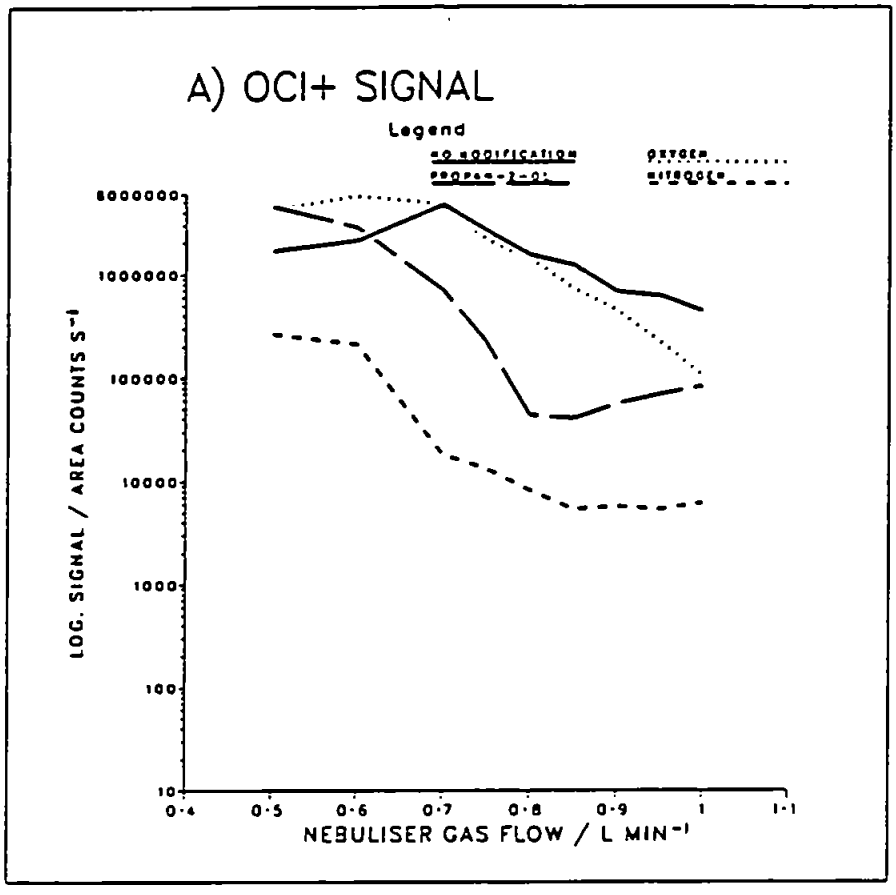

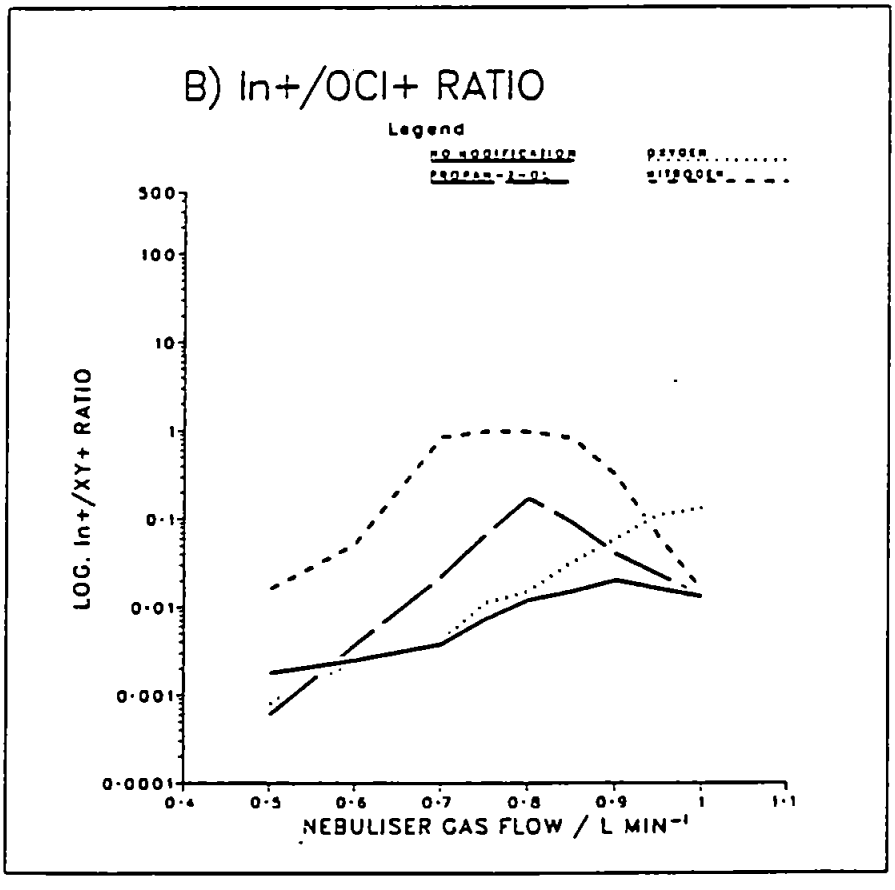

Figure 6.9 Effect of nebuliser gas flow on: A) OCl^+ signal; and B) In^+/OCl^+ ratio, using the various method modifications

had the opposite effect at a nebuliser gas flow rate below 0.70 l min^{-1}, and a similar though lesser effect above this gas flow (Fig. 6.9).

In general, the behaviour of the ArC^+, ArN^+, ArO^+, CCl^+, NCl^+ and OCl^+ polyatomic ions with respect to the various method modifications tends to suggest that these ions form in competition with $ArCl^+$ and $ArAr^+$. It should be noted that these polyatomic ions may also cause major interferences in ICP-MS, and that at least one of the method modifications for each has been shown to reduce the signal caused by the interfering species and increase the In^+/xy^+ ratio. Two further examples of the effect of nebuliser gas flow on $ArOH^+$ and $ClCl^+$ signals are shown in Figs. 6.10 and 6.11 for the four different methods. The effect of N_2 introduction was again to reduce the $ArOH^+$ signal (Fig. 6.10A) and increase the $In^+/ArOH^+$ ratio (Fig. 6.10B). Oxygen introduction and the propan-2-ol spike had similar but less pronounced effects. Likewise, the $ClCl^+$ signal and $In^+/ClCl^+$ ratio (Fig. 6.11) were affected by the method modifications in the same way but to a much greater extent.

The results are summarised in Table 6.3 for a nebuliser flow rate of 0.85 l min^{-1}. As can be seen, the method modifications did not result in such large increases in the In^+/xy^+ ratios for the polyatomic ions in Table 6.3 compared to those in Table 6.2, with perhaps the exception of $In^+/ClCl^+$. Nevertheless, in general the ratios were

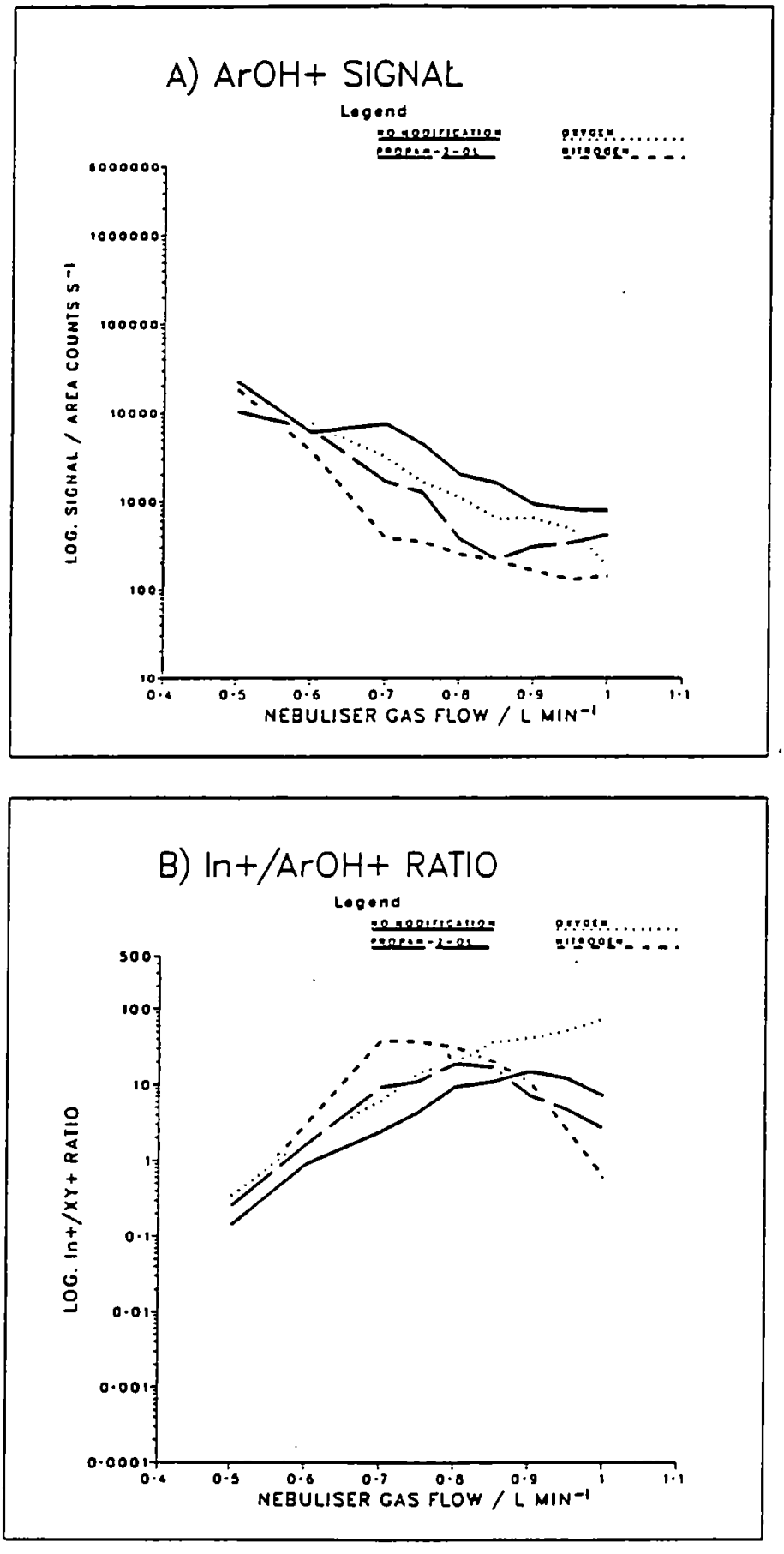

Figure 6.10 Effect of nebuliser gas flow on: A) $ArOH^+$ signal; and B) $In^+/ArOH^+$ ratio, using the various method modifications

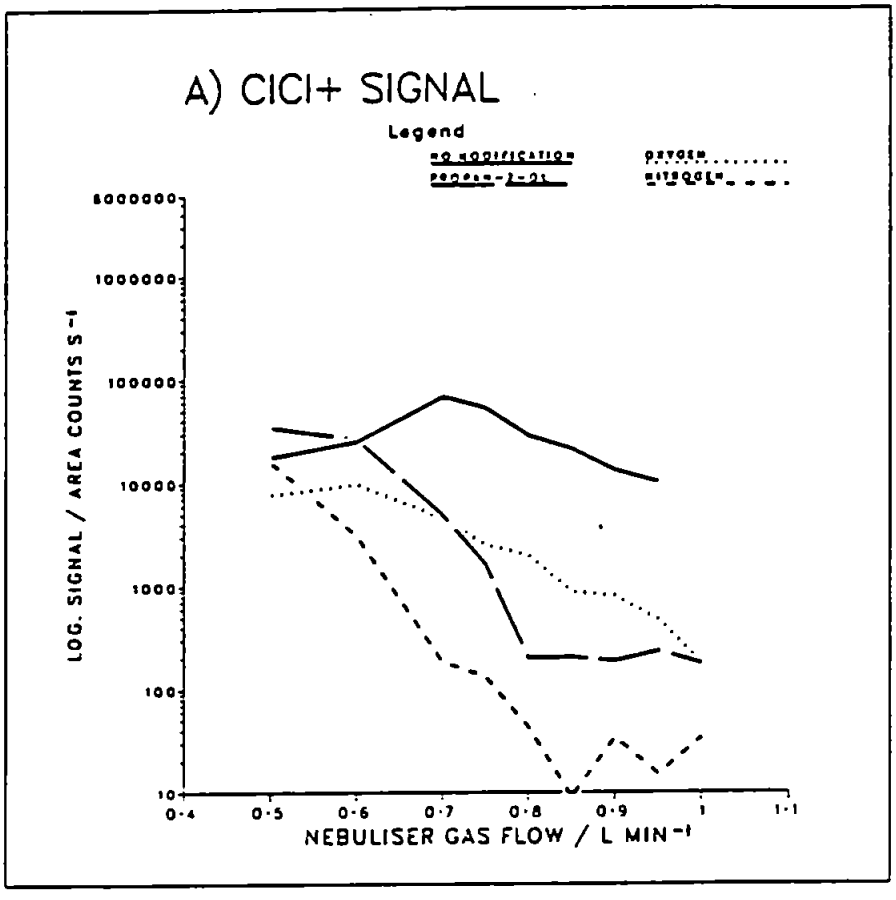

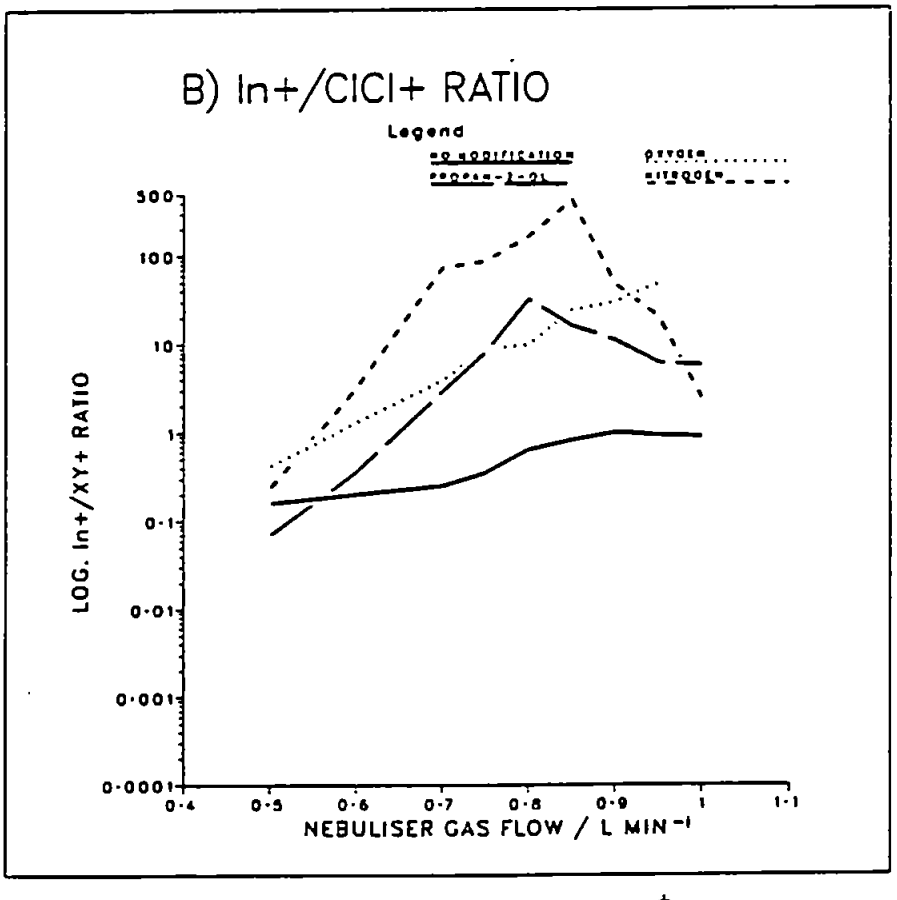

Figure 6.11 Effect of nebuliser gas flow on: A) $ClCl^+$ signal; and B) $In^+/ClCl^+$ ratio, using the various method modifications

Table 6.3 In^+ response and In^+/xy^+ ratios using the four methods and a nebuliser gas flow of 0.85 l min^{-1}

Method Modification	In^+ signal/ area counts s^{-1}	In^+/xy^+ ratios							
		In^+/CCl^+	In^+/NCl^+	In^+/OCl^+	In^+/ArC^+	In^+/ArN^+	In^+/ArO^+	$In^+/ArOH^+$	$In^+/ClCl^+$
None	18,213	70	1.14	0.015	0.95	0.66	0.67	11	0.8
Propan-2-ol spike	3,646	0.12	0.32	0.090	0.036	0.31	0.34	17	10
O_2 introduction	23,198	264	6.35	0.032	3.3	3.1	0.35	36	11
N_2 introduction	4,333	117	0.45	0.81	3.9	-	1.9	20	200

increased provided, of course, that the organic solvent or molecular gas that was introduced did not contribute to the formation of the species.

The effect of increasing propan-2-ol and N_2 concentrations on the In^+, $ArCl^+$ and $ArAr^+$ signals is shown in Fig. 6.12. The $ArCl^+$ and $ArAr^+$ signals decreased rapidly up to a propan-2-ol concentration of 5% (v/v), and thereafter decreased more gradually up to a concentration of 80% where they started to increase once more (Fig. 6.12A). The In^+ signal also decreased sharply up to a propan-2-ol concentration of 20% (v/v) after which it rose steadily (Fig. 6.12A). However, the initial sharp decrease in In^+ signal was far less pronounced than the decreases in $ArCl^+$ and $ArAr^+$ signals. A propan-2-ol concentration of 10% (v/v) was considered most convenient to achieve effective minimisation of the polyatomic ion signals. Contrastingly, as the proportion of N_2, in a constant total gas flow, was increased the $ArCl^+$ and $ArAr^+$ signals increased slightly while the In^+ signal decreased rapidly (Fig. 6.12B). Hence, it was decided that the minimum flow-rate of N_2 allowable by the mass-flow controller (i.e. 0.03 l min^{-1}) was optimum.

The effect of nebuliser gas flow with N_2 introduction at different powers is shown in Fig. 6.13A for $ArCl^+$ signal and Fig. 6.13B for $ArAr^+$ signal. These results indicate that higher power necessitates a higher nebuliser gas flow for minimum polyatomic ion signal.

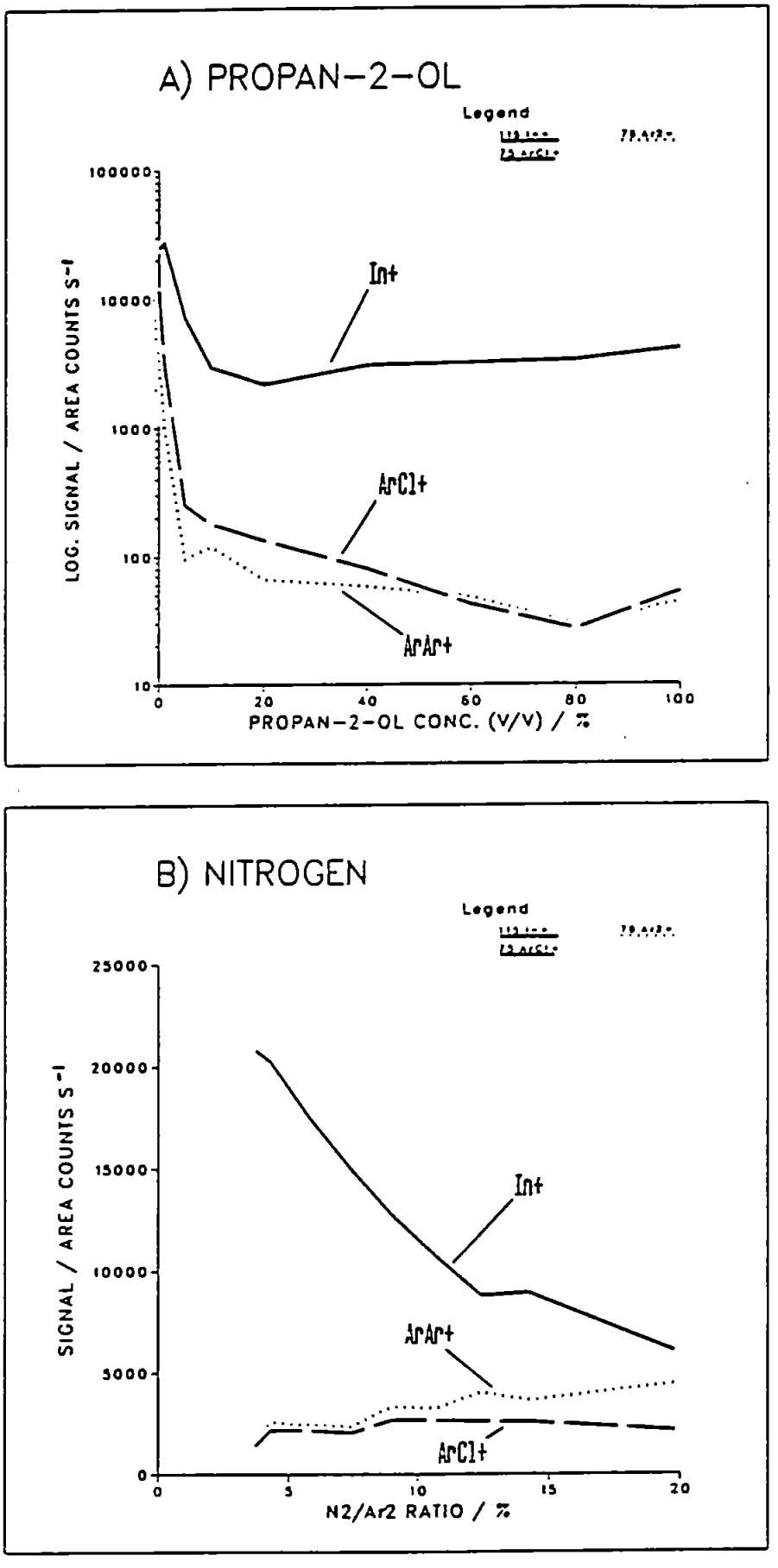

Figure 6.12 Effect of increasing: A) propan-2-ol concentration; and B) nitrogen concentration on the signals for In^+, $ArCl^+$ and $ArAr^+$

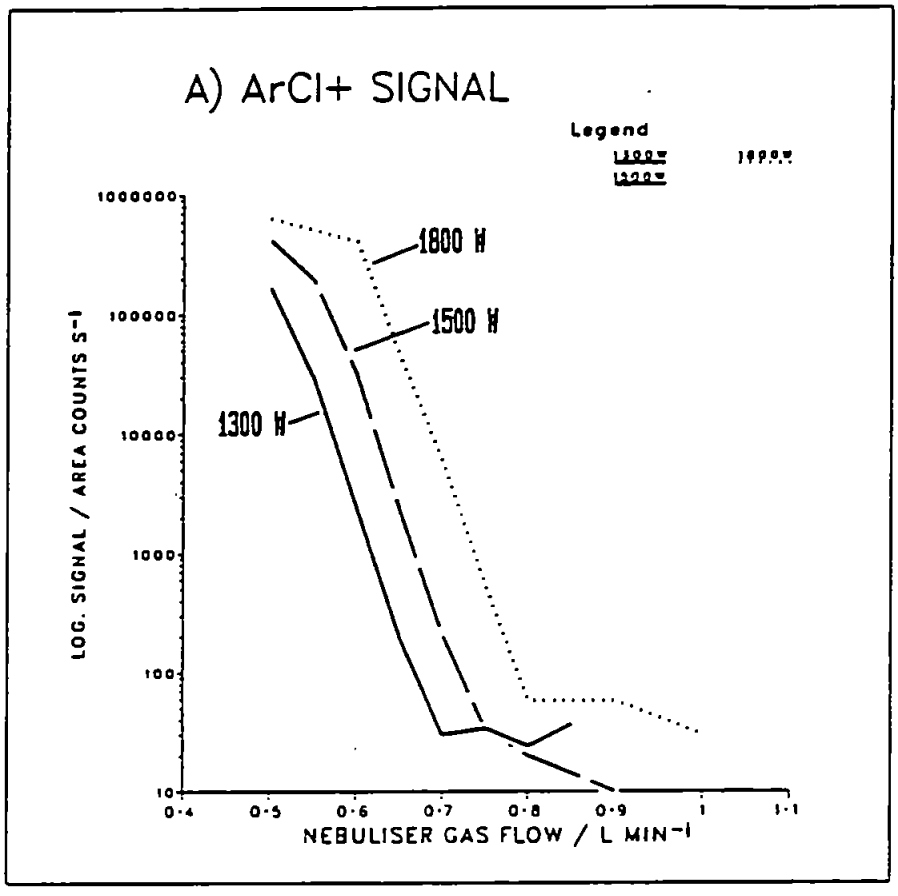

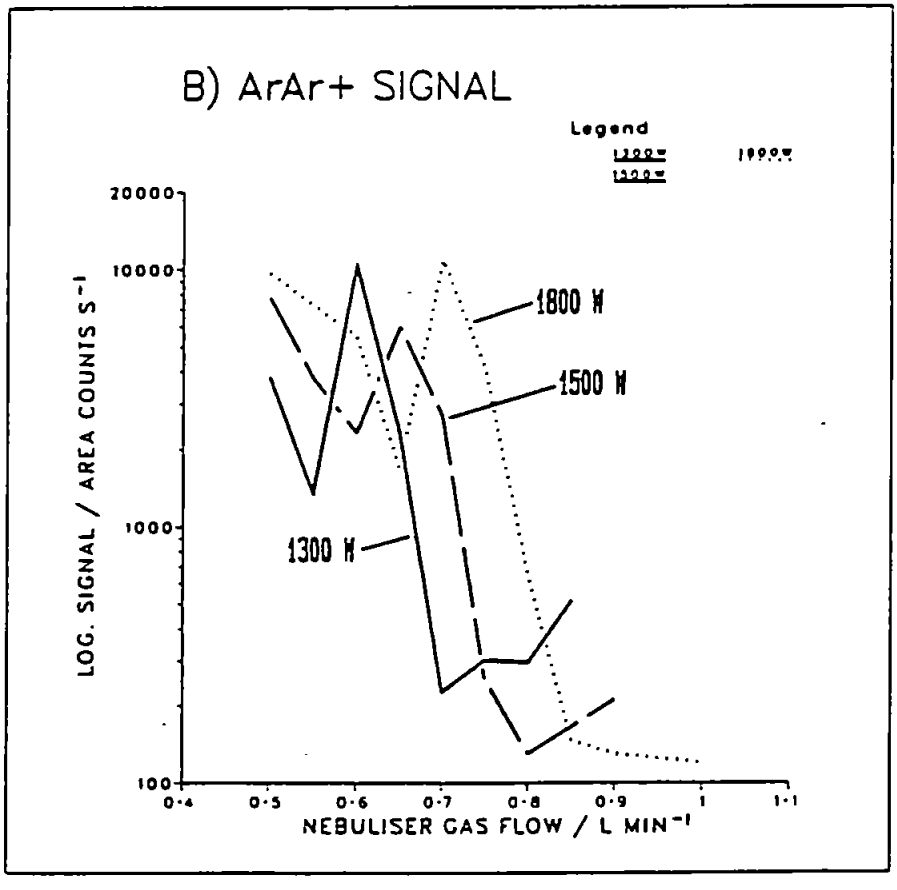

Figure 6.13 Effect of nebuliser gas flow on signals for: A) $ArCl^+$; and B) $ArAr^+$ at different powers during nitrogen introduction

6.4 Determination of Arsenic and Selenium

6.4.1 Procedure

Standards containing known concentrations of As and Se were spiked with various concentrations of hydrochloric acid (Aristar grade, BDH) and run as samples calibrated with solutions prepared in dilute nitric acid (2 + 98) (Aristar grade, BDH) using In (100 ng ml^{-1}) as an internal standard. The four different method modifications were used and recoveries for As and Se compared. Different nebuliser gas flows were used for each of the methods, as these were found to give the best compromise for the minimisation of interference while still maintaining as much of the In^+ signal as possible, as determined in the preliminary experiments. Nebuliser gas flows are given in Table 6.4. Other operating conditions were the same as those given in Table 6.1.

6.4.2 Results and Discussion

A brief summary of the effects of the four methods on the signals for In^+ and the interfering ions is given in Table 6.5. Ion intensities should be compared with the reference values, obtained by operating the instrument with a nebuliser gas flow of 0.85 l min^{-1} which has been found to give the best In^+ signal under normal conditions.

When no method modification was used, some reduction in $ArCl^+$ signal was observed by increasing the nebuliser gas flow from 0.85 to 1.00 l min^{-1}, although this was accompanied by a much greater decrease in the In^+ signal,

Table 6.4 Nebuliser gas flows used for As and Se determination in conjunction with the different method modification

Parameter	Method Modification			
	None	Propan-2-ol spike	O_2 Introduction	N_2 Introduction
Ar Nebuliser gas flow/l min^{-1}	1.00	0.80	1.00	0.87
O_2 Nebuliser gas flow/l min^{-1}	0	0.03	0.03	0
N_2 Nebuliser gas flow/l min^{-1}	0	0	0	0.03

Table 6.5 Signals for In^+ and In^+/xy^+ ratios for polyatomic ions interfering with As and Se at different operating conditions and using various method modifications. All results were obtained in dilute HCl (3+97)

Method Modification	$^{115}In^+$ signal/ area counts s^{-1}	In^+/xy^+ ratios			
		$^{115}In^+/^{40}Ar^{35}Cl^+$	$^{115}In^+/^{40}Ar^{36}Ar^+$	$^{115}In^+/^{40}Ar^{37}Cl^+$	$^{115}In^+/^{40}Ar^{38}Ar^+$
Reference*	18,213	0.19	2.2	0.62	12
None	5,521	0.79	1.5	2.9	8.3
Propan-2-ol spike	7,263	35	112	134	242
O_2 introduction	13,599	65	504	148	680
N_2 introduction	4,333	144	58	255	255

and an increase in the $ArAr^+$ signal (Table 6.5).

All three method modifications resulted in a decrease in In^+ signal. However, the relative reduction in the $ArCl^+$ and $ArAr^+$ signals was much greater, resulting in reduced interferences, as discussed in Section 6.3.2 and shown in Table 6.5.

These results are confirmed by the data contained in Table 6.6, which shows the effect of increasing HCl concentration on the recovery factors for As and Se. As can be seen, ^{75}As recovery was enhanced by a factor of 2.45 to 13.8 times and ^{78}Se by 1.18 to 3.08 times when no method modification was used. Recoveries much closer to unity were obtained when the method modifications were employed, the best performances being obtained by spiking with propan-2-ol or by the introduction of N_2 into the nebuliser gas flow, rather than by the introduction of O_2 only, which is undesirable anyway due to its detrimental effect on the lifetime of the sampling cone.

It should be noted that the determinations were undertaken without subtraction of a HCl blank solution since the samples were meant to mimic those containing unknown concentrations of chloride salts. Hence, As and Se contamination in the HCl used for spiking may also have caused enhancements to an unknown extent.

Table 6.6 Effect of increasing hydrochloric acid concentration on the recoveries of 100 ng ml^{-1} As and Se using different method modifications

Method Modification	Dilute HCl Concentration	Recovery factor*		
		^{75}As	^{77}Se	^{78}Se
None	1 + 99	2.45	8.83	1.18
	2 + 98	4.18	18.3	1.70
	4 + 96	7.05	35.1	2.04
	8 + 92	13.8	74.5	3.08
Propan-2-ol spike	1 + 99	1.02	1.51	1.00
	2 + 98	1.05	1.30	1.03
	4 + 96	1.15	1.69	1.09
	8 + 92	1.07	2.28	1.07
O_2 introduction	1 + 99	1.75	5.58	1.12
	2 + 98	2.16	9.39	0.73
	4 + 96	3.52	16.2	1.17
	8 + 92	4.95	25.9	1.52
N_2 introduction	1 + 99	0.97	1.21	0.94
	2 + 98	1.06	1.16	1.11
	4 + 96	1.12	1.13	0.95
	8 + 92	1.25	1.16	0.96

* Ratio of concentration found using the signal for the isotope shown to concentration added (i.e. 100 ng ml^{-1})

6.5 Conclusions

The introduction of an organic solvent or molecular gas into the ICP has been shown to cause dramatic reductions in polyatomic ion interferences in ICP-MS, facilitating the interference-free determination of As and Se. It is likely that the methods described will result in improved accuracy for the determination of other elements which suffer from polyatomic ion interferences in ICP-MS, although the use of alternative gases may be necessary.

CHAPTER 7

CONCLUSIONS AND SUGGESTIONS FOR FURTHER WORK

The project was successful in meeting many of its original objectives as well as others not initially forseen, especially in the field of ICP-MS.

The inductively coupled plasma has been successfully optimised for organic solvent introduction using the multivariate simplex optimisation procedure. The necessity of multivariate optimisation has been demonstrated by the identification of optimum operating conditions that differed in important respects from those determined by workers using univariate optimisation procedures. The conclusions were further supported by relating the operating conditions to fundamental properties of the plasma such as the behaviour of hard and soft spectral lines, rotational and excitation temperature. The application of computer aided tomography could well make an important contribution to the understanding of these properties. Additionally, trace elements have been determined in several organic samples by ICP-AES using novel methods of sample introduction such as slurry atomisation.

A study of matrix effects caused by an organic solvent in ICP-MS was performed. These effects were successfully eliminated by employing a novel method of sample introduction, namely the simultaneous nebulisation of organic and aqueous phases, together with internal

standardisation. Further work in this area could include the evaluation of the technique for more volatile organic solvents and the analysis of real organic samples, especially organic polymers solubilised in a suitable solvent.

Two different torches, namely the standard and low-flow torches were optimised for ICP-MS using simplex optimisation. Various criteria of merit were shown to differ markedly using the low-flow compared to the standard torch, and further investigation of different torch designs is evidently necessary for this technique. The low-flow torch was shown to form a much more stable plasma when organic solvents were introduced in comparison to the standard torch, and was evaluated for the semi-quantitative determination of trace elements in organic samples. Further studies of novel methods of sample introduction for organic solvents in ICP-MS are proposed, particularly flow injection, thermospray and glass frit nebulisation, especially for volatile solvents.

Finally, the effect of an organic solvent and molecular gases on polyatomic ion interferences in ICP-MS was investigated. Substantial reduction in, and in some cases the elimination of polyatomic species was achieved, allowing the interference free determination of As and Se. This area of work merits much more extensive study. Many more molecular gases could be introduced into the ICP and their effects on fundamental properties in the plasma,

expansion region and ion beam explored, thereby yielding a greater understanding of the mechanisms of formation of polyatomic ions, and the ionisation processes occurring in ICP-MS.

MEETINGS ATTENDED

(i) Analytical Division of the RSC, meeting on 'Research and Development Topics in Analytical Chemistry', 8th and 9th July, 1987, Glasgow.

(ii) Atomic Spectroscopy Group and Western Region jointly with the Peninsula Section of the RSC, meeting on 'New Perspectives in Atomic Spectroscopy', 3rd and 4th September, 1987, Plymouth.

(iii) Analytical Division in conjunction with the Scottish Region of the RSC, 'Professor Ottaway Memorial Meeting', 5th and 6th November, 1987, Edinburgh.

(iv) North East Region, Atomic Spectroscopy and Molecular Spectroscopy Groups jointly with the UV Spectrometry Group and Atomic Spectrometry Updates of the RSC, meeting on 'Recent Advances in Atomic and Molecular Spectroscopy', 29th and 30th March, 1988, Hull.

(v) Atomic Spectroscopy Group of the RSC jointly with the Spectroscopy Group of the Institute of Physics, 'Fourth Biennial National Atomic Spectroscopy Symposium', 29th June - 1st July, 1988, York.

(vi) Analytical Division of the RSC, meeting on '25th Anniversary of the Research and Development Topics in Analytical Chemistry', 18th -19th July, 1988, Plymouth.

(vii) Austrian Society for Microchemistry and Analytical Chemistry jointly with the German Working Group for Applied Spectroscopy, '1989 European Winter Conference on Plasma Spectrochemistry', 8th - 14th January, 1989, Reutte, Austria.

(viii) Atomic Spectroscopy Group jointly with the North East Region of the RSC, meeting on 'Inductively Coupled Plasma Mass Spectrometry', 15th February, 1989, Middlesbrough.

(ix) Analytical Division of the RSC, meeting on 'Research and Development Topics in Analytical Chemistry', 21st and 22nd March, 1989, Dublin.

(x) '3rd Surrey Conference on Plasma Source Mass Spectrometry', 16th - 19th July, 1989, Guildford.

LECTURES AND ASSOCIATED STUDIES

(i) RSC Lecture, 30th October, 1986, Plymouth Polytechnic, Dr. J.D.R. Thomas, 'Liquid and Enzyme Membrane Electrodes'.

(ii) RSC Lecture, 23rd January, 1987, Exeter University, Professor J. Miller, 'Illumination in Analytical Chemistry'.

(iii) RSC Lecture, 20th February, 1987, Plymouth Polytechnic, Dr. A. Ure, 'Atomic and Ion Spectra'.

(iv) SERC Vacation School 13th - 18th September, 1987, UMIST, 'Instrumentation and Analytical Science'.

(v) RSC Lecture, 13th November, 1987, Plymouth Polytechnic, Dr. A. Howard, 'Speciation'.

(vi) RSC Lecture, 29th January, 1988, Plymouth Polytechnic, Professor A. Townsend, 'Flow Injection Analysis - The First Decade'.

(vii) RSC Lecture, 7th October, 1988, Plymouth Polytechnic, Professor C.A. McAuliffe, 'The Binding and Activation of Sulphur Dioxide by Manganese Complexes'.

(viii) Research visit, 18th October, 1988, ICI Brixham.

(ix) RSC Lecture, 20th January, 1989, Plymouth Polytechnic, Dr. P.J. Worsfold, 'Flow Injection: Hands-off Analysis'.

(x) RSC Lecture, 17th February, 1989, Plymouth Polytechnic, Professor M. Barber, 'Modern Mass Spectrometry'.

(xi) Departmental Research Colloquia, weekly meetings, October 1986 to September 1989.

PRESENTATIONS AND PUBLICATIONS

Resulting from the work reported in this thesis the following papers have been presented and published.

Presentations

(i) 'Simplex Optimisation of an Inductively Coupled Plasma - Atomic Emission Spectrometer for Organic Solvent Introduction'.

Paper presented at the Fourth Biennial National Atomic Spectroscopy Symposium, 29th June - 1st July, 1988, York.

(ii) 'Optimum Conditions for Inductively Coupled Plasma - Atomic Emission Spectrometry with Organic Solvents'.

Poster presented at Research and Development Topics in Analytical Chemistry, 18th and 19th July, 1988, Plymouth.

(iii) 'The Importance of Multivariate Optimisation for ICP-AES and Organic Solvent Introduction'.

Paper presented during a research visit to ICI Brixham, 18th October, 1988.

(iv) 'Organic Samples and ICP-MS. Are They Compatible?'.

Paper presented at the 1989 European Conference on Plasma Spectrochemistry, 8th - 14th January, 1989, Reutte, Austria.

(v) 'Internal Standardisation for Plasma Spectrometry'.

Poster presented at Research and Development Topics in Analytical Chemistry, 21st and 22nd March, 1989, Dublin.

(vi) 'A Study of the Effects of Molecular Gases on Polyatomic Ion Interferences in ICP-MS'.

Paper presented at the 3rd Surrey Conference on Plasma Source Mass Spectrometry, 16th - 19th July, 1989, Guildford.

Publications

(i) Ebdon, L., and Evans, E.H.,

'The Inductively Coupled Plasma - An Analytical Tool with Growing Application'.

European Spectroscopy News, 1988, 79, 9.

(ii) Ebdon, L., and Evans, E.H.,

'Simple Approach to the Reduction of Polyatomic Ion Interferences on Arsenic and Selenium in Inductively Coupled Plasma - Mass Spectrometry'.

J. Anal. At. Spectrom., 1989, 4, 299.

(iii) Ebdon, L., Evans, E.H., and Barnett, N.W.,

'Simplex Optimisation of an Inductively Coupled Plasma for Organic Solvent Introduction',

J. Anal. At. Spectrom. 1989, 4, 505.

REFERENCES

1. Sychra, V., Lang, I., and Sebor, G., Prog. Anal. At. Spectrosc., 1981,4, 341.
2. Greenfield, S., Jones, I.L., and Berry, C.T., Analyst, 1964, 89, 713.
3. Wendt, R.H., and Fassel, V.A., Anal. Chem., 1965, 37, 920.
4. Boumans, P.W.J.M., (Ed.), Inductively Coupled Plasma Emission Spectrometry Parts 1 and 2, Wiley-Interscience, New York, 1987.
5. Fassel, V.A., Peterson, C.A., Abercrombie, F.N., and Kniseley, R.N., Anal. Chem., 1976, 48, 516.
6. Merryfield, R.N., and Loyd, R.C., Anal. Chem., 1979, 51, 1965.
7. Brown, R.J., Spectrochim. Acta, 1983, 38B, 283.
8. Algeo, J.D., Heine, D.R., Phillips, H.A., Hoek, F.B.G., Schneider, M.R., Freelin, J.M., and Denton, M.B., Spectrochim. Acta, 1985, 40B, 1447.
9. Granchi, M.P., Biggerstaff, J.A., Hilliard, L.J., and Grey, P., Spectrochim. Acta, 1987, 42B, 169.
10. Ohls, K., and Hutsch, B., ICP Inf. Newslett., 1986, 12, 176.
11. Shabanova, L.N., Buchbinder, G.L., and Gilbert, E.N., Zh. Anal. Khim., 1985, 40, 1221.
12. Nygaard, D.D., and Sotera, J.J., Spectroscopy (Springfield, Oregon), 1986, 1, 42.
13. Barnes, R.M., Khosah, R.P., Mahanti, H.S., and Ullman, A.H., Spectrochim. Acta, 1983, 38B, 291.

14. Miyazaki, A., Kimura, A., and Umezaki, Y., Anal. Chim. Acta, 1981, 127, 93.

15. Miyazaki, A., Kimura, A., Bansho, K., and Umezaki, Y., Anal. Chim. Acta, 1982, 144, 213.

16. Miyazaki, A., Kimura, A., and Umezaki, Y., Anal. Chim. Acta, 1982, 138, 121.

17. Seeverens, P.J.H., Klaassen, E.J.M., and Maessen, F.J.M.J., Spectrochim. Acta, 1983, 38B, 727.

18. Miyazaki, A., and Bansho, K., Spectrochim. Acta, 1987, 42B, 227.

19. Thompson, M., and Zao, L., Analyst, 1985, 110, 229.

20. Windsor, D.L., and Bonner Denton, M., Appl. Spectrosc., 1978, 32, 366.

21. Hausler, D.W., and Taylor, L.T., Anal. Chem., 1981, 53, 1223.

22. Irgolic, K.J., and Hobill, J.E., Spectrochim. Acta, 1987, 42B, 269.

23. Nygaard, D.D., Schleicher, R.G., and Sotera, J.J., Appl. Spectrosc., 1986, 40, 1074.

24. Nygaard, D.D., and Sotera, J.J., Appl. Spectrosc., 1987, 41, 703.

25. Barrett, P., and Pruskowska, E., Anal. Chem., 1984, 56, 1927.

26. Xu, J., Kawaguchi, H., and Mizuike, A., Anal. Chim. Acta, 1983, 152, 133.

27. Boorn, A.W., Cresser, M.S., and Browner, R.F., Spectrochim. Acta, 1980, 35B, 823.

28. Boorn, A.W., and Browner, R.F., Anal. Chem., 1982, 54, 1402.

29. Blades, M.W., and Caughlin, B.L., Spectrochim. Acta, 1985, 40B, 579.

30. Boumans, P.W.J.M., and Lux-Steiner, M.Ch., Spectrochim. Acta, 1982, 37B, 97.

31. Botto, R.I., Spectrochim. Acta, 1987, 42B, 181.

32. Maessen, F.J.M.J., Seeverens, P.J.H., and Kreuning, G., Spectrochim. Acta, 1984, 39B, 1171.

33. Maessen, F.J.M.J., Kreuning, G., and Balke, J., Spectrochim. Acta, 1986, 41B, 3.

34. Kreuning, G., and Maessen, F.J.M.J., Spectrochim. Acta, 1987, 42B, 677.

35. Kreuning, G., and Maessen, F.J.M.J., Spectrochim. Acta, 1989, 44B, 367.

36. Houk R.S., Fassel, V.A., Flesch, G.D., Svec, H.J., Gray, A.L., and Taylor, C.E., Anal. Chem., 1980, 52, 2283.

37. Gray, A.L., and Date, A.R., Analyst, 1983, 108, 1033.

38. Tan, S.H., and Horlick, G., Appl. Spectrosc., 1986, 40, 445.

39. Vaughan, M.A., and Horlick, G., Appl. Spectrosc., 1986, 40, 434.

40. Gray, A.L., and Williams, J.G., J. Anal. At. Spectrom., 1987, 2, 599.

41. Campbell, M.J., and Delves, H.T., J. Anal. At. Spectrom., 1989, 4, 235.

42. Ting, B.T.G., and Janghorbani, M., Spectrochim. Acta, 1987, 42B, 21.

43. Longerich, H.P., Fryer, B.J., and Strong, D.F., Spectrochim. Acta, 1987, 42B, 39.

44. Price Russ III, G., and Bazan, J.M., Spectrochim. Acta, 1987, 42B, 49.

45. Park, C.J., and Hall, G.E.M., J. Anal. At. Spectrom., 1987, 2, 473.

46. Wang, X. Viczian, M., Lasztity, A., and Barnes, R.M., J. Anal. At. Spectrom., 1988, 3, 821.

47. Beauchemin, D., McLaren, J.W., Willie, S.N., and Berman, S.S., Anal. Chem., 1988, 60, 687.

48. Beauchemin, D., Siu, K.W.M., and Berman, S.S., Anal. Chem., 1988, 60, 2587.

49. Beauchemin, D., McLaren, J.W., and Berman, S.S., J. Anal. At. Spectrom., 1988, 3, 775.

50. McLaren, J.W., Beauchemin, D., and Berman, S.S., Spectrochim. Acta., 1988, 43B, 413.

51. Date, A.R. and Hutchison, D., J. Anal. At. Spectrom., 1987, 2, 269.

52. Doherty, W., Spectrochim. Acta, 1989, 44B, 263.

53. Longerich, H.P., Fryer, B.J., Strong, D.F., and Kantipuly, C.J., Spectrochim. Acta, 1987, 42B, 75.

54. Date, A.R., and Stuart, M.E., J. Anal. At. Spectrom., 1988, 3, 659.

55. Hieftje, G.M., and Vickers, G.H., Anal. Chim. Acta, 1989, 216, 1.

56. Date, A.R., and Gray, A.L., (Eds.), Applications of Inductively Coupled Plasma Mass Spectrometry, Blackie, Glasgow, 1989.

57. Boorn, A., Fulford, J.E., and Wegscheider, W., Mikrochim. Acta, 1985, 2, 171.

58. Hutton, R.C., J. Anal. At. Spectrom., 1986, 1, 259.

59. Hausler, D., Spectrochim. Acta, 1987, 42B, 63.

60. Thompson, J.J., and Houk, R.S., Anal. Chem., 1986, 58, 2541.

61. Jiang, S., and Houk, R.S., Spectrochim. Acta, 1988, 43B, 405.

62. Beauchemin, D., Bednas, M.E., Berman, S.S., McLaren, J.W., Sui, K.W.M., and Sturgeon, R.E., Anal. Chem., 1988, 60, 2209.

63. Beauchemin, D., Sui, K.W.M., McLaren, J.W., and Berman, S.S., J. Anal. At. Spectrom., 1989, 4, 285.

64. Heitkemper, D., Creed, J., Caruso, J., and Fricke, F.L., J. Anal. At. Spectrom., 1989, 4, 279.

65. Meyer, G.A., Spectrochim. Acta, 1987, 42B, 201.

66. Brotherton, T., Barnes, B., Vela, N., and Caruso, J., J. Anal. At. Spectrom., 1987, 2, 389.

67. Nisamaneepong, W., Haas, D.L., and Caruso, J.A., Spectrochim. Acta, 1985, 40B, 3.

68. Brotherton, T.J., Pfannerstill, P.E., Creed, J.T., Heitkemper D.T., Caruso, J.A., and Pratsinis, S.E., J. Anal. At. Spectrom., 1988, 4, 341.

69. Ng, K.C., and Caruso, J.A., Anal. Chem., 1983, 55, 2032.

70. Ng, R.C., Kaiser, H., and Meddings, B., Spectrochim. Acta, 1985, 40B, 63.

71. Lancione, R.L., and Evans, S.J., 1986 Pittsburgh Conference and Exposition on Analytical Chemistry and Applied Spectroscopy, Atlantic City, N.J., USA, 10th - 14th March, 1986.

72. Spendley, W., Hext, G.R., and Himsworth, F.R., Technometrics, 1962, 4, 441.

73. Nelder, J.A., and Mead, R., Comput. J., 1965, 7, 308.

74. Yarbro, L.A., and Deming, S.N., Anal. Chim. Acta, 1974, 73, 391.

75. Deming, S.N., and Parker, L.R., C.R.C. Crit. Rev. Anal. Chem., 1978, 7, 187.

76. Ebdon, L., Cave, M.R., and Mowthorpe, D.J., Anal. Chim. Acta, 1980, 115, 179.

77. Cave, M.R., Kaminaris, D.M., Ebdon, L., and Mowthorpe, D.J., Anal. Proc., 1981, 18, 12.

78. Carpenter, R., and Ebdon, L., J. Anal. At. Spectrom., 1986, 1, 265.

79. Ebdon, L., and Carpenter, R.C., Anal. Chim. Acta, 1987, 200, 551.

80. Ebdon, L., and Carpenter, R., Anal. Chim. Acta, 1988, 209, 135.

81. Moore, G.L., and Böhmer, R.G., J. Anal. At. Spectrom., 1987, 2, 819.

82. Werner, P., and Friege, H., Appl. Spectrosc., 1987, 41, 32.

83. Greenfield, S., Salman, M.S., Thomsen, M., and Tyson, J.F., J. Anal. At. Spectrom., 1989, 4, 55.

84. Greenfield, S., and Thorburn-Burns, D., Anal. Chim. Acta, 1980, 113, 205.

85. Kalivas, J.H., Appl. Spectrosc., 1987, 41, 1338.

86. Moore, G.L., Humphries-Cuff, P.J., and Watson, A.E., Spectrochim. Acta, 1984, 39B, 915.

87. Belchamber, R.M., Betteridge, D., Wade, A.P., Cruickshank, A.J., and Davison, P., Spectrochim. Acta, 1986, 41B, 503.

88. Norman, P., Ph.D. Thesis, Plymouth Polytechnic, CNAA, 1987.

89. Wiese, W.L., and Furh, J.R., J. Chem. Ref. Data, 1975, 4, 263.

90. Ebdon, L., and Cave, M.R., Analyst, 1982, 107, 172.

91. Greenfield, S., Jones, I.L., and Berry, C.T., Analyst, 1964, 89, 713.

92. Fuller, C.W., Hutton, R.L., and Preston, B., Analyst, 1981, 103, 913.

93. Ebdon, L., and Collier, A.R., Spectrochim. Acta, 1988, 43B, 355.

94. Ebdon, L., and Wilkinson, J.R., J. Anal. At. Spectrom., 1987, 2, 39.

95. Ebdon, L., and Wilkinson, J.R., J. Anal. At. Spectrom., 1987, 2, 325.

96. Ebdon, L., and Collier, A.R., J. Anal. At. Spectrom., 1988, 3, 557.

97. Halicz, L., and Brenner, I.B., Spectrochim. Acta, 1987, 42B, 207.

98. Verbeek, A.A., and Brenner, I.B., J. Anal. At. Spectrom., 1989, 4, 23.

99. Broekaert, J.A.C., Leis, F., Raeymaekers, B., and Zaray, G., Spectrochim. Acta, 1988, 43B, 339.

100. Raeymaekers, B., Graule, T., Broekaert, J.A.C., Adams, F., and Tschöpel, P., Spectrochim. Acta, 1988, 43B, 923.

101 Sparkes, S., and Ebdon, L., Anal. Proc., 1986, 23, 410.

102 Ambrose, A.J., Ebdon, L., Foulkes, M.E., and Jones, P., J. Anal. At. Spectrom., 1989, 4, 219.

103. Williams, J.G., Gray, A.L., Norman, P., and Ebdon, L., J. Anal. At. Spectrom., 1987, 2, 469.

104. Ebdon, L., Foulkes, M.E., Parry, H.G.M., and Tye, C.T., J. Anal. At. Spectrom., 1988, 3, 753.

105. Sparkes, S.T., and Ebdon, L., J. Anal. At. Spectrom., 1988, 3, 563.

106. Gray, A.L., and Date, A.R., Analyst, 1983, 108, 1033.

107. Olivares, J.A., and Houk, R.S., Anal. Chem., 1986, 58, 20.

108. Pickford, C.J., and Brown, R.M., Spectrochim. Acta, 1986, 41B, 183.

109. Gray, A.L., Spectrochim. Acta, 1986, 41B, 151.

110. Beauchemin, D., McLaren, J.W., and Berman, S.S., Spectrochim. Acta, 1987, 42B, 467.

111. Gregoire, D.C., Appl. Spectrosc., 1987, 41, 897.

112. Gregoire, D.C., Spectrochim. Acta, 1987, 42B, 895.

113. Tan, S.H., and Horlick, G., J. Anal. at. Spectrom., 1987, 2, 745.

114. Thompson, J.J., and Houk, R.S., Appl. Spectrosc., 1987, 41, 801.

115. Gillson, G.R., Douglas, D.J., Fulford, J.E., Halligan, K.W., and Tanner, S.D., Anal. Chem., 1988, 60, 1472.

116. Crain, J.S., Houk, R.S., and Smith, F.G., Spectrochim. Acta, 1988, 43B, 1355.

117. Vandecasteele, C., Nagels, M., Vanhoe, H., and Dams, R., Anal. Chim. Acta, 1988, 211, 91.

118. Marshall, J., and Franks, J., Presented at the 1989 European Conference on Plasma Spectrochemistry, Reutte, Austria, 8th - 14th January, 1989. Paper No. P2-48.

119. Long, G.L., and Bolton, J.S., Spectrochim. Acta, 1987, 42B, 581.

120. Long, S.E., and Brown, R.M., Analyst, 1986, 111, 901.

121. Vaughan, M.A., Horlick, G., and Tan, S.H., J. Anal. At. Spectrom., 1987, 2, 765.

122. Evans, E.H., Ebdon, L., and Barnett, N.W., Presented at the 1989 European Conference on Plasma Spectrochemistry, Reutte, Austria, 8th - 14th January, 1989. Paper No. P2-44.

123. Gordon, J.S., van der Plas, P.S.C., and de Galan, L., Anal. Chem., 1988, 60, 375.

124. Schmit, J., and Chauvette, A., J. Anal. At. Spectrom., in the press.

125. Gray, A.L., Houk, R.S., and Williams, J.G., J. Anal. At. Spectrom., 1987, 2, 13.

126. Douglas, D.J., and French, J.B., J. Anal. At. Spectrom., 1988, 3, 743.

127. Houk, R.S., Schoer, J.K., and Crain, J.S., J. Anal. At. Spectrom., 1987, 2, 283.

128. Munro, S., Ebdon, L., and McWeeny, D.J., J. Anal. At. Spectrom., 1986, 1, 211.

129. Date, A.R., Cheung, Y.Y., and Stuart, M.E., Spectrochim. Acta, 1987, 42B, 3.

130. Hutton, R.C., and Eaton, A.N., J. Anal. At. Spectrom., 1987, 2, 595.

131. Zhu, G., and Browner, R.F., J. Anal. At. Spectrom., 1988, 3, 781.

132. Jiang, S.J., Palmieri, M.D., Fritz, J.S. and Houk, R.S., Anal. Chim. Acta, 1987, 200, 559.

133. Lyon, T.D.B., Fell, G.S., Hutton, R.C., and Eaton, A.N., J. Anal. At. Spectrom., 1988, 3, 601.

134. Plantz, M.R., Fritz, J.S., Smith, F.G., and Houk, R.S., Anal. Chem., 1989, 61, 149.

135. Branch, S., Ebdon, L., and O'Neill, P., Presented at the 3rd Surrey Conference on Plasma Source Mass Spectrometry, 16th - 19th July, 1989.

136. Janghorbani, M., and Ting, B.T., Anal. Chem., 1989, 61, 701.

137. Hall, G.E.M., Pelchat, J.C., Boomer, D.W., and Powell, M., J. Anal. At. Spectrom., 1988, 3, 791.

138. McLaren, J.W., Beauchemin, D., and Berman, S.S., J. Anal. At. Spectrom., 1987, 2, 277.

139. Lyon, T.D.B., Fell, G.S., Hutton, R.C., and Eaton, A.N., J. Anal. At. Spectrom., 1988, 3, 265.

140. Montaser, A., Chan, S., and Koppenaal, D., Anal. Chem., 1987, 59, 1240.

141. Koppenaal, D.W., and Quinton, L.F., J. Anal. At. Spectrom., 1988, 3, 667.

142. Brown, P.G., Davidson, T.M., and Caruso, J.A., J. Anal. At. Spectrom., 1988, 3, 763.